MONTICELLO
NUCLEAR POWER PLANT

QUALIFICATION OF REACTOR PHYSICS METHODS
FOR
APPLICATION TO MONTICELLO
NSPNAD-8609

NORTHERN STATE
NUCLEAR ANAL

NSP

MONTICELLO NUCLEAR GENERATING PLANT

QUALIFICATION OF REACTOR PHYSICS METHODS

For

APPLICATION TO MONTICELLO

NSPNAD-8609

Revision 0

September 1986

Principal Contributors

Roger O Anderson, NSP
Clifford Bonneau, NSP
Keith Dehnbostel, NSP
Peter Pankratz, NSP
Doug Shilts, NSP
Rick Streng, NSP
Tim Tasto, NSP
Jack Fisher, URA
Rod Grow, UAI

Prepared by Rick Streng Date 9/4/86

Reviewed by Clifford Bonneau Date 9/4/86

Approved by Roger O. Anderson Date 9/10/86

Abstract

This document is a Topical Report describing the Northern States Power Company (NSP) qualification of reactor physics methods for application to the Monticello Nuclear Plant.

This document addresses the reactor model description, qualification and quantification of reliability factors and applications to operations and reload safety evaluations of the Monticello plant.

TABLE OF CONTENTS

TABLE OF CONTENTS

LIST OF TABLES

LIST OF FIGURES

LIST OF FIGURES (Continued)

LIST OF FIGURES (Continued)

LIST OF FIGURES (Continued)

1.0 INTRODUCTION

This report addresses the reactor model description, qualification and quantification of reliability factors, applications to operations and reload safety evaluations of the Monticello Nuclear Plant (Mnt).

A summary description of the computer codes is given in Section 2. This report stresses the aspects of implementation of the NSP model; the individual code descriptions are referenced in Appendix B.

Whenever possible, directly observable parameters (such as reactor critical K-eff and measured incore detector fission rates) are utilized. The Mnt data used in this evaluation span cycles 7 through 10. In order to be completely objective in the choice of data to be used for the comparisons, all Mnt cycles 7 through 10 measurements were reviewed and qualified prior to initiating the comparison calculations.

After the measured data to be used in the benchmark process had been defined, the model calculations were performed and comparisons are presented in this report as part of the quantification of the NSP model calculational uncertainties and reliability factors. A statistical approach was used to derive the uncertainties. These uncertainties are consistent with the model application procedures and methodology.

The uncertainties are evaluated by direct comparison to experimental data.

In order to provide a continuing verification of the conservatism of the reliability factors determined by Mnt cycles 7 through 10 data, ongoing comparisons are made each cycle using the statistical methods described in this report. A discussion of the reliability factors is provided in Section 3.

The methods for use of the model and the reliability factors are described relative to reactor operation and reload safety evaluation in Sections 4 and 5.

2.0 GENERAL CHARACTERISTICS OF THE NSP CALCULATIONAL MODEL

The Monticello (Mnt) calculational model is very similar to the calculational model already approved for our Prairie Island (PI) units (see Reference 1). This has been intentionally done in order to simplify the methods, make the use of these methods more efficient, make it easier to cross train personnel, and to simplify the review process. A flow diagram of the Monticello model is shown in Figure 2.0.1. For ease of comparison the Prairie Island model is shown in Figure 2.0.2. The code acronyms used in these figures are defined in Appendix B.

In general, the CASMO-II[2] program is used to generate the lattice physics parameters for input to both PDQ7/HARMONY[3,4] and to the Nuclear Data Handling System (NDH). CASMO-II produces initial nuclide concentrations, depletion and product chain data, and tables of microscopic and macroscopic cross sections varying with burn-up for input to the XY diffusion-depletion in PDQ7/HARMONY. Cross Section data for PDQ7/HARMONY are generated by a capture fraction matching procedure between PDQ7 and CASMO-II. For Mnt, PDQ7 is used primarily to generate generic normalization parameters for NDH and generic adjustment factors for local peaking factor generation. The use of generic rather than cycle specific normalization factors is the most significant difference between the modeling techniques of Mnt and PI. CASMO-II generates void and exposure dependent K_∞, M^2, $\nu\Sigma_f$, and $\kappa\Sigma_f$ assembly information in curve fits and table lookup formats for input to the NDH program. NDH is a derivative of the Flare based EPRI NODE-B program described in the Advanced Recycle Methodology Program (ARMP)[5] documentation. The NDH program contains the following improvements over the NODE-B program.

- Automates the collection and processing of data.
- 24 axial nodes per assembly versus 12.
- 50 fuel types are represented versus 13.
- Changes in reactivity are represented by $\Delta\rho$ rather than by $\Delta K/K$.
- Doppler is treated as a function of exposure and water density in addition to being a function of fuel temperature.
- The exposure weighted void term (V_{ijk}) is treated explicitly.
- A samarium correction has been added.
- An (optional) normalization factor has been added on M^2
- Control rod tip correction factor has been added.
- A routine has been added to calculate kinetics parameters for input to transient analyses models.
- The inlet flow distribution is calculated by EPRI-THERM-B in the void loop.
- A new array was added to explicitly treat control rod history.
- The radial albedos are void dependent.
- The cold base K_∞ is a function of temperature.
- $\Delta\rho/N_{xe}$ is input on a Table as a function of void history and exposure versus calculating $\Delta K/K$ for xenon internally.
- A correction factor was added to K_∞ to account for the fact that a bundle was on the core periphery and then moved to the inside of the core.
- Spectrum correction factors were added to correct for the extrapolated flux in the power calculation.

Other minor changes have been made such as input and output edits, but the primary calculational sequence and physics methodology have been preserved from the EPRI-NODE-B program.

The SIGMA program calculates the predicted reaction rates using NDH nodal power distributions. The program then determines the uncertainties associated with the measured and calculated incore detector signals for each statepoint. The SPM code then combines all the statepoints to calculate overall uncertainties.

It is recognized that the procedures used for the construction and application of the Mnt model are as much a part of the model definition as are the codes. It is essential, therefore, that the procedures used to calculate inputs for safety analysis be the same as those used in the model benchmarking and qualification process. This is particularly true in the calculation of core power distributions and local peaking factors in which the results are heavily dependent on the procedure used to normalize the nodal model. In view of the importance of model normalization, it is appropriate to identify the key aspects of the procedures used for Monticello and their application to future safety related calculations.

The Monticello nodal model has been normalized to plant measurements for cycles 7 through 10. Those parameters that have been normalized to plant data have been constrained to retain a single set of values for all of the benchmark results presented in this document. These will also be used for future safety related calculations. Generic normalization factors have been generated from normalization of the nodal model to ¼ core depleted PDQ7 models at zero, forty, and seventy percent void for cycles 5 and 6 and at forty percent void for cycle 7.

In addition to the main sequence computer codes, a number of auxiliary computer codes are employed to provide a user tailored code package. These auxiliary computer codes are not basic to the physics methodology, but are vital for automation and transformation of the large volume of calculated and measured parameters required for core analysis. The computer code descriptions are summarized in Appendix B.

Figure 2.0.1

FLOW CHART,CASMO/NDH MODEL

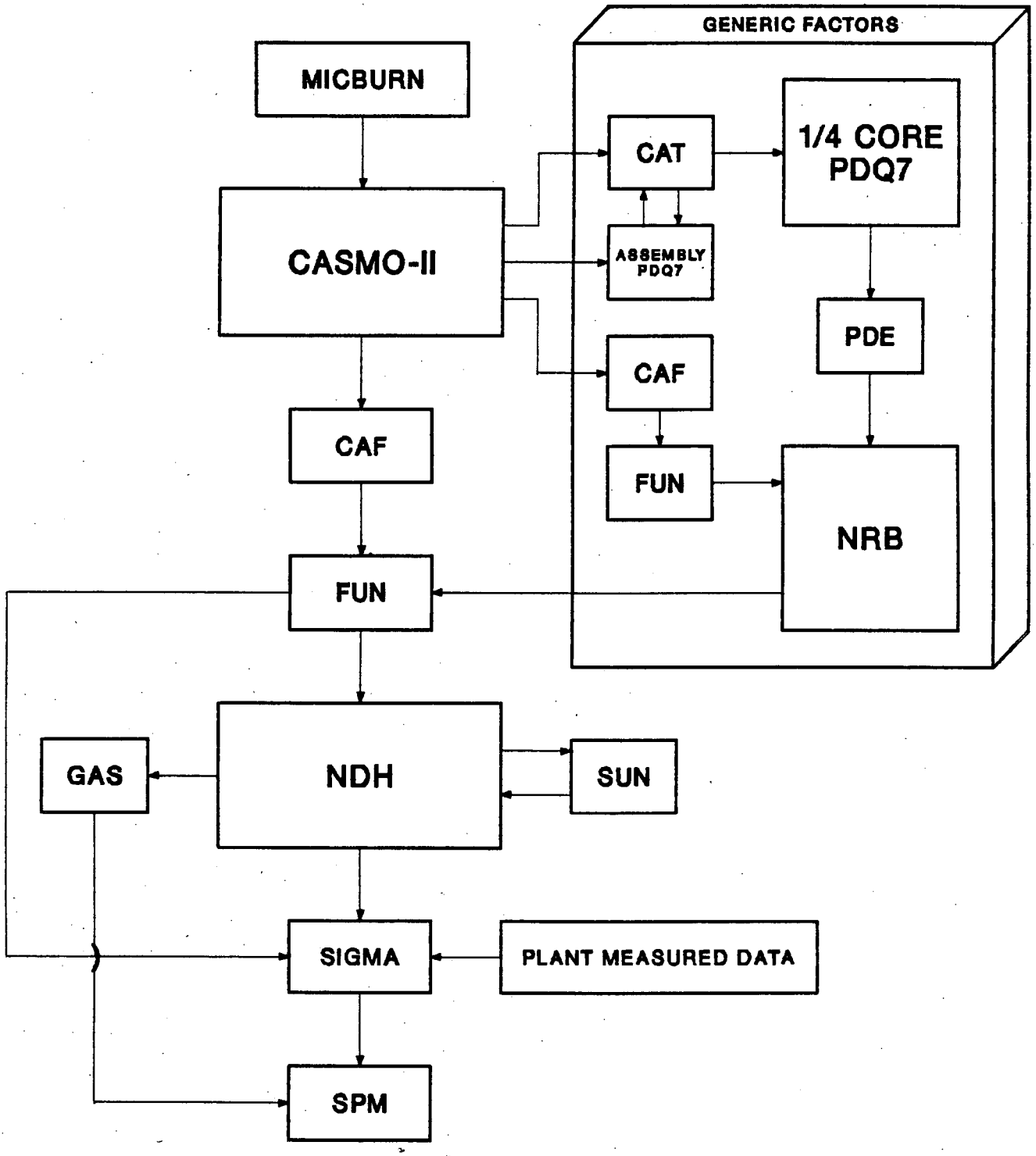

Figure 2.0.2

FLOW CHART,CASMO/PDQ7/DP5 MODEL

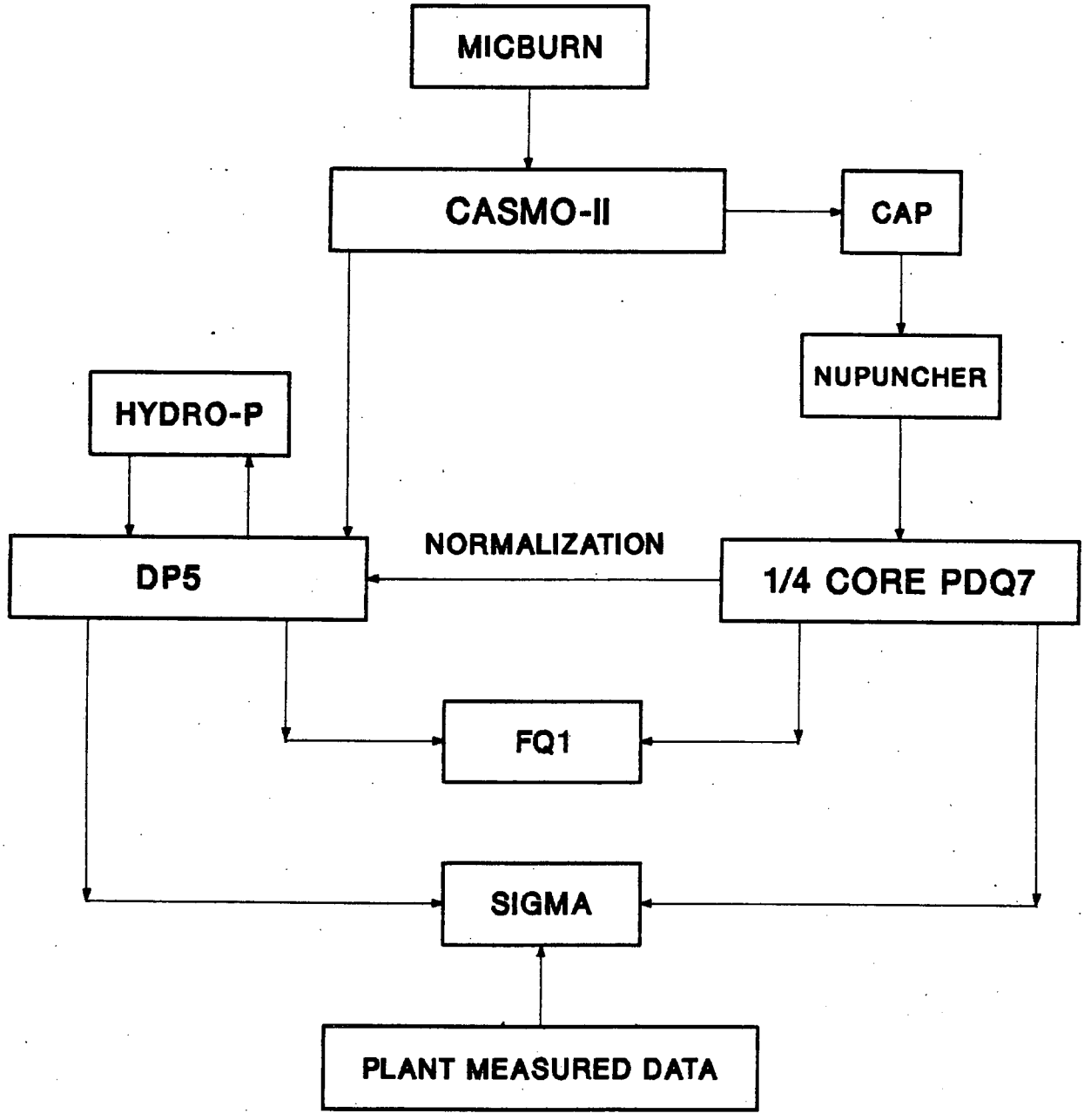

3.0 MODEL VERIFICATION AND RELIABILITY FACTOR DETERMINATION

The NSP models have been benchmarked against Mnt measurements made during cycles 7 thru 10 for the CASMO/NDH model to quantify the reliability factors to be used in safety related calculations. The resultant reliability factors and biases are summarized in Table 3.0.1. The remainder of this section is a detailed account of the derivation of these factors.

The term reliability factor (RF) is used to describe the allowances to be used in safety related calculations to assure conservatism. The uncertainty factor (1σ) is used to describe the actual model accuracy. The reliability factor is always larger than the uncertainty factor.

The term bias is used to describe the statistical difference between an observed or measured distribution and the calculated value.

Appendix A describes the statistical methods used in the evaluation of the uncertainties in the following sections.

During each cycle, measured and calculated parameters will be compared in order to verify and update the reliability factors determined in this section. Results of the verification and an update for each parameter will be documented in the reload safety evaluation for the reload in which the updated values will be used. The updates to the reliability factors will be in accordance with the methods outlined in this section and in Appendix A.

TABLE 3.0.1

Reliability Factors for Monticello

PARAMETER	Reliability Factor (expressed as applied)	Reliability Factor (expressed as %)	Bias
APLHGR	$RF_{TPF} = .111$	11.1	0
LHGR	$RF_{TPF} = .111$	11.1	0
MCPR	$RF_{RPF} = .081$	8.1	0
Rod Worth	$RF_{RODS} = .10$	10.0	0
Void Coefficient	$RF_{VOIDS} = .10$	10.0	0
Doppler Coefficient	$RF_{DOP} = .10$	10.0	0
Delayed Neutron Parameters			
ℓ^*	$RF_{\ell^*} = .04$	4.0	0
β	$RF_{\beta} = .04$	4.0	0

3.1 Control Rod Worth

Control rod worths in a BWR cannot be directly measured. Control rod worths can be inferred from various reactor critical conditions. The approach taken is to benchmark the NSP model to these critical conditions. The data base includes 8 few rod criticals and 14 sequence criticals taken at temperatures ranging from 68 °F to 200 °F. This data represents the actual critical statepoints in cycles 7 through 10. All measured statepoints have been included. The results of the comparisons are shown in Table 3.1.1.

The standard deviation of the calculated K_{eff} at the critical positions is .0019. This difference includes the measurement uncertainty as well as the calculational uncertainty. The typical amount of reactivity being held down by rods is on the order of 10% ΔK. Using this value we can calculate an uncertainty in rod worth by dividing the standard deviation by this worth, i.e. .19% ΔK / 10% ΔK = 2.0%. For convervatism the rod worth reliability factor (RF_{rods}) is defined as 10%.

Figures 3.1.1 through 3.1.4 present graphs of control rod notch inventory versus cycle exposure for hot critical conditions for cycles 7 through 10. The best estimate is the predicted control rod notch inventory using CASMO/NDH with the ±1%ΔK reactivity anomaly shown. Measured rod notch inventory is indicated as a dot for each statepoint. All measured values are within the ± 1%ΔK bounds. This indicates the well behaved prediction of the model and supports the use of the conservative rod worth reliability factor used above.

TABLE 3.1.1

MEASURED TO CALCULATED

ROD WORTH COMPARISON

Cycle	Notches Withdrawn	Core Ave. Exposure	Temp. °F	K_{eff}
7	154	9.748	101	.9995
	1480	9.748	102	1.0015
	1492	9.748	118	.9991
	1494	9.748	130	.9989
	1508	12.033	133	.9992
	1514	12.033	172	.9975
8	152	12.119	123	.9975
	120	12.119	123	1.0006
	124	12.119	122	.9991
	1416	12.119	122	1.0016
	1492	12.119	127	1.0046
	1464	12.119	125	1.0019
	1504	12.389	141	1.0037
9	148	13.368	99	.9990
	130	13.368	97	.9994
	846	13.368	102	1.0003
	828	13.368	109	1.0013
	1494	16.403	134	.9971
10	152	13.520	138	.9996
	154	13.520	139	1.0016
	1458	13.520	142	.9999
	1478	13.520	145	.9999

Mean K_{eff} = 1.0001 σ = .0019

Figure 3.1.1
Control Notch Worth Inventory Versus Exposure
Cycle 7

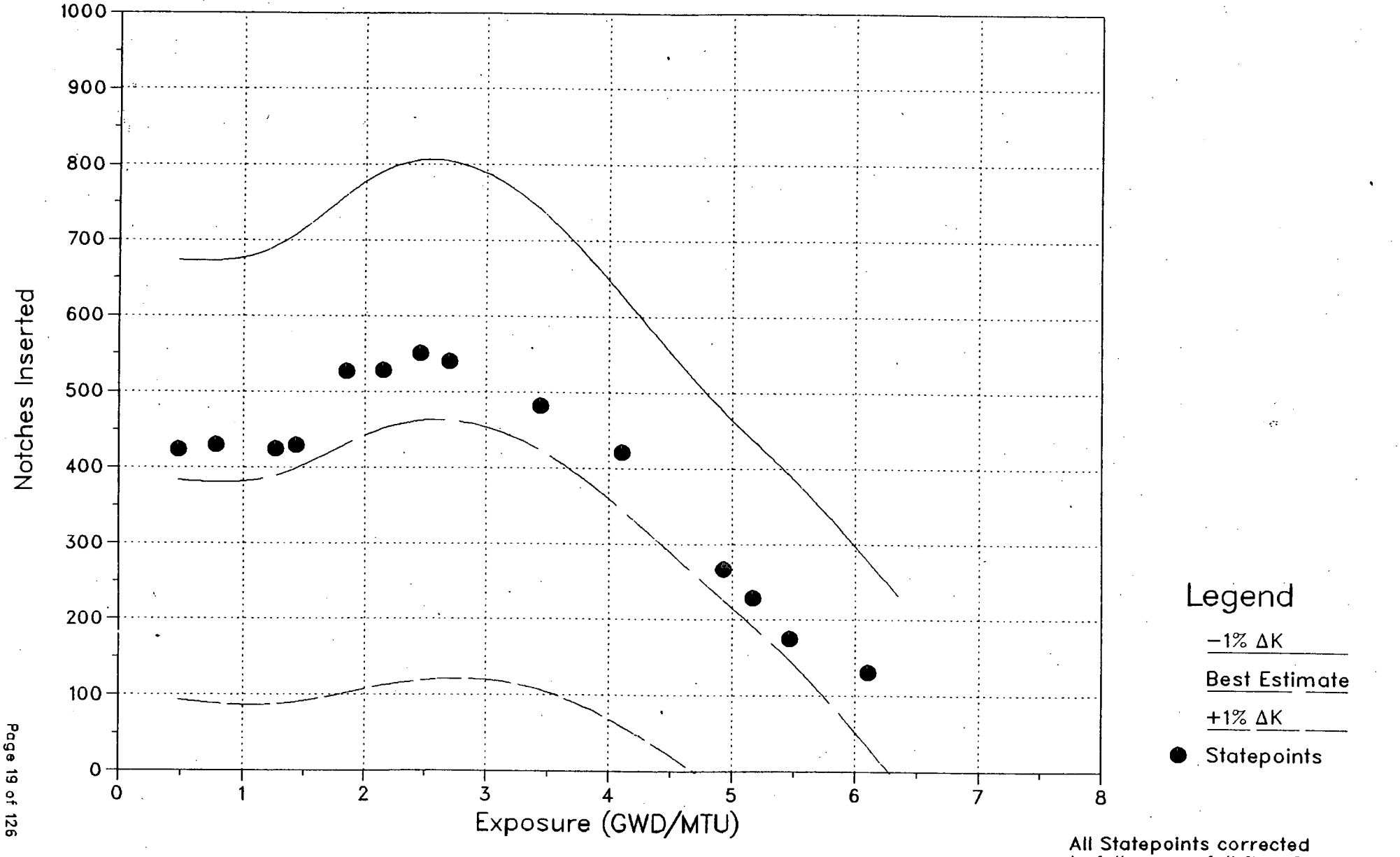

All Statepoints corrected
to full power, full flow Conditions

Figure 3.1.2
Control Notch Worth Inventory Versus Exposure
Cycle 8

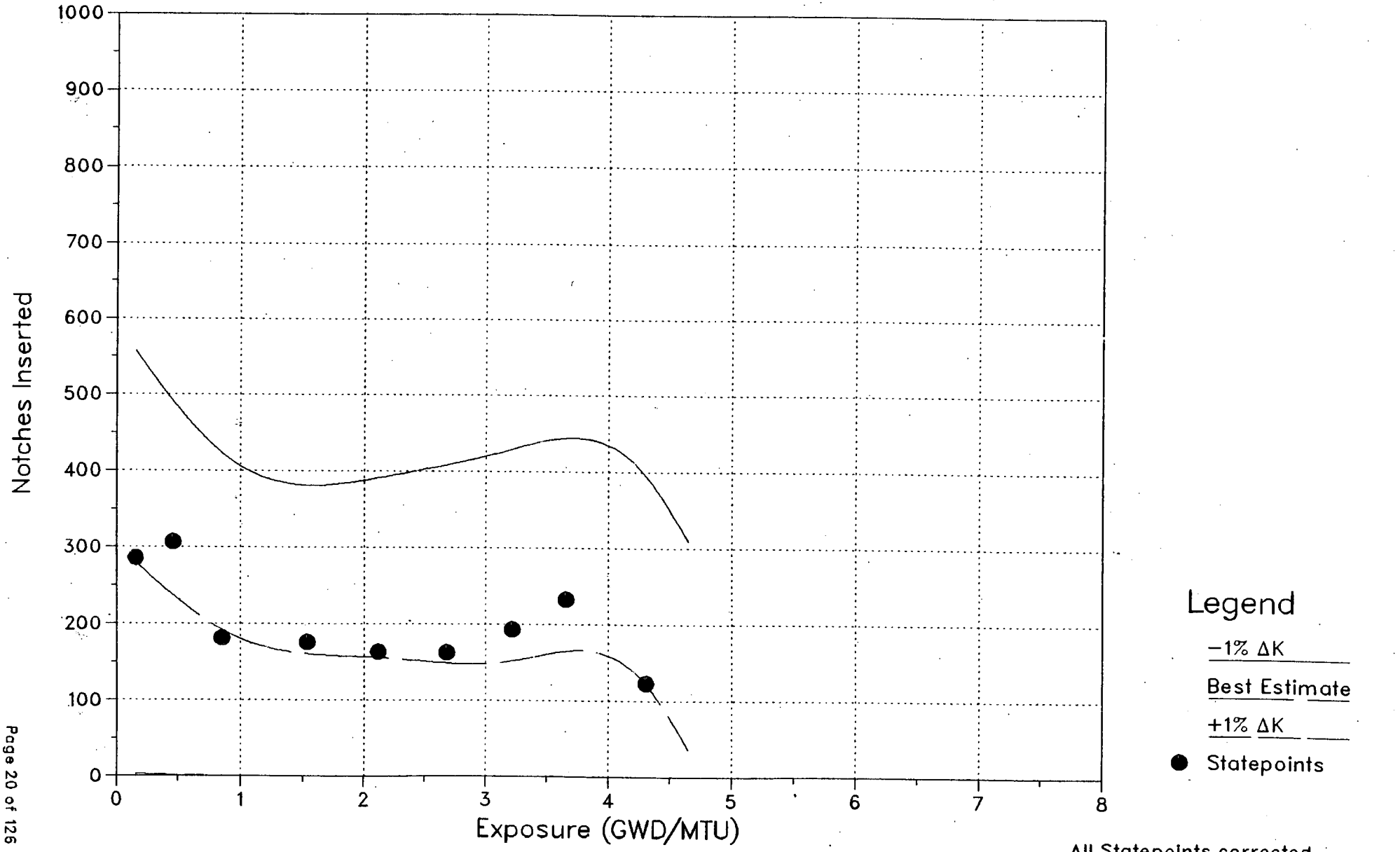

Figure 3.1.3
Control Notch Worth Inventory Versus Exposure
Cycle 9

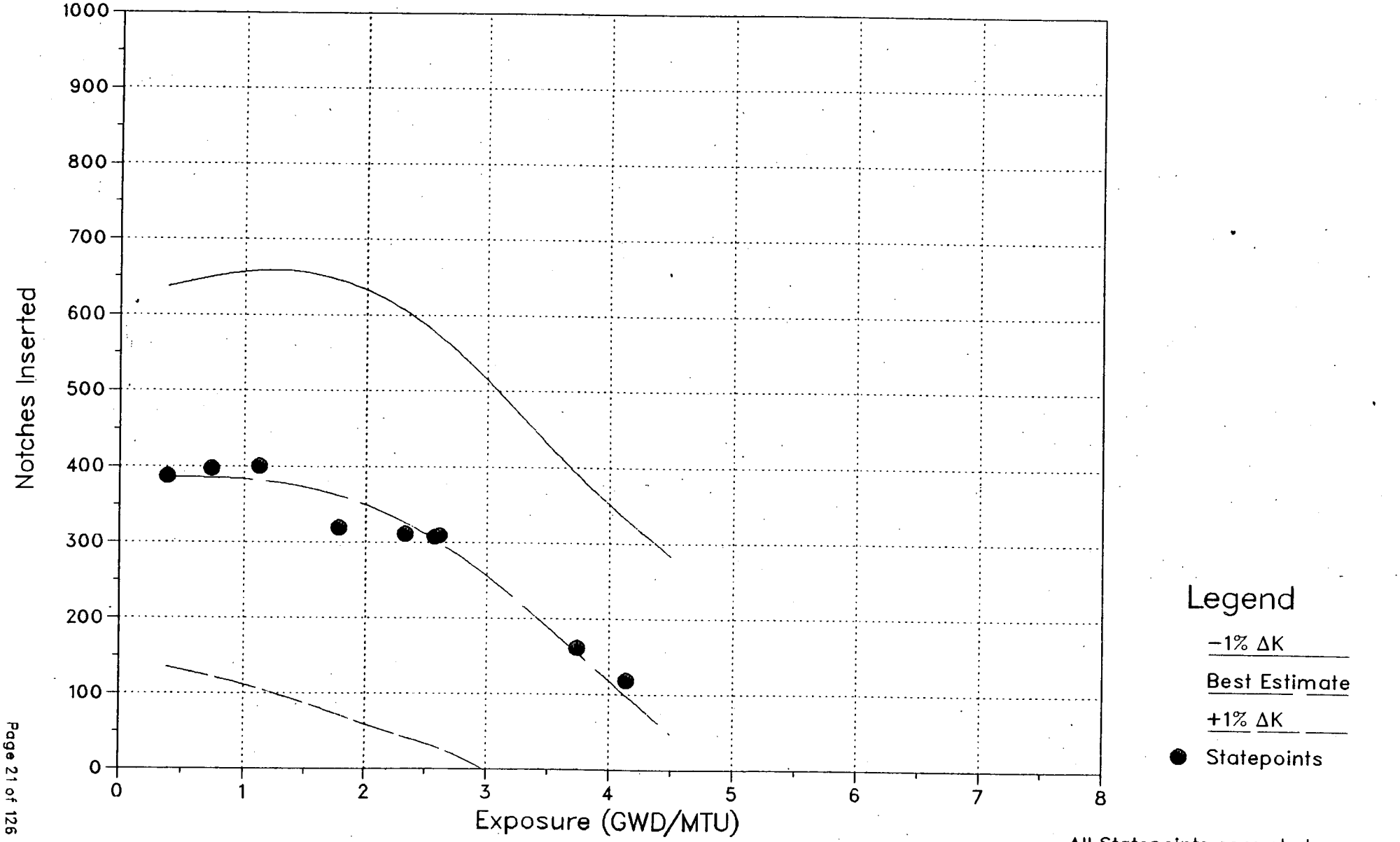

All Statepoints corrected
to full power, full flow Conditions

Figure 3.1.4
Control Notch Worth Inventory Versus Exposure
Cycle 10

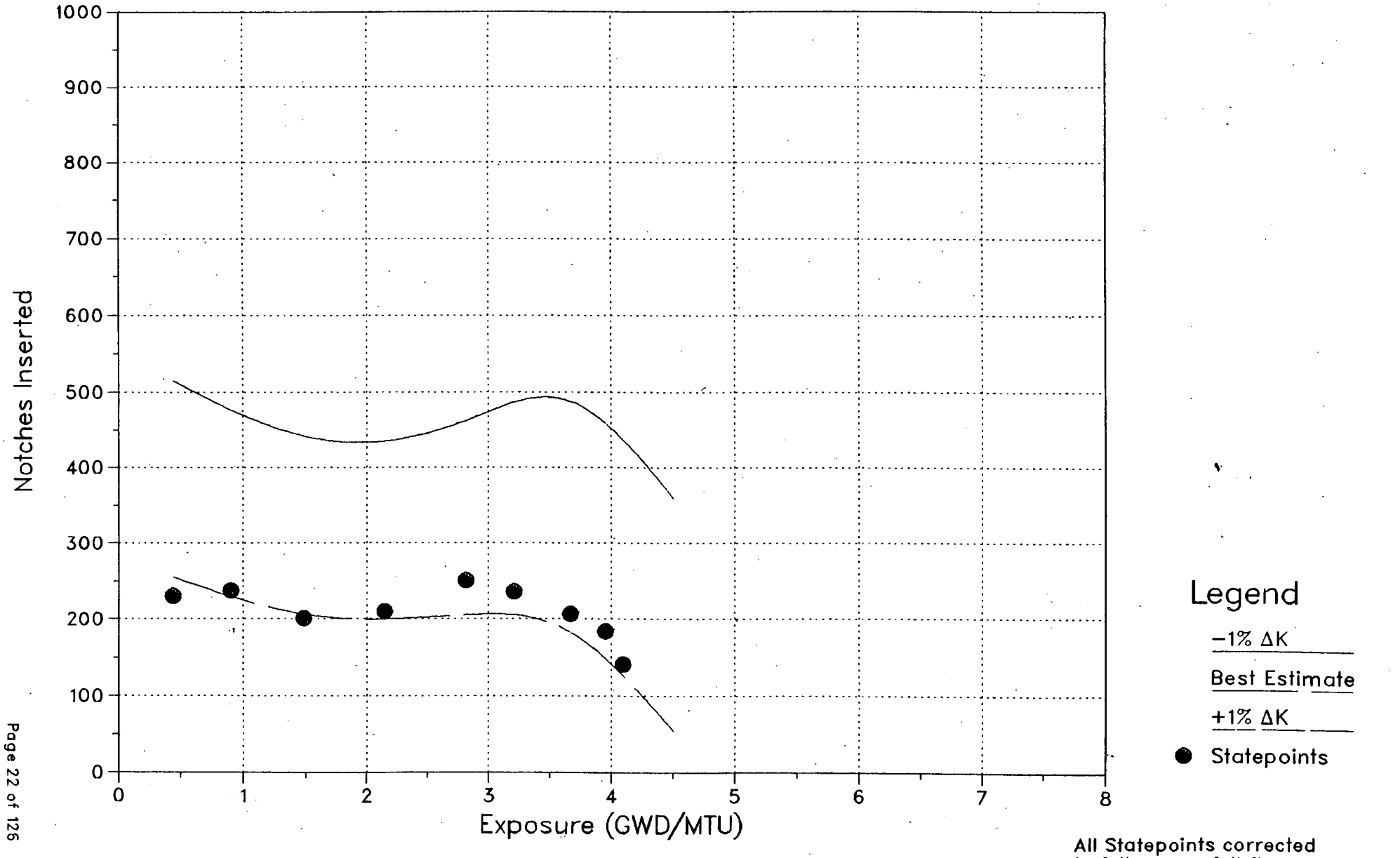

3.2 Temperature Coefficient

The range of values of moderator temperature coefficients encountered in current BWR lattices does not include any that are significant from the safety point of view. The small magnitude of this coefficient, relative to that associated with steam voids and combined with the long time-constant associated with transfer of heat from the fuel to the coolant, makes the reactivity contribution of moderator temperature change insignificant during rapid transients.

For the reasons stated above, current core design criteria do not impose limits on the value of the temperature coefficient, and effects of minor design changes on the coefficient usually are not calculated.

3.3 Void Coefficient

The void coefficient in a BWR cannot be directly measured, i.e., there are always present the effects of other parameters such as control rods, Doppler coefficient, xenon etc. The magnitude of the uncertainty in the void coefficient can be inferred, however, from comparisons of predicted versus measured critical statepoints where the effect of the other parameters is minimized. Table 3.3.1 gives calculated values for the measured critical statepoints from EOC coastdown for cycles 7 thru 10. All of these cases are at the all rods out condition. Table 3.3.2 gives the calculated values for the measured critical statepoints for a one pump trip at EOC 7, again at the all rods out condition. The standard deviation of the calculated $K_{eff's}$ is ±.0018 ΔK for the coastdown cases and ± .0007ΔK for the one pump trip cases. The total reactivity held down by voids for the average void fraction (38%) in the core at these conditions is on the order of 3% ΔK. An average %ΔK/%V can be calculated from Table 3.3.1 which represents the error in the predicted and measured value. % ΔK/% ΔV = .0077. Multiplying by the average percent void gives the error in terms of ΔK. % ΔK = .0077 * 38% = 0.29. Therefore the uncertainty in void can be calculated by dividing by the total void worth at 38% which gives 0.29 / 3% = 9.8% uncertainty. This uncertainty includes components of error from exposure, xenon and Doppler. Therefore, a reliability factor of 10% in void coefficient is deemed appropriately conservative for safety related calculation. The results from Table 3.3.2 also demonstrate the stability of the analysis during a xenon transient.

Table 3.3.1

EOC COASTDOWN STATEPOINTS

Cycle	Exposure GWD/MTU	Power %	Void %	K_{eff}
7	6.345	100	36.9	.9909
	6.954	91	33.6	.9902
	7.636	79	27.6	.9909
8	4.651	100	38.4	.9923
	5.565	90	34.8	.9908
	6.104	83	30.9	.9924
9	4.496	99	36.1	.9939
	5.570	83	30.5	.9938
	6.163	72	26.5	.9949
	6.555	64	23.6	.9960
10	4.507	100	37.2	.9929
	5.886	80	29.5	.9932
	6.371	71	26.2	.9943

Mean K_{eff} = .9928 σ =.0018

Table 3.3.2

ONE PUMP TRIP STATEPOINT AT EOC 7

Hours after trip	% Power	% Void	K_{eff}
0.0	76	28.0	.9916
0.01	54	28.5	.9927
2.0	57	29.1	.9913
4.0	62	29.1	.9907
10.0	62	29.2	.9909
24.0	62	29.5	.9910

Mean K_{eff}= .9914 σ ± .0007

3.4 Doppler Coefficient

Measurements can be made in a power reactor which are directed at determining the Doppler coefficient at various power levels. In a BWR the uncertainty associated with such measurements (e.g. rod repositioning, void feedback) are such that results are not reliable for direct validation of the calculational model. Consequently, an indirect approach is taken.

The primary variable in the calculation of Doppler effects using the CASMO/NDH model is the fuel temperature. A change in fuel temperature associated with a power change results in a reactivity change due to the change in the resonance absorption.

The algorithm in NDH that determines the model change in reactivity due to the fuel temperature change uses data calculated by CASMO (i.e. $\Delta\rho/°F$). The approach is to determine the accuracy of CASMO in calculating the change in the resonance integral (RI) due to a known fuel temperature increase, then use engineering judgement to bound this uncertainty to assure conservatism.

Comparisons of EPRI-CPM and CASMO calculations to experiments performed at the Kritz facility[6,7,8] in Sweden have determined that the uncertainty of CASMO is well within the measurement uncertainty. See also reference 1, 3-9 thru 3-12 for additional supporting data from the EPRI ARMP documentation. In view of this, a 10% reliability factor placed on the Doppler coefficient is judged adequate to assure a conservative value.

3.5 Isotopics

The benchmarking of CASMO to Yankee and Saxton data is thoroughly discussed in reference 1.

3.6 Power Distribution Reliability Factor Determination

The purpose of this section is to discuss the methods used to determine the power distribution reliability factors. Reliability factors have been determined for the local fuel pin power in a node and for the total fuel bundle power. These factors can then be applied to the calculation of the linear heat generation rate (LHGR), the average planar linear heat generation rate (APLHGR) and the critical power ratio (CPR) respectively.

The statistics presented in Sections 3.6.1, 3.6.2 and 3.6.3 follow those presented in the Prairie Island Topical, see reference 1. Since this way of presenting power distribution statistics is not the common practice in the industry, Section 3.6.4 has been added which presents data in a form directly comparable to other published BWR power distribution data. This has been done to enhance the review process and make comparison to standard published data easier.

3.6.1 Local Power Distribution

The model reliability factor for calculating power distributions is based on comparisons of measured and predicted traversing incore probe (TIP) flux detector signals for normal operating core conditions.

The signals from the detectors are corrected by the on-site process computer to account for such things as detector sensitivity, drift, and background. It is these corrected signals, or reaction rates, which have been compared to simulated reaction rates calculated with the NSP models in order to derive model reliability factors.

The reliability factor RF is defined as a single value of $\Delta TPF/TPF_m$ such that TPF_c (I,J,K) times 1 + $\Delta TPF/TPF_m$ has a 95% probability at a 95% confidence level of being conservative with respect to TPF_m (I,J,K). The subscripts c and m denote calculated and measured values. TPF (I,J,K) is the total pin peaking factor for all I,J,K locations in the core. This value cannot be measured directly. What is measured by the detector system is the reaction rate in the instrument thimble. This measured reaction rate is a local value. $RR_m = \phi\Sigma_f$ (measured).

These values are measured at 48 axial locations in each thimble. The CASMO/NDH model has been used to calculate the reaction rates in the instrument thimbles. $RR_c = \phi\Sigma_f$(calculated). The observed difference distribution (ODD) has then been calculated by simply taking the relative difference of these two values:

$ODD = (RR_m - RR_c) / RR_m$ for all measured locations in the core.

It is important to note that the ODD is not the difference between nodal powers but rather is the difference between local fission rate values. It is assumed that the ODD is equal to $\Delta TPF/TPF_m$. This is a valid assumption since the calculated and measured reaction rates are local fission rate values as is the TPF, the only difference is the location.

The observed difference distribution determined above includes the uncertainties in the calculational model as well as the uncertainties in the measurement instrumentation. The calculational model uncertainty includes uncertainty in the calculation of the nodal power and in the conversion factors from nodal power to the pin power which is taken to be the same as the total uncertainty in the calculated reaction rates. Therefore, the total uncertainty in the local pin power can be written as follows:

$$RF_{TPF} = \sigma_{TPF.95}$$

where $\sigma_{TPF.95}$ is determined from the ODD determined above.

The simulated detector signals are calculated in a manner which is consistent with the calculation of local power peaking factors for the purpose of safety evaluations; see Section 5.1. The first step is to compute the power distribution under consideration. The resolution used is 24 axial levels per fuel assembly.

The simulated detector signals are obtained by using one node at each axial level to predict a nodal power density for that assembly at that level. This power is then converted to a local relative reaction rate at the location of the detector. The conversion factors are calculated for each assembly location as a function of assembly exposure and void history using the CASMO model, and a generic rod insertion and radial placement term obtained from a fine mesh ¼ core PDQ7 calculation. The 24 axial values in each detector location are then synthesized into a continuous function over the axial height of the fuel.

The grid flux depressions are then superimposed on the synthesized function using an empirical function designed to match the characteristics of flux depressions measured with tip detectors. The effect of the grid flux depressions is to raise the flux level in the axial region between grids while depressing the flux in the grid region.

A total of 44 core statepoints, or tip traces were chosen for the purpose of comparing measured and simulated in-core reaction rates for the CASMO/NDH model. These statepoints span operating cycles 7 through 10 of Monticello. The specific core conditions for each of the statepoints are given in Table 3.6.1.

Typical examples of the comparisons of measured and predicted reaction rates are provided in Figures 3.6.1 through 3.6.36. The data is presented in sets of three figures, one set for each TIP trace, three maps per cycle (BOC, MOC, EOC). The first figure in each set presents the differences between the measured and predicted integral reaction rates for all instrumented locations. The instrumented core locations are indicated with circles in each of the figures. The second and third figures of

each set present axial comparisons in two specific instrumented core locations. The measurements are shown as triangles at the 48 axial levels. The predicted reaction rates are represented as circles. The two core locations were chosen as typical of regions of high power density.

The method of normalizing the calculated and measured reaction rates is to adjust the average of all 24 detectors at 48 locations to the fraction of rated thermal power for each statepoint. This normalization technique is used to put the measured and predicted values on a common basis which is consistent with the definition of the local peaking factors. The measurement uncertainty in core thermal power is accounted for in the transient and LOCA analysis.

The distribution of observed differences between measured and calculated instrument signals for all 44 core statepoints was determined. For each trace, 8 of the 48 axial values were excluded from consideration. This included the top and bottom 4 points. These are areas of steep flux gradients, and small errors in instrument position result in large differences in measured to calculated values. Since the reaction rates in these areas are always smaller (e.g., the high power point will never occur in top or bottom) these values were excluded from the determination of the observed differences density function. The reliability factors being developed here will include the measurement uncertainty as well as the calculational uncertainty. However, known problems with the TIP measurement system such as TIP tube mislocation and channel bowing make the measurement uncertainty very large relative to the calculational uncertainty. In order to minimize the impact of these large measurement uncertainties on reliability factor determination, the following procedure was used to quantify the measurement error and eliminate the worst values from the data base. First, a 95%/95% confidence level was determined from the observed difference density function determined above. Note that this distribution includes all TIPs. Then a thorough review was made of all the data which was greater than the 95/95 confidence limit. The following criteria were then established to eliminate selected data:

One: if a TIP's data was greater than the 95/95 confidence level at one statepoint and stayed outside of this level for the rest of the cycle, that TIP's data was eliminated.

Two: if a TIP's data varied throughout the cycle about the 95/95 confidence level, i.e. sometimes higher sometimes lower, then the TIP trace was compared to its symetric pair. If the comparison showed large deviations, the data was eliminated.

All other data was retained in the data base. The total number of nodal observations used was 37396. The total number of observations eliminated was 4839.

The resulting observed differences density function was tested for normality using the Kolomogorov D test. The results demonstrated that this function differed significantly from a normal distribution. Therefore, all subsequent statistical analysis has been performed using the methods described in Appendix A.2. To ensure a conservative reliability factor at all power levels, the sample was divided into subsamples as a function of power (see Figure 3.6.43). A

standard deviation was calculated for each subsample using the methods described in Appendix A.2. Figure 3.6.43 shows a distinct power dependence for the absolute difference. Therefore, to assure conservatism in the application, the reliability factor will be applied as a relative rather than an absolute value. The distribution of observed differences is shown in Figure 3.6.37. The following statistics therefore represent the total data base as described above using relative differences.

The first step using this method is to determine the mean relative difference of the measured to calculated values (μmc) and the standard deviation (σmc):

$$\mu mc = \frac{\sum_{i=1}^{n} e_i}{n} = -.008$$

$$\sigma mc = \left[\frac{\sum_{i=1}^{n} (e_i - \mu mc)^2}{n-1} \right]^{\frac{1}{2}} = .070$$

where: e_i = ith observed difference

n = total number of observations

The second step is to transform the e_i to standard measure using the following formula:

$$Z_i = \frac{e_i - \mu mc}{\sigma mc}$$

and the resulting variates Z were then sorted into ascending order (see Figure 3.6.38). A value of Z was chosen as an estimate of the 95th percentile of the distribution, i = 35527. This gives the 95th percentile of Z to be

$$Z_{35527} = Q_{95} = 1.566$$

which implies that 95% of the errors are likely to be less than 1.566 standard deviations from the mean. It remains then to calculate a 95% confidence interval on Q_{95} using the following formula

$$\text{Var } Q_{95} = \frac{q(1-q)}{n f_1^2}$$

where:

q = the quantile (.95)
n = number of independent observations in sample
f_1 = ordinate of the density function of the distribution function at the abscissa q

Due to the dependence of the observed differences with axial height, the total number of observations was reduced by a factor of three to determine the total number of independent observations. The factor of three was taken from the Prairie Island topical, Reference 1. This was assumed conservative since the PWR shows more dependence than the BWR.

It is necessary to obtain an estimate of $f_1(.95)$, and this was done by applying a linear regression analysis on a short interval of the cumulative distribution function (CDF) of Z in the region of the 95th percentile (see Figure 3.6.39). The estimated slope of the CDF (estimated from the straight line in Figure 3.6.39) is an estimate of the ordinate density function. The slope is calculated as .120.

This gives

$$\text{Var } Q_{95} = \frac{.95(1-.95)}{(37396/3 \text{ X } .120^2)} = .00026$$

and $\sigma_{Q95} = (\text{Var } Q_{95})^{\frac{1}{2}} = .016$

The estimate of the upper limit on Q_{95} is

$$K_c \, \sigma_{Q95} = 1.645 * .016 = .027$$

thus:

$$1.566 - .027 \leq Q_{95} \leq 1.566 + .027$$

The upper limit is then 1.566 + .027 = 1.593 which gives the following as the 95% confidence level that the calculated reaction rate (RRc) will be conservative with respect to the measured reaction rate (RRm).

$$RRm = RRc * (1 \pm 1.593 \, \sigma mc) = RRc * (1 \pm 1.593 * .070)$$
$$RRm = RRc * (1 \pm .111)$$
therefore $\sigma_{TPF.95} = .111$

Note that this value includes measurement error which adds to the conservativeness of the calculation.

3.6.2 Integrated Power Distribution

The model reliability factors for calculating power distributions are based on comparisons of integrated measured and predicted TIP trace signals obtained from normal operating core conditions.

The reliability factor RF is defined as a single value of $\Delta RPF/RPF_m$ such that RPF(I,J) calculated times 1 + $\Delta RPF/RPF_m$ has a 95% probability at a 95% confidence level of being conservative with respect to the measured RPF(I,J). The subscripts c and m will be used to denote calculated and measured values. RPF(I,J) is the integrated peaking factor determined for all I,J locations in the core. This value cannot be measured directly. What is measured by the detector system is the reaction rate in the instrument thimble. This measured reaction rate is a local value. $IRR_m = \phi\Sigma_f$ (measured). These values are determined at each thimble by integrating the 48 measured axial locations. The three-dimensional model CASMO/NDH has been used to calculate the reaction rate in the instrument thimbles. $IRR_c = \phi\Sigma_f$ (calculated). The observed difference distribution (ODD) has then been calculated by simply taking the relative difference of these two values

$ODD = (IRR_m - IRR_c)/IRR_m$ for all measured locations in the core.

The observed difference distribution determined above includes the uncertainties in the calculational model, the uncertainties in the measurement instrumentation, and the uncertainties in conversion factors from nodal power to instrument value. The calculational model uncertainty includes uncertainty in the calculation of the nodal powers as well as uncertainties in the local pin powers. Therefore the uncertainty in the local integrated pin power can be written as follows

$$RF_{\Delta RPF} = \sigma_{RPF.95}$$

where $\sigma_{RPF.95}$ is determined from the ODD.

The distribution of observed differences between measured and calculated integrated instrument signals for all 44 statepoints was determined for the CASMO/NDH model and is shown in Figure 3.6.40. All 48 axial values were used to calculate the integrated value. The TIP traces eliminated by the screening criteria in Section 3.6.1 were also eliminated from the integral data base. The total number of integrated observations used was 935.

The observed difference density function was tested for normality using the Kolomogorov D test and was found to vary significantly from a normal distribution. Therefore, all subsequent statistical analysis has been performed using the methods described in Appendix A.2 on the entire sample. The cumulative distribution function and the CDF in the region of the 95th percentile are given in Figures 3.6.41 and 3.6.42 respectively. The significant parameters calculated for this distribution are as follows:

$$\mu mc = -.003$$
$$\sigma mc = .047$$
$$Q_{95} = 1.612$$
$$\sigma_{Q95} = .055$$
$$K_c\sigma_{Q95} = .097$$
$$IRRm = IRR_c * (1 \pm .081)$$
$$\sigma_{RPF.95} = .081$$

where: IRRm = Integrated reaction rate measured
IRRc = Integrated reaction rate calculated

No dependence of the observed difference with position was found. Therefore, n was not reduced.

3.6.3 Gamma Scan Comparisons

Gamma scan measurements were made on 31 discharged fuel bundles at the EOC 8 and on 57 bundles at the EOC 9. Individual rod measurements were performed on four bundles at twelve axial levels, two at EOC8 and two at EOC9. See references 11 and 12 for complete detailed information on the measurement technique and results. Figures 3.6.44 and 3.6.45 show the assembly locations that were gamma scanned at EOC 8 and EOC 9 respectively. The results of these gamma scans have been used to determine the accuracy of the CASMO/NDH model power distribution calculation.

The approach used in the comparison is identical to that used in Sections 3.6.1 and 3.6.2 when comparing to the detector reaction rates. Figures 3.6.46 thru 3.6.51 give typical comparisons from the EOC 8 and EOC 9 gamma scans. The first figure presents the radial comparison and the next two figures present the axial comparisons of two high power density bundles.

The following is a comparison of the CASMO/NDH to TIP comparison and the CASMO/NDH to gamma scan comparison. Since the gamma scan is a 'snapshot' in time it has been compared to TIP comparisons made at the EOC 8 and EOC 9 only. Since there are not sufficient data points to compare at a 95/95 level, only the standard deviations are compared.

For the relative integral comparison 48 CASMO/NDH to TIP and 88 CASMO/NDH to gamma scan values are used.

CASMO/NDH to integral TIP (EOC 8 and 9 only)

$$\mu = -.005$$
$$\sigma = .055$$

CASMO/NDH to integral gamma scans

$$\mu = .003$$
$$\sigma = .031$$

For the relative local comparison 1920 CASMO/NDH to TIP comparisons and the local gamma scan are used. To obtain the local gamma scans 1123 CASMO/NDH to nodal gamma scan comparisons are statistically combined with 48 CASMO/NDH pin to assembly gamma scans.

CASMO/NDH to local TIP (EOC 8 and 9 only)

$$\mu_L = -.009$$
$$\sigma_L = .080$$

CASMO/NDH to nodal gamma scan

$$\mu_n = -.032$$
$$\sigma_n = .074$$

CASMO/NDH to pin to assembly gamma scan

$$\mu_p = .016$$
$$\sigma_p = .026$$

CASMO/NDH to local gamma scan

$$\sigma_L = (\sigma^2_n + \sigma^2_p)^{\frac{1}{2}}$$
$$= (.074^2 + .026^2)^{\frac{1}{2}} = .078$$

Since the standard deviations for the gamma scans are less than the TIP for both the integral (.031 < .055) and local (.078 < .080) comparisons the reliability factors used from the CASMO/NDH to TIP comparisons in sections 3.6.1 and 3.6.2 are conservative. The calculational technique for the TIP and gamma scan are the same, i.e., CASMO/NDH with PDQ generic factors.

3.6.4 Standard Power Distribution Comparison

The following is a presentation of the power distribution using the industry standard format. Published power distribution data is usually presented in tables of axial, radial and nodal comparisons and is usually compared at the 1σ level. Note that the entire data base is used.

3.6.4.1 Axial Power Distribution Comparisons

Table 3.6.2 presents axial peak-to-average comparisons for selected statepoints from cycles 7 through 10. Table 3.6.3 presents axial peak-to-average comparisons for selected gamma scan comparisons at EOC 8 and EOC 9. The following results are taken from the entire data base presented in sections 3.6.1, 3.6.2 and 3.6.3.

Simulator to measured TIP traces

Unrodded	Rodded
n = 647	n = 288
μ = .003	μ = -.010
σ = .036	σ = .035

Simulator to Gamma Scan

Unrodded
n = 88
μ = -.011
σ = .026

This data shows excellent agreement with other published data.

3.6.4.2 Radial Power Distribution Comparisons

Table 3.6.4 presents radial peak-to-average comparisons from selected statepoints from cycles 7 through 10. Table 3.6.5 presents radial peak to average comparisons for selected gamma scans from EOC 8 and EOC 9. The following results are taken from the entire data base presented in Section 3.6.1, 3.6.2 and 3.6.3.

Simulator to measured TIP traces

$\mu = -.003$
$\sigma = .047$

Simulator to Gamma Scan

$\mu = .003$
$\sigma = .031$

This data shows excellent agreement to other published data.

3.6.4.3 Nodal Power Distributions Comparisons

Table 3.6.6 presents the nodal standard deviations for the 20 axial planes from the EOC 8 and EOC 9 gamma scans. The following results are taken from the entire data base presented in Sections 3.6.1, 3.6.2 and 3.6.3.

Simulator to measured TIP traces

$\mu = -.008$
$\sigma = .070$

Simulator to Gamma Scans

$\mu = -.032$
$\sigma = .074$

This data shows excellent agreement to other published data.

3.7 Delayed Neutron Parameters

This section deals with determining reliability factors for values which can be calculated but not measured. In these cases, an argument may be made for the general magnitude of the reliability factor without making direct comparisons between measured and predicted values.

The importance of the reliability of the calculated values of the delayed neutron parameters is primarily associated with the core β_{eff}. The uncertainties in the calculation of β_{eff} are composed of several components, the most important of which are listed below:

a) Experimental values of β, and λ, by nuclide;
b) Calculation of the spatial nuclide inventory;
c) Calculation of core average β as a flux weighted average over the spatial nuclide inventory;
d) Calculation of β_{eff} from the core average as $\beta_{eff} = I*\beta$, where I = importance factor.

The experimental determination of the β's and λ's are assumed to be accurate to within 1%. The most important nuclide concentrations with respect to core β are U^{238}, U^{235} and Pu^{239}. Tables 3.4.1 and 3.4.2 in reference one indicate that the uncertainty in the calculation of these parameters is about 0.3% for CASMO. Therefore, components a) and b) above are combined as 1.3% for CASMO.

The uncertainty in the calculation of a core average β depends on the relative flux weighting of the individual assemblies in the core. For demonstration purposes, consider a four region core, each with a different average burnup and average β. This is typical of advanced BWR cycles in that about a fourth of the core has seen three previous cycles, a fourth two previous cycles, a fourth one previous cycle and a fourth is the feed fuel. Typical regional β's are given below:

Region 1 (fourth cycle fuel)	$\beta = 0.0050$
Region 2 (third cycle fuel)	$\beta = 0.0055$
Region 3 (second cycle fuel)	$\beta = 0.0065$
Region 4 (feed fuel)	$\beta = 0.0070$

The effect of errors in the calculated flux distribution can be evaluated in terms of the effect on the core average β. As a base case, flux weighting factors are all set to 1.0. In this case, the core average $\beta = 0.006$. Using a maximum error in the regional flux weighting of 7.0%, the worst error in the calculation of the core average β is obtained by increasing the weight of the Region 1 fuel and decreasing the weight of the Region 4 fuel. It should be noted that the average relative weighting factor is unity. The revised β is calculated as follows:

$\beta(1) \times 1.07 = .00535$
$\beta(2) \times 1.00 = .0055$
$\beta(3) \times 1.00 = .0065$
$\beta(4) \times 0.93 = .00651$
$\beta = .00597$, which yields a -0.5% error for component c) above.

The last uncertainty component, d), concerns the reduction of core average β to obtain β_{eff} by using the importance factor. Since this reduction is computed to be about 3 to 4%, an error of 10% in this computation would lead to an error in β_{eff} of less than 0.5%.

The sum of the errors for these four factors for CASMO is as follows:

$$1.3\%(a+b) + 0.5\%(c) + 0.5\%(d) = 2.3\%$$

For conservatism the realibility factor for delayed neutron parameters is set at 4%.

3.8 Effective Neutron Lifetime

An argument similar to the delayed neutron parameter argument is applied to the determination of the effective neutron lifetime (ℓ^*) uncertainty. The uncertainty components which go into the calculation of ℓ^* are as follows:

a) Experimental values of microscopic cross sections;
b) Calculation of the spatial nuclide inventory; and
c) Calculation of the core average effective neutron lifetime, ℓ^*, as a flux weighted average over the spatial nuclide inventory which includes the effects of leakages.

Uncertainties for components a) and b) are assumed to be the same as described for the calculation of β_{eff}, that is, 1% uncertainty in the experimental determination of nuclear cross section and .3% uncertainty in the determination of the spatial nuclide inventory for CASMO. The core average neutron lifetime depends on flux weighting of local absorption lifetimes ℓ^*. If a conservative estimate of the error in regional power sharing (7%) is used in determining the impact on the core average lifetime (ℓ^*), the error in lifetime is on the order of 1.0%. Combining all of these uncertainties linearily results in a total uncertainty of 2.3% for CASMO. Therefore, a 4% reliability factor will be applied to the neutron lifetime calculation when applied to safety related calculations.

TABLE 3.6.1

FULL POWER STATEPOINTS

Cycle	Exposure (GWD/MTU)	% of Full Power	% Rod Density	K_{eff}	Tip Trace Used
7	0.482	100.	6.61	.9908	*
	0.783	100.	6.61	.9904	*
	1.265	100.	6.89	.9895	
	1.434	100.	6.89	.9893	*
	1.851	100.	8.82	.9884	
	2.152	100.	8.82	.9886	*
	2.456	100.	8.68	.9879	
	2.702	100.	8.82	.9883	*
	3.442	100.	7.58	.9897	*
	4.109	100.	7.02	.9883	*
	4.928	100.	3.99	.9900	*
	5.169	100.	3.72	.9900	
	5.466	100.	2.62	.9899	*
	6.105	100.	1.79	.9902	*
	6.345	100.	0.0	.9909	
	6.954	91.	0.0	.9902	
	7.636	78.	0.0	.9909	*
8	0.156	100.	4.68	.9919	*
	0.464	100.	4.82	.9930	*
	0.855	100.	2.89	.9932	*
	1.537	100.	2.89	.9926	*
	2.119	100.	2.48	.9918	
	2.682	100.	2.48	.9914	*
	3.220	99.	2.48	.9906	
	3.568	97.	4.41	.9905	*
	4.306	100.	1.79	.9921	*
	4.651	100.	0.0	.9924	*
	5.565	90.	0.0	.9908	*
	6.104	83.	0.0	.9924	*

TABLE 3.6.1
(continued)

FULL POWER STATEPOINTS

Cycle	Exposure (GWD/MTU)	% of Full Power	% Rod Density	K_{eff}	Tip Trace Used
9	0.384	100.	6.47	.9920	*
	0.738	100.	6.47	.9916	*
	1.124	100.	6.34	.9917	*
	1.782	100.	5.10	.9918	*
	2.327	100.	4.96	.9915	*
	2.570	100.	4.96	.9917	
	2.614	100.	4.96	.9915	*
	3.737	100.	2.34	.9929	
	4.140	99.	1.93	.9935	*
	4.496	99.	0.0	.9939	
	4.839	95.	0.0	.9937	*
	5.570	83.	0.0	.9938	*
	6.163	72.	0.0	.9949	*
	6.555	64.	0.0	.9960	*
10	0.444	100.	3.75	.9946	*
	0.905	100.	3.75	.9938	*
	1.489	100.	3.20	.9927	*
	2.148	100.	3.17	.9920	*
	2.814	100.	3.86	.9915	*
	3.211	100.	3.72	.9917	*
	3.667	100.	2.89	.9920	*
	3.955	100.	2.89	.9925	*
	4.096	100.	2.62	.9926	
	4.507	100.	1.93	.9929	*
	5.886	80.	0.0	.9932	*
	6.051	77.	0.0	.9938	*
	6.371	71.	0.0	.9943	*

TABLE 3.6.2

Axial Power Distribution Comparison
CASMO / NDH to TIP Scans

Cycle	Location	Rod	Peak to Average TIP	Calculated	% Difference
10	44-29	Out	1.256	1.317	-4.8
10	20-37	Out	1.216	1.261	-3.7
9	20-13	Out	1.498	1.539	-2.8
7	44-29	Out	1.418	1.446	-2.0
7	44-29	Out	1.624	1.640	-1.0
8	12-13	Out	1.310	1.313	-.2
8	44-29	Out	1.638	1.632	.3
10	28-45	Out	1.539	1.524	1.0
8	20-13	Out	1.440	1.416	1.7
9	28-45	Out	1.554	1.516	2.4
9	29-29	Out	1.397	1.350	3.4
7	20-25	Out	1.399	1.339	4.4
9	28-13	Out	1.408	1.303	7.4
7	12-21	In	1.499	1.585	-5.8
7	28-21	In	1.307	1.353	-3.5
7	20-37	In	1.409	1.435	-1.8
10	20-37	In	1.329	1.334	-.4
8	12-29	In	1.597	1.576	1.3
10	12-29	In	1.554	1.487	4.3

TABLE 3.6.3

Axial Power Distribution Comparisons
CASMO/NDH to Gamma Scans

Peak to Average

Cycle	Location	Rod	Gamma Scan	Calculated	% Difference
8	25-42	Out	1.326	1.378	-3.95
8	13-30	Out	1.255	1.277	-1.75
8	41-26	Out	1.351	1.374	-1.72
8	29-22	Out	1.293	1.348	-4.26
8	21-16	Out	1.229	1.257	-2.32
8	39-14	Out	1.302	1.350	-3.71
8	41-10	Out	1.360	1.385	-1.86
8	39-06	Out	1.478	1.477	0.04
9	15-40	Out	1.299	1.300	-0.08
9	13-38	Out	1.297	1.301	-0.28
9	39-34	Out	1.419	1.416	-0.17
9	27-26	Out	1.522	1.510	0.74
9	33-22	Out	1.343	1.329	1.08
9	31-20	Out	1.373	1.335	2.77
9	15-16	Out	1.317	1.341	-1.81
9	29-14	Out	1.419	1.448	-2.05
9	39-14	Out	1.337	1.415	-5.83
9	27-10	Out	1.444	1.477	-2.32
9	41-10	Out	1.505	1.491	0.88
9	39-08	Out	1.550	1.546	0.24
9	33-06	Out	1.563	1.531	2.05
9	29-04	Out	1.646	1.664	-1.10
9	31-02	Out	1.898	1.746	8.03

TABLE 3.6.4

Radial Power Distribution Comparisons
CASMO/NDH to TIP Trace

Cycle	Location	Exposure	TIP	Calculated	% Difference
8	28-37	3.568	1.071	1.059	-1.1
7	28-37	6.105	1.124	1.083	-3.0
10	28-29	3.955	1.120	1.061	-5.2
8	20-37	3.568	1.068	1.037	-2.9
8	28-29	4.651	1.035	1.043	-.8
10	12-21	3.211	1.055	1.066	-1.0
9	36-13	2.327	1.118	1.061	5.1
7	12-21	.482	1.111	1.091	1.7
9	12-37	1.124	1.011	1.031	-2.1
10	36-13	3.955	1.064	1.070	-.5
10	36-37	.905	1.169	1.136	2.8
7	20-13	3.442	1.084	1.089	-.5
9	20-13	.384	1.117	1.080	3.3
7	12-21	4.109	1.058	1.070	-1.2
8	20-29	.156	1.135	1.133	-.2
10	28-29	2.148	1.203	1.165	3.1
10	28-29	2.814	1.219	1.178	3.3
10	20-29	3.211	1.133	1.117	1.4
8	20-29	2.682	1.154	1.129	2.2
8	36-37	4.651	1.060	1.060	-.1
7	28-31	5.466	1.070	1.099	-2.7
9	28-21	4.140	1.038	1.032	.5
8	20-21	2.682	1.185	1.146	3.3
10	12-29	3.955	1.118	1.039	7.0
7	20-29	4.109	1.076	1.098	-2.1
7	28-21	2.152	1.093	1.089	.4
8	20-25	3.568	1.032	1.061	-2.8
8	36-29	.156	1.134	1.139	-.4
9	20-45	2.327	1.038	1.083	-4.3
8	28-37	.464	1.103	1.088	1.3

TABLE 3.6.5

Radial Power Distribution Comparisons
CASMO/NDH to Gamma Scan

Cycle	Location	Gamma Scan	Calculated	% Difference
8	25-42	1.087	1.092	-0.53
	13-30	1.065	1.101	-3.40
	41-26	1.147	1.091	4.90
	29-22	1.206	1.194	0.97
	21-16	1.269	1.269	-0.06
	39-14	.978	.979	-0.06
	41-10	.512	.498	2.68
	39-06	.289	.284	1.74
9	15-40	1.327	1.334	-0.50
	13-38	1.321	1.334	-1.00
	39-34	1.083	1.078	0.42
	27-26	1.071	1.058	1.27
	33-22	1.117	1.150	-2.97
	31-20	1.132	1.156	-2.18
	15-16	.972	1.029	-5.85
	29-14	1.090	1.079	1.00
	39-14	1.286	1.294	-0.63
	27-10	1.014	.996	1.75
	41-10	.508	.485	4.37
	39-08	.412	.406	1.66
	33-06	.523	.511	2.25
	29-04	.527	.535	-1.55
	31-02	.216	.224	-4.10

TABLE 3.6.6

Nodal Power Distribution Standard Deviations
In 20 Axial Planes

Planes	Planar Standard Deviation
3	.052
4	.052
5	.048
6	.044
7	.045
8	.047
9	.044
10	.048
11	.047
12	.051
13	.042
14	.043
15	.040
16	.042
17	.032
18	.038
19	.030
20	.029
21	.030
22	.029

Plane 24 = Top

Figure 3.6.1

Measured and Calculated Integrated Detector Responses

BOC 7

0.783 GWD/MTU , A Sequence

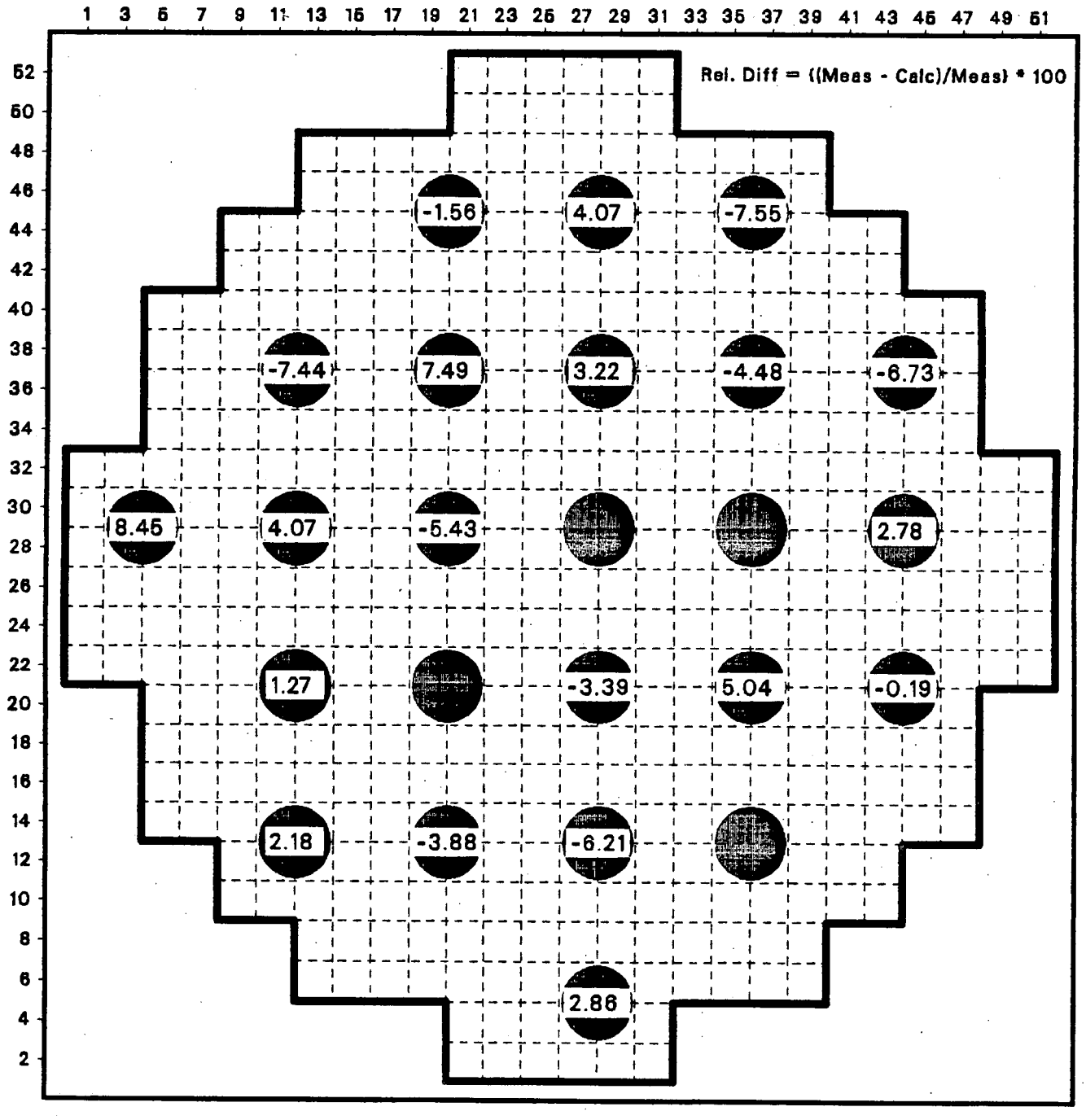

Figure 3.6.2

Measured and Calculated Detector Response

BOC Cycle 7, Trace 28-45

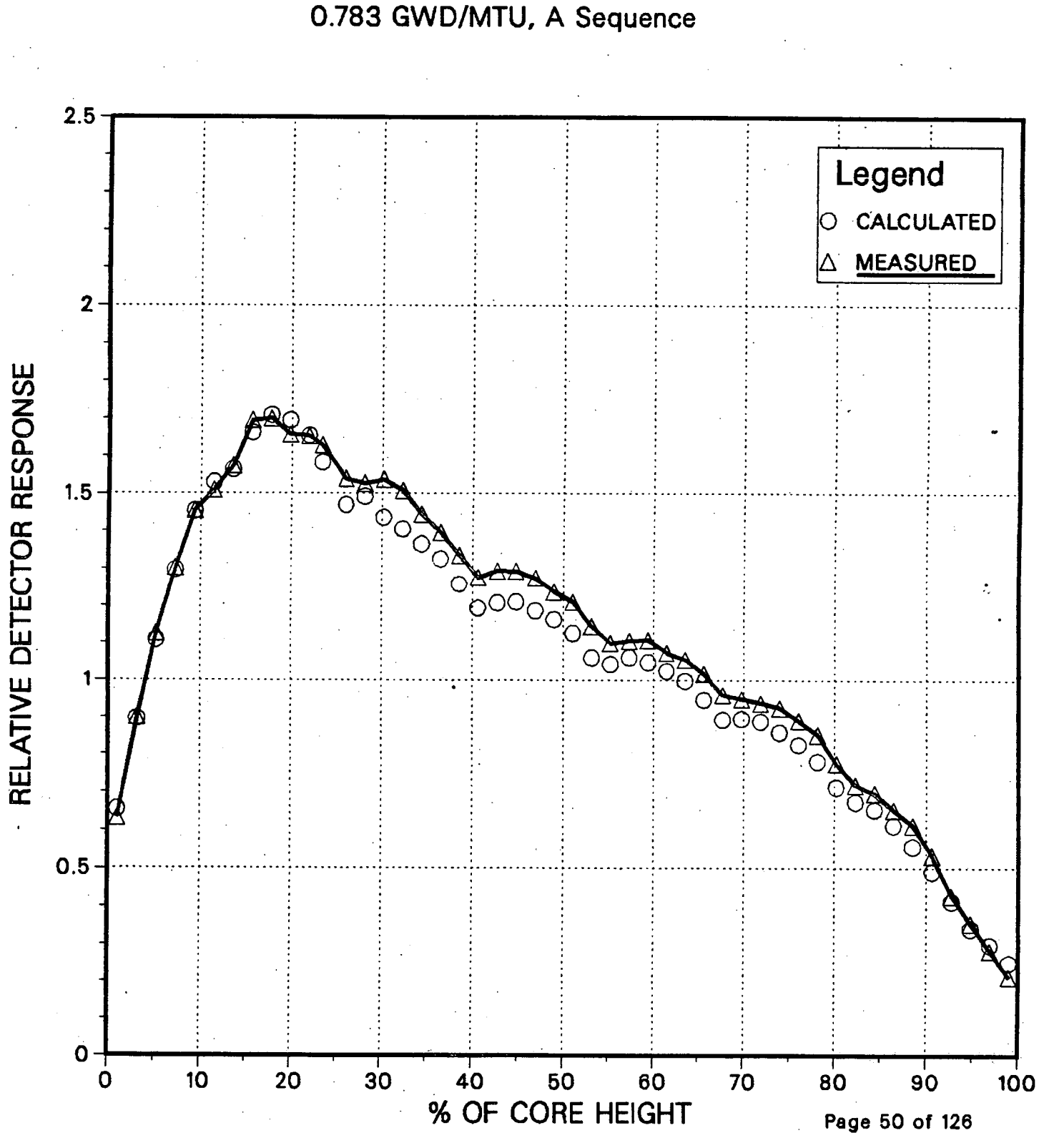

Figure 3.6.3

Measured and Calculated Detector Response

BOC Cycle 7, Trace 12-29

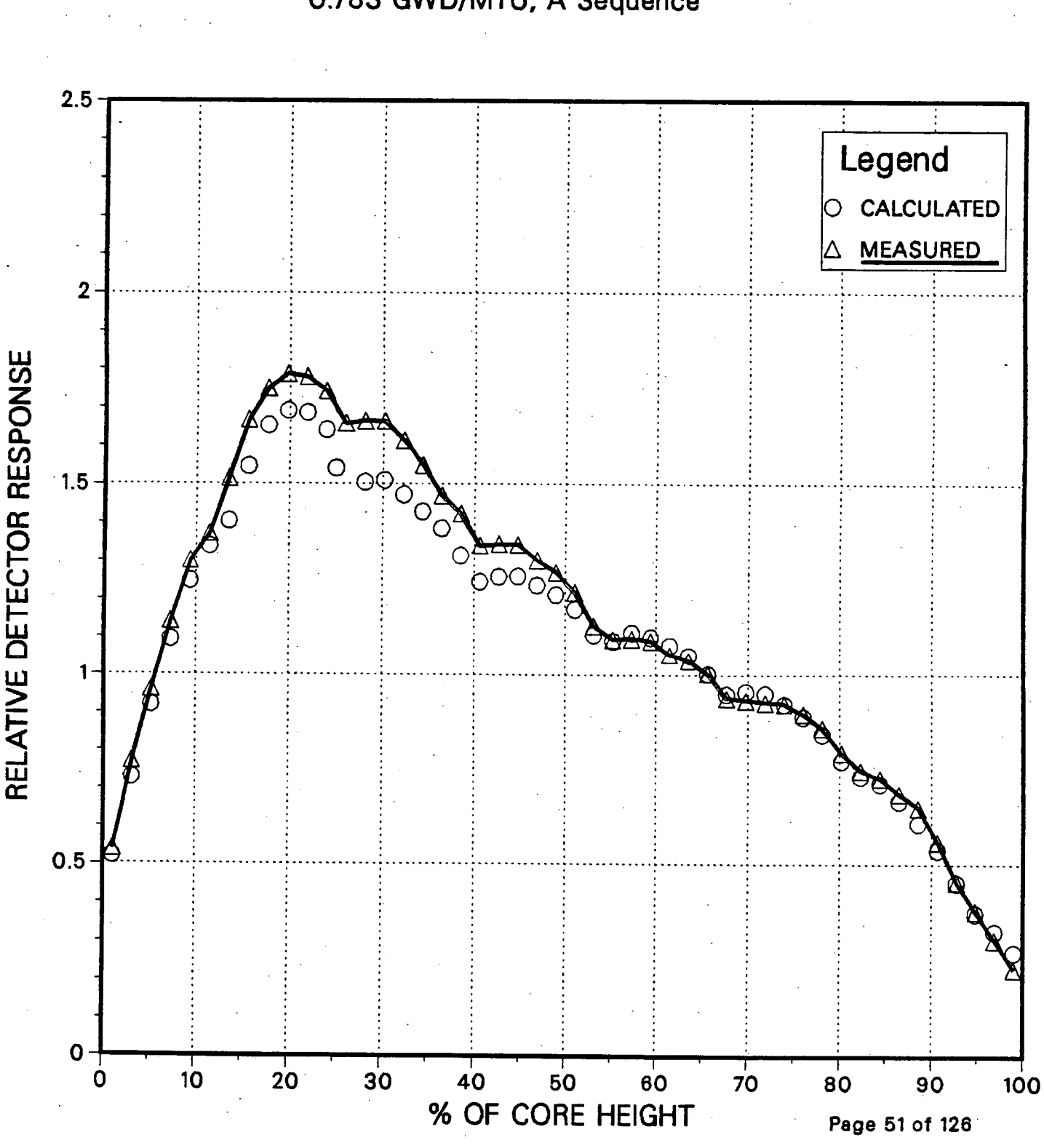

Figure 3.6.4

Measured and Calculated Integrated Detector Responses

MOC 7

2.702 GWD/MTU , B Sequence

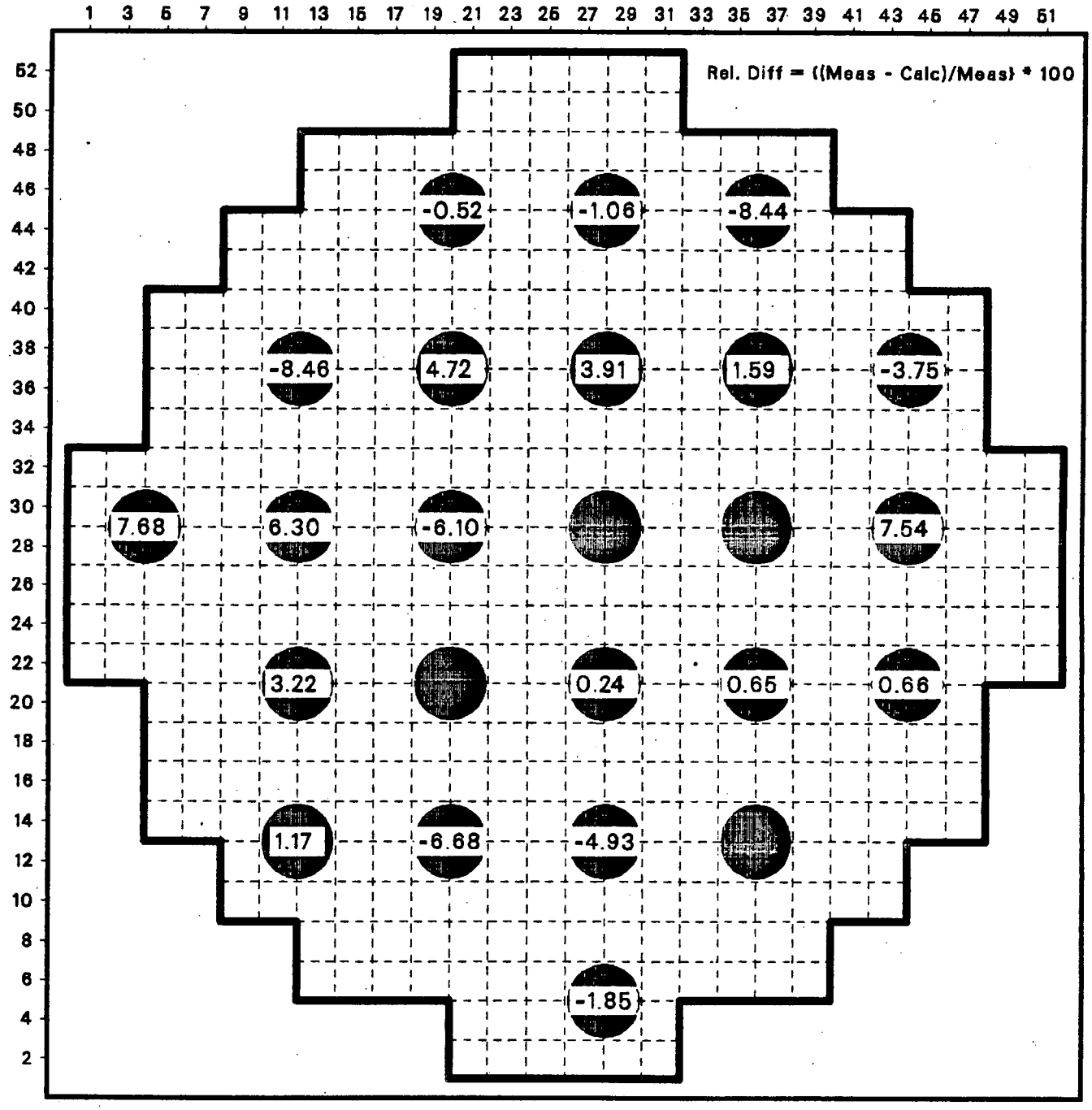

Figure 3.6.5

Measured and Calculated Detector Response

MOC Cycle 7, Trace 12-21

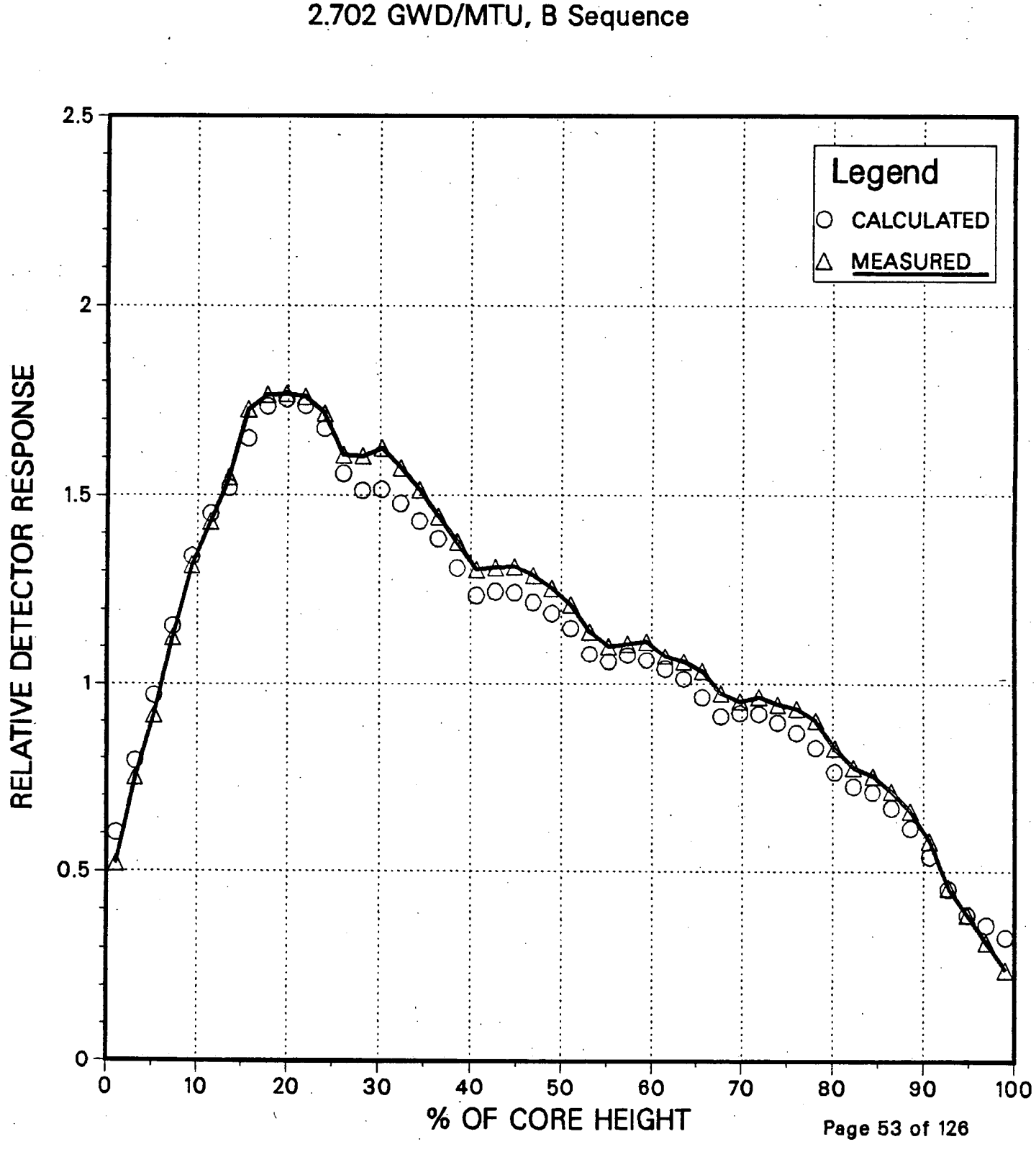

Figure 3.6.6

Measured and Calculated Detector Response

MOC Cycle 7, Trace 28-37

2.702 GWD/MTU, B Sequence

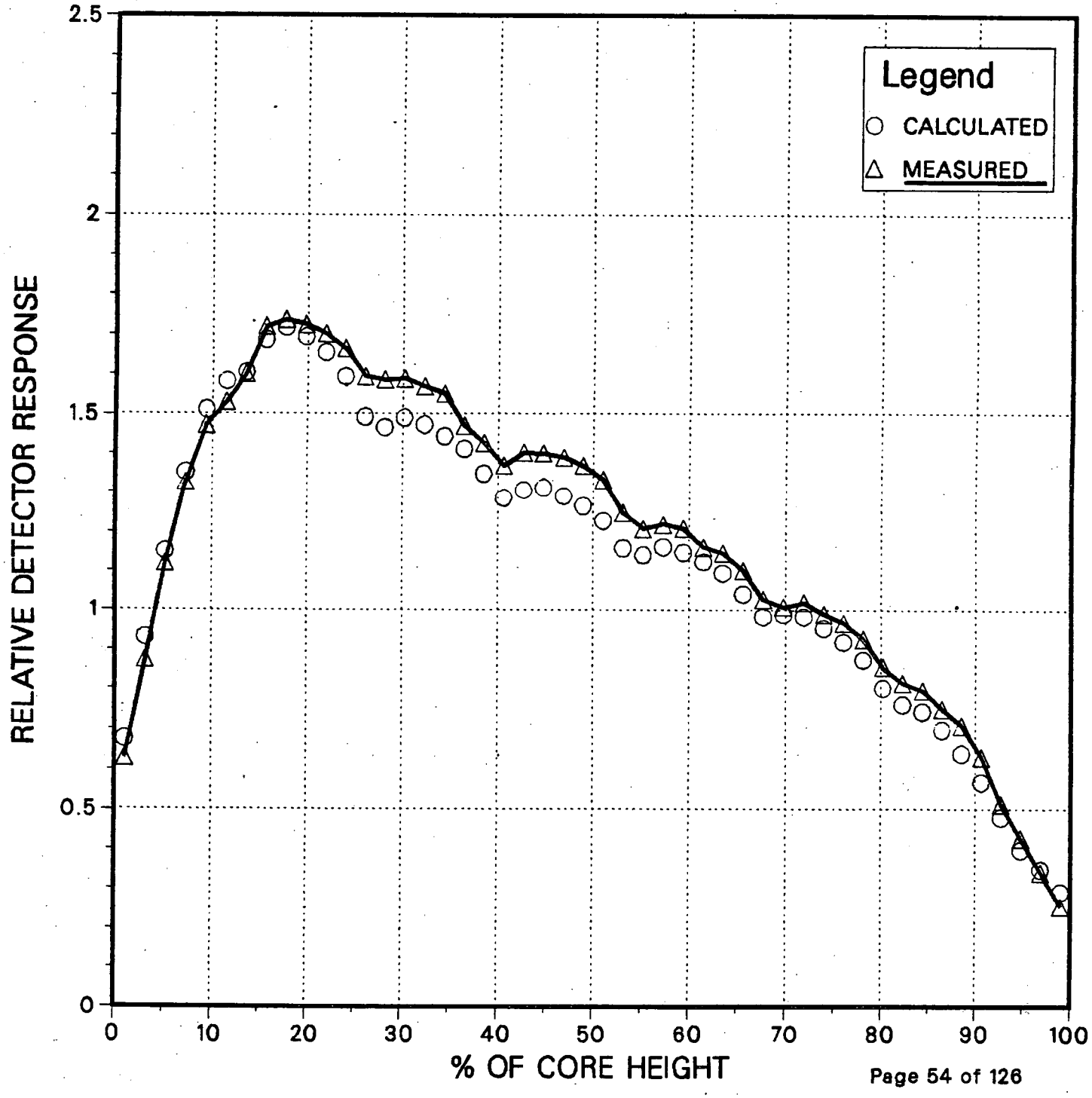

Figure 3.6.7

Measured and Calculated Integrated Detector Responses

EOC 7

6.105 GWD/MTU , ARO

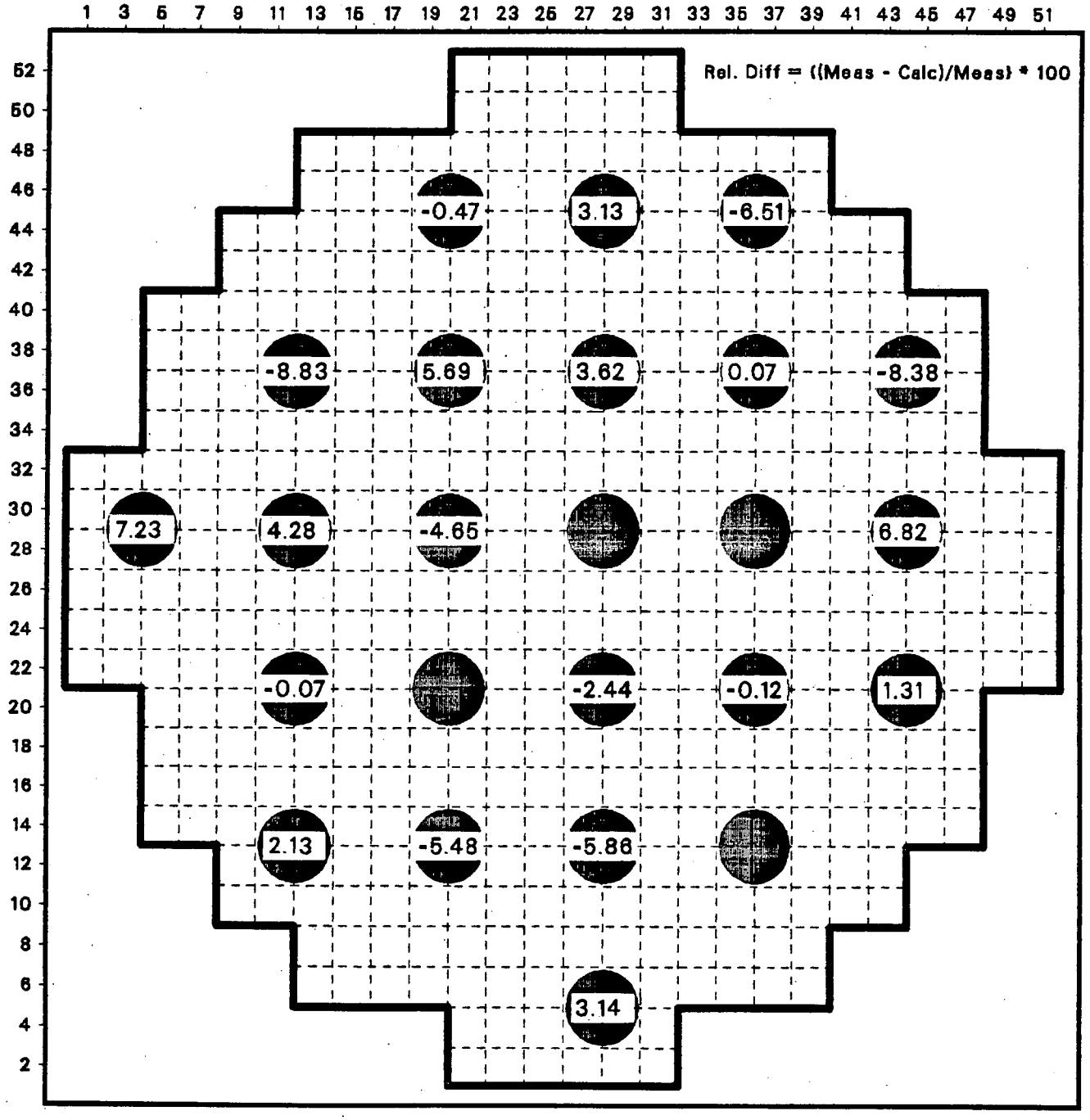

Figure 3.6.8

Measured and Calculated Detector Response

EOC Cycle 7, Trace 12-29

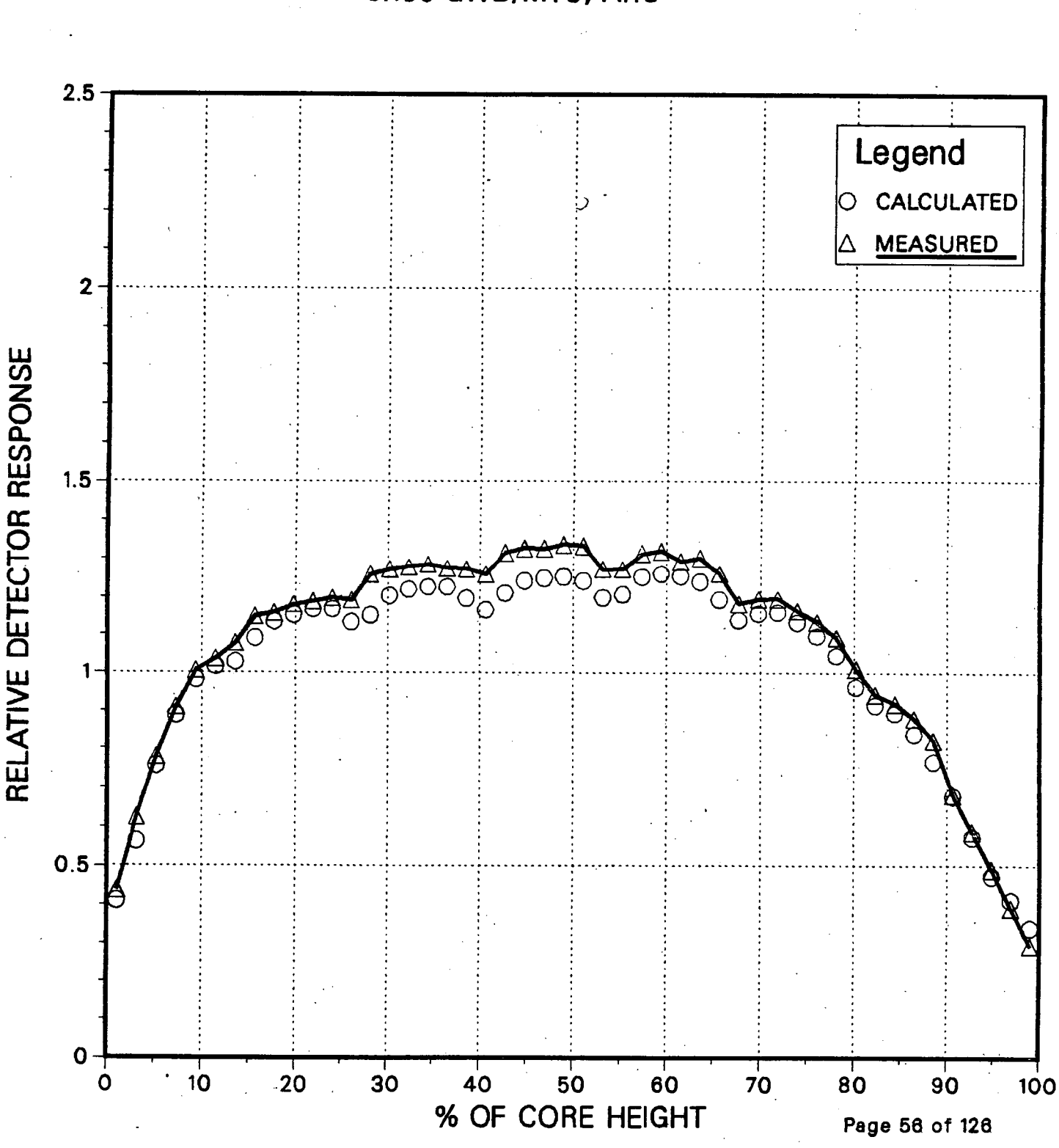

Figure 3.6.9

Measured and Calculated Detector Response

EOC Cycle 7, Trace 28-37

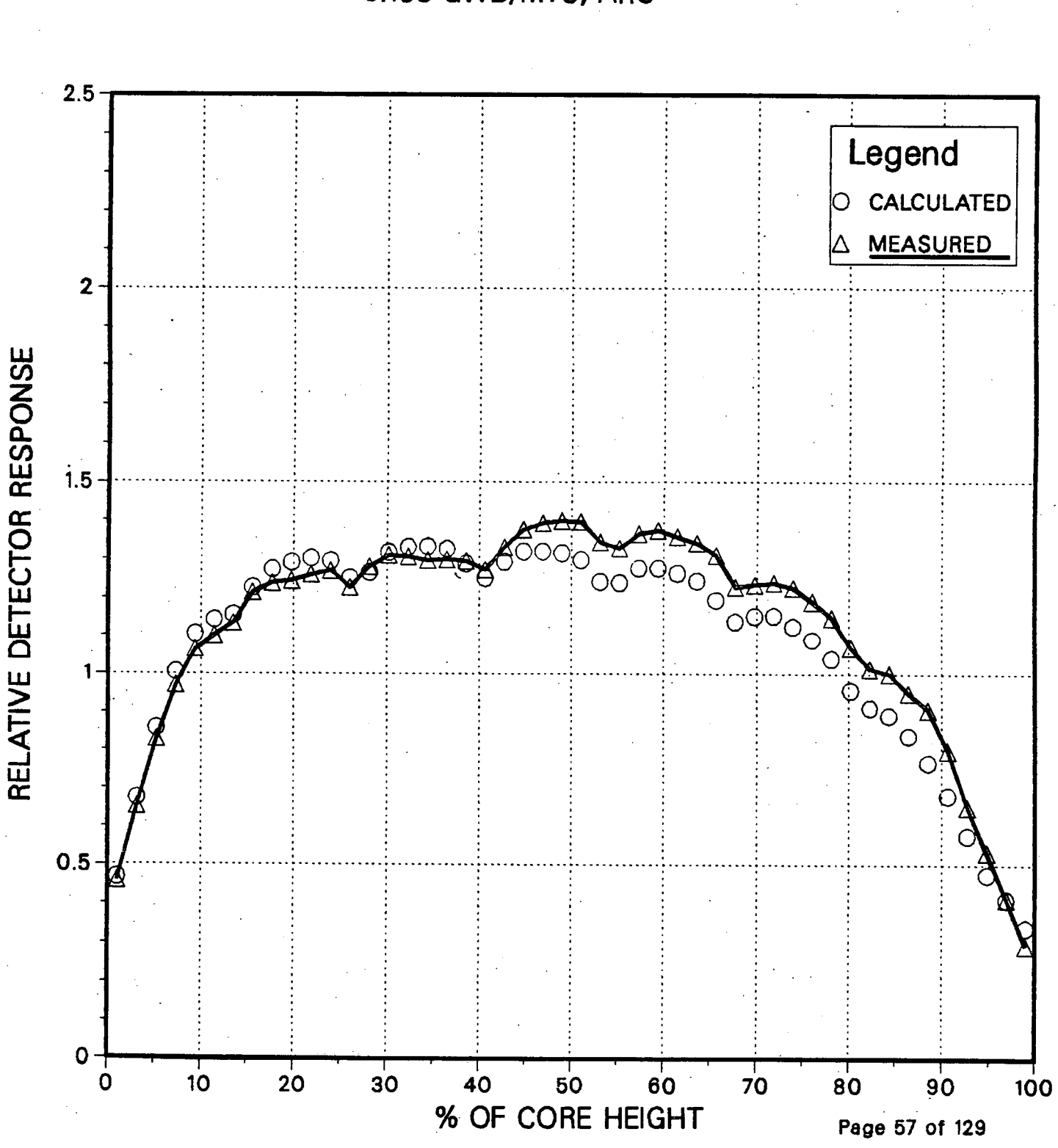

Figure 3.6.10

Measured and Calculated Integrated Detector Responses

BOC 8

0.855 GWD/MTU , A Sequence

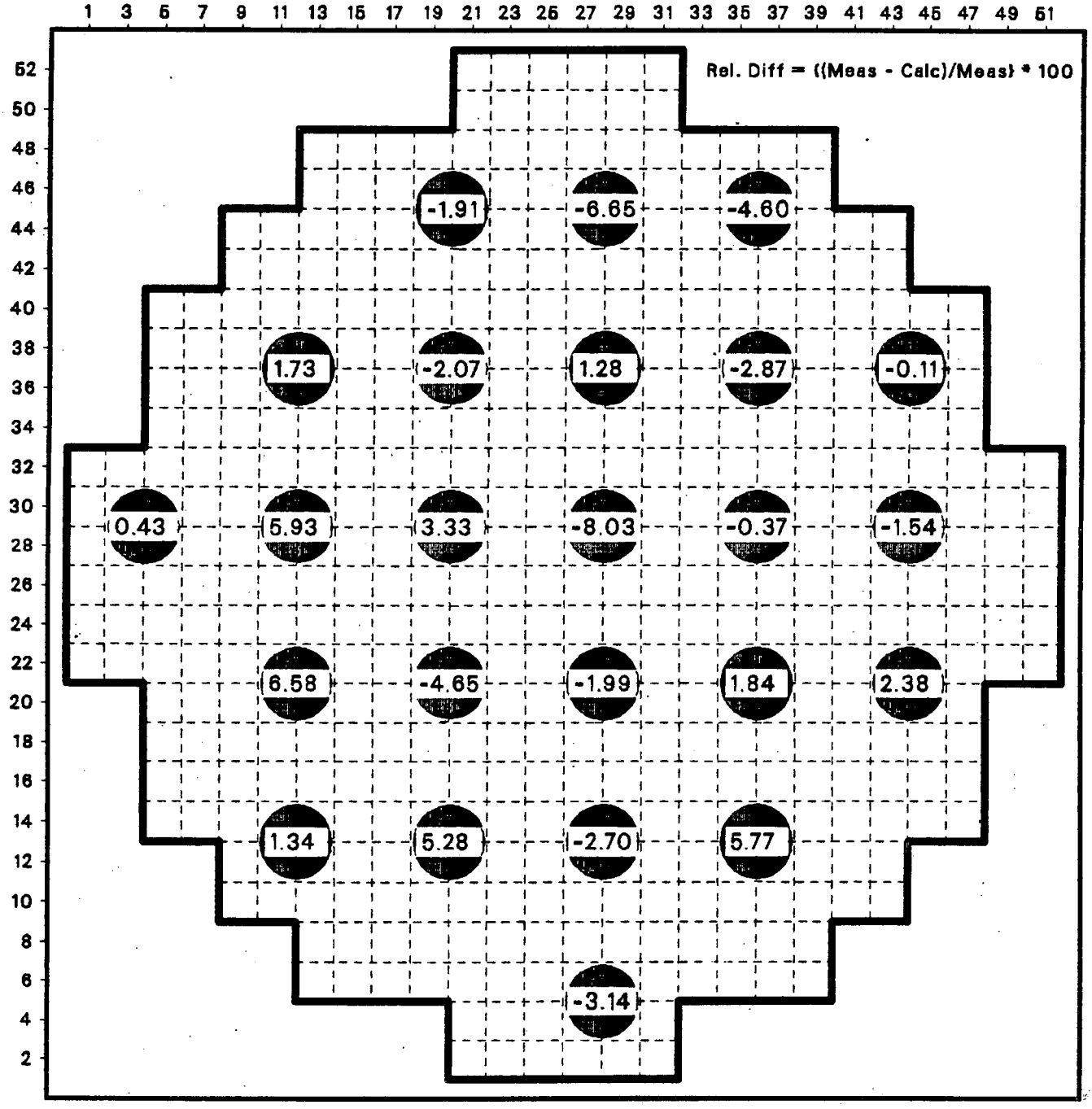

Figure 3.6.11

Measured and Calculated Detector Response

BOC Cycle 8, Trace 20-29

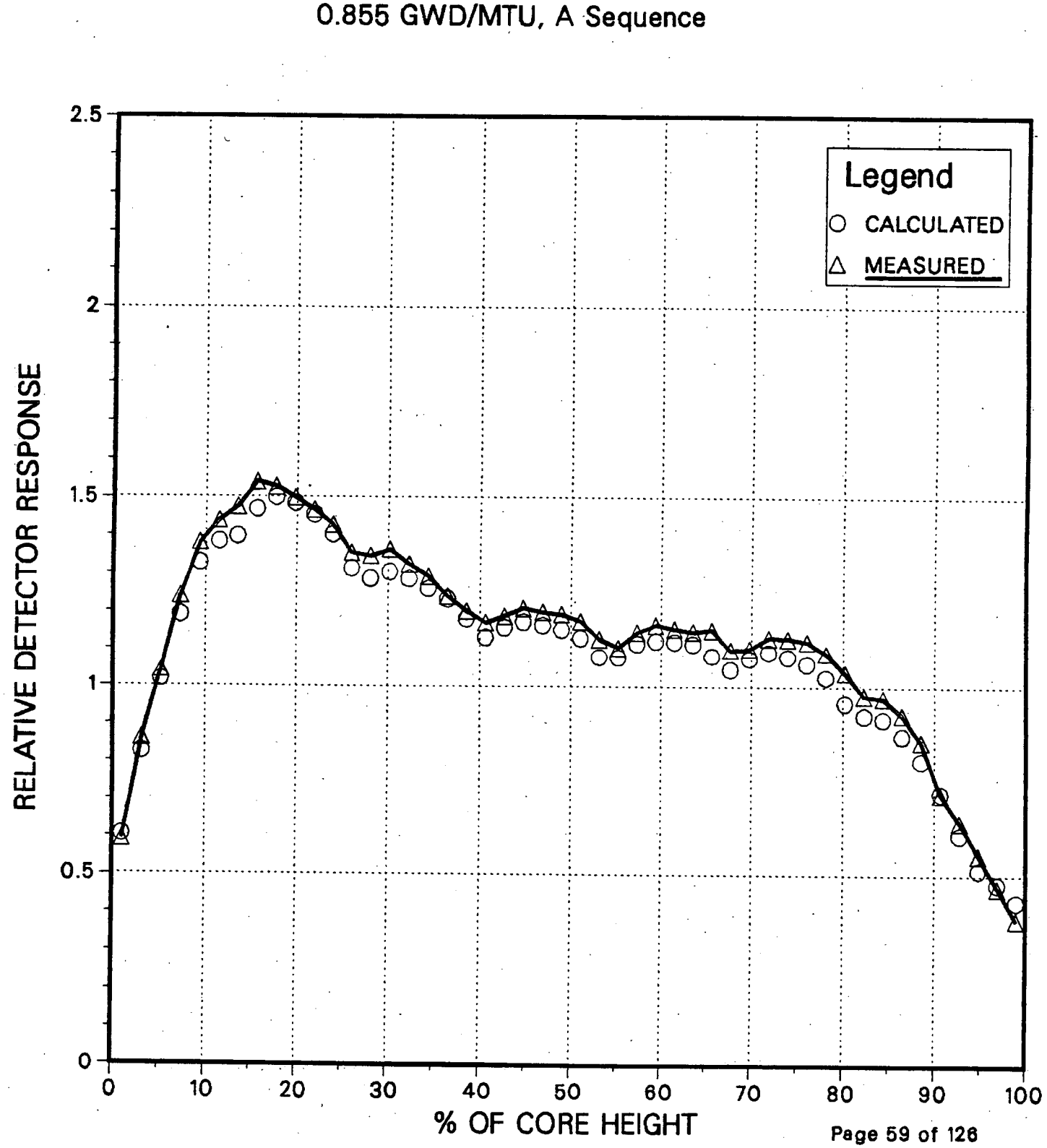

Figure 3.6.12

Measured and Calculated Detector Response

BOC Cycle 8, Trace 20-21

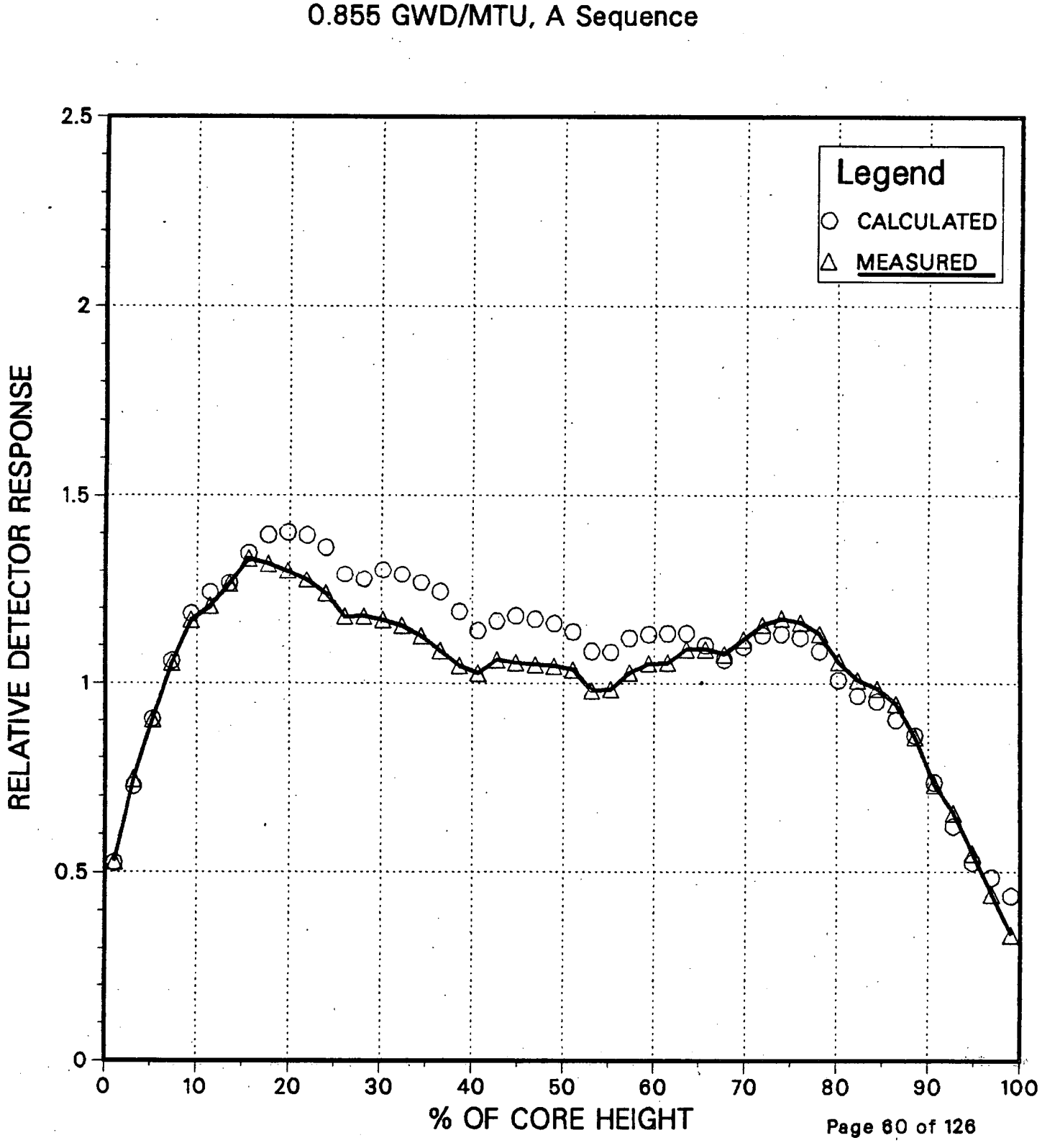

Figure 3.6.13

Measured and Calculated Integrated Detector Responses

MOC 8

2.682 GWD/MTU , B Sequence

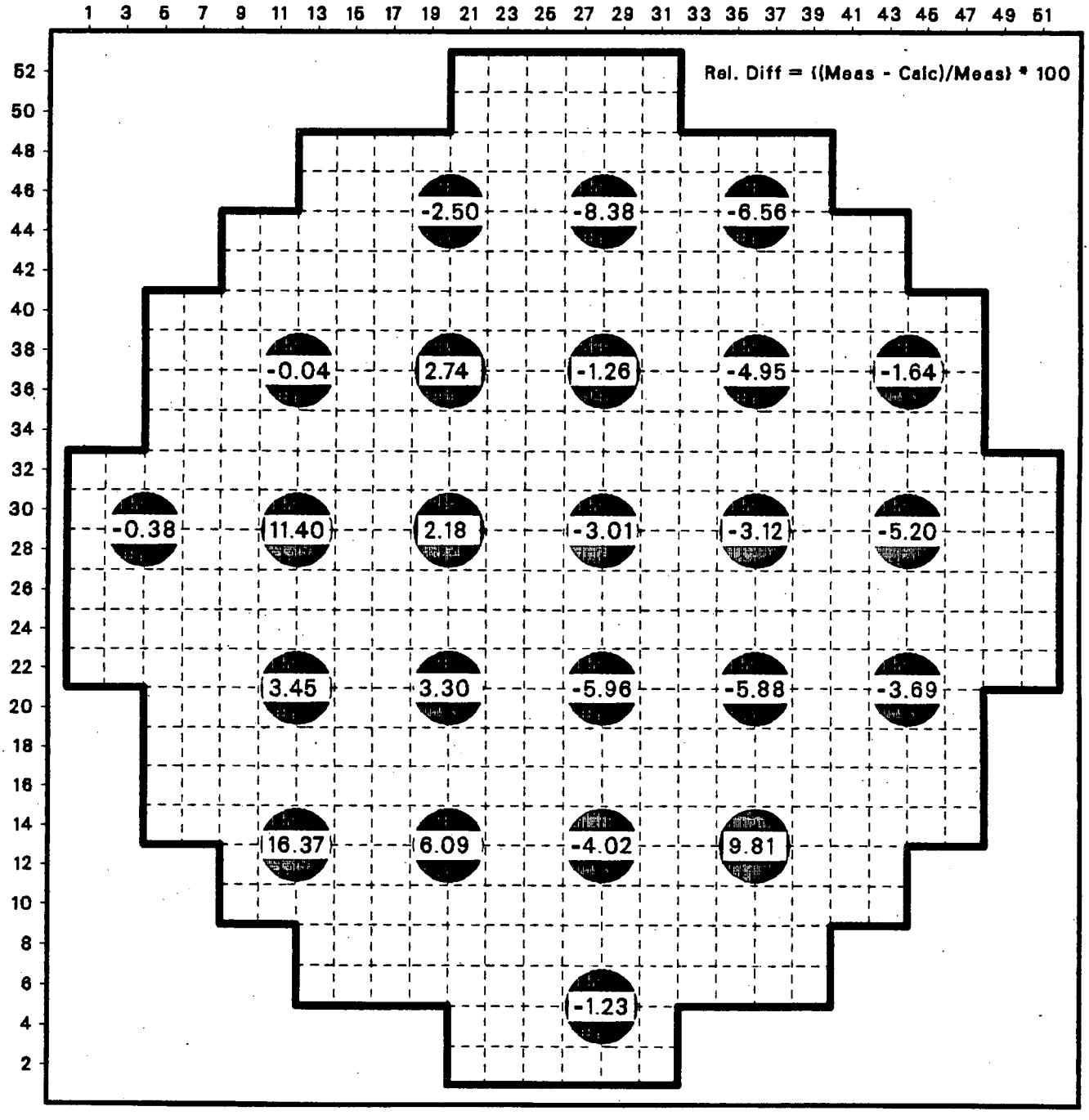

Figure 3.6.14

Measured and Calculated Detector Response

MOC Cycle 8, Trace 36-19

2.682 GWD/MTU, B Sequence

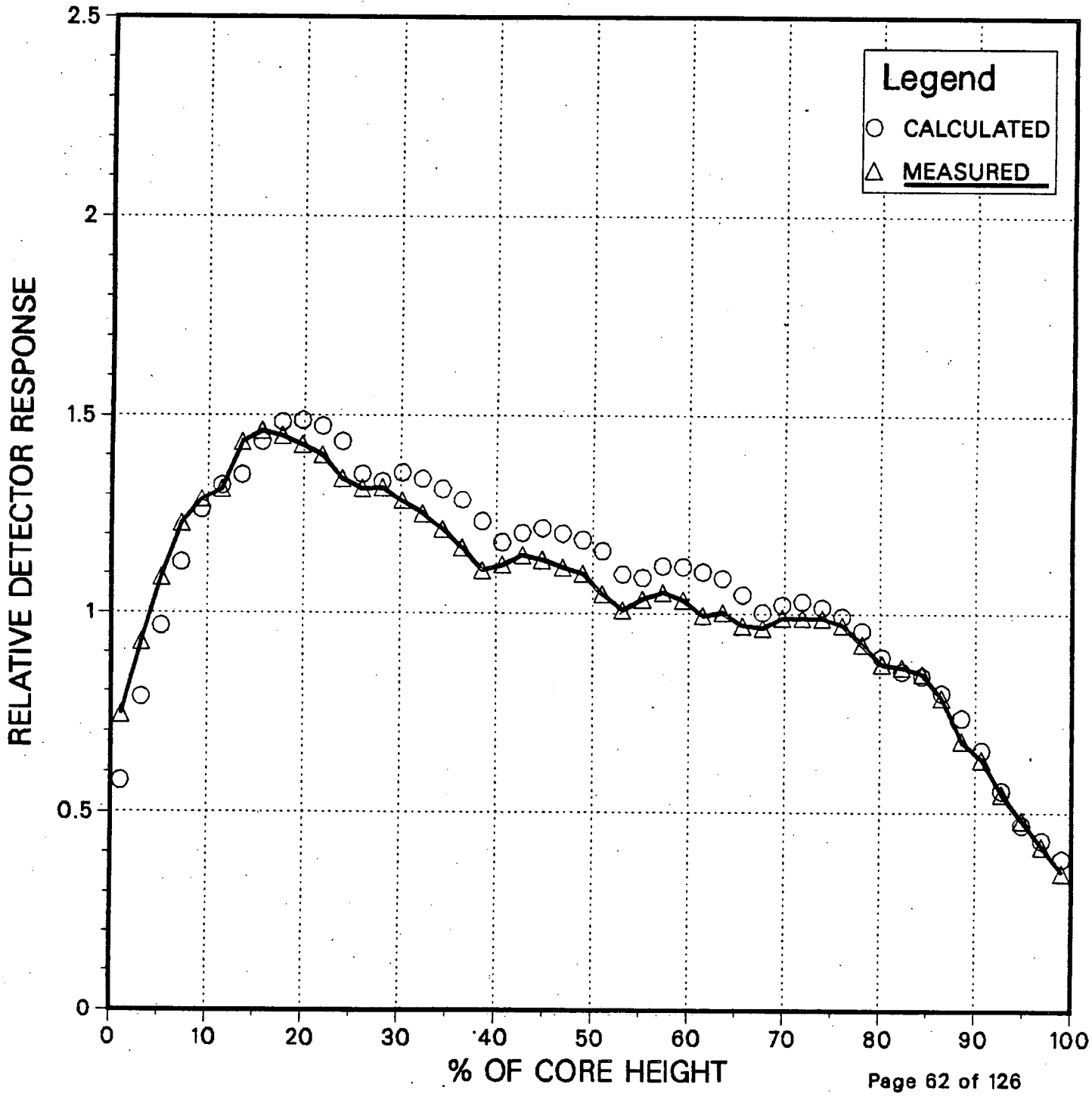

Figure 3.6.15

Measured and Calculated Detector Response

MOC Cycle 8, Trace 20-21

2.682 GWD/MTU, B Sequence

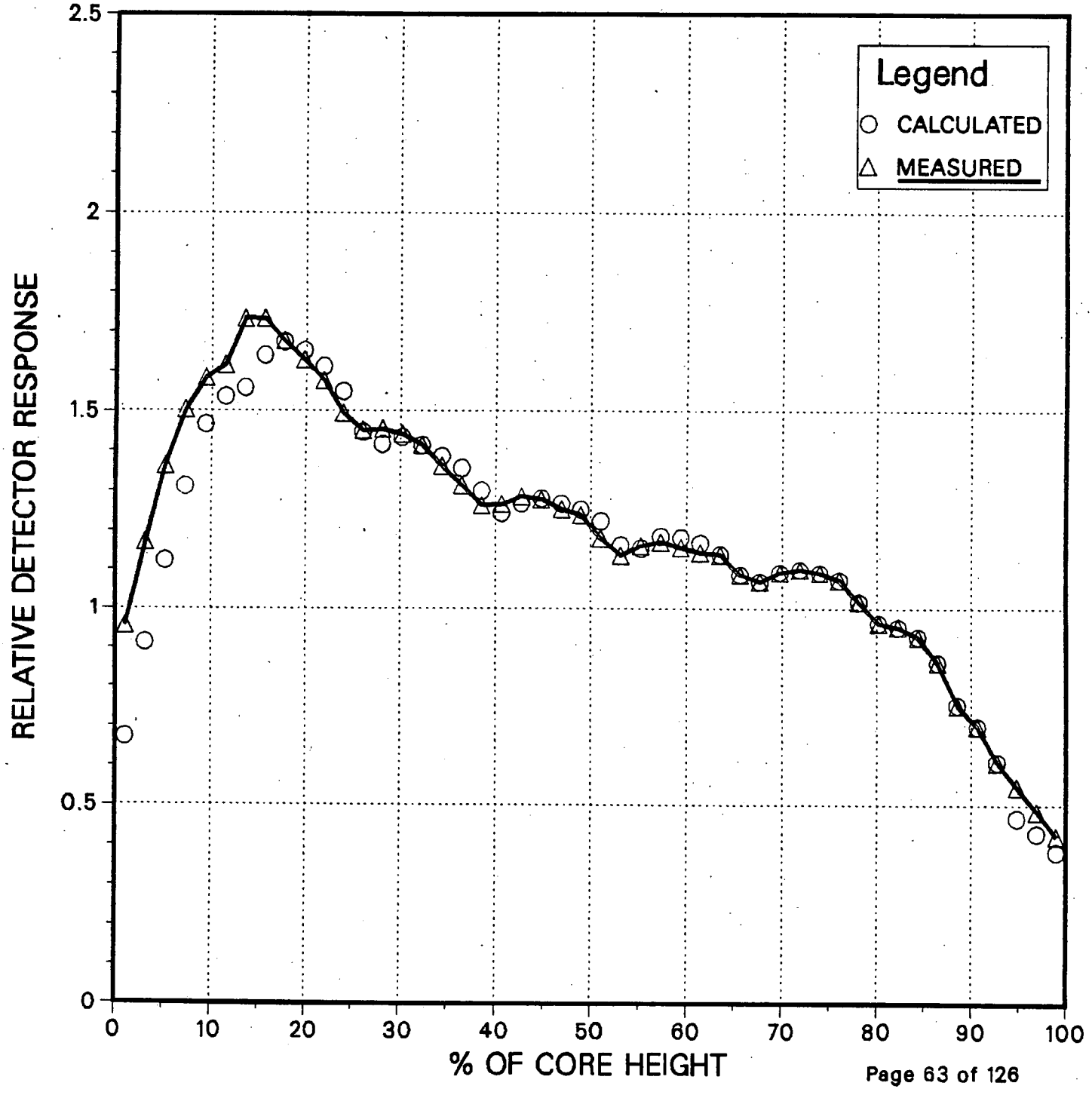

Figure 3.6.16

Measured and Calculated Integrated Detector Responses

EOC 8

4.651 GWD/MTU , ARO

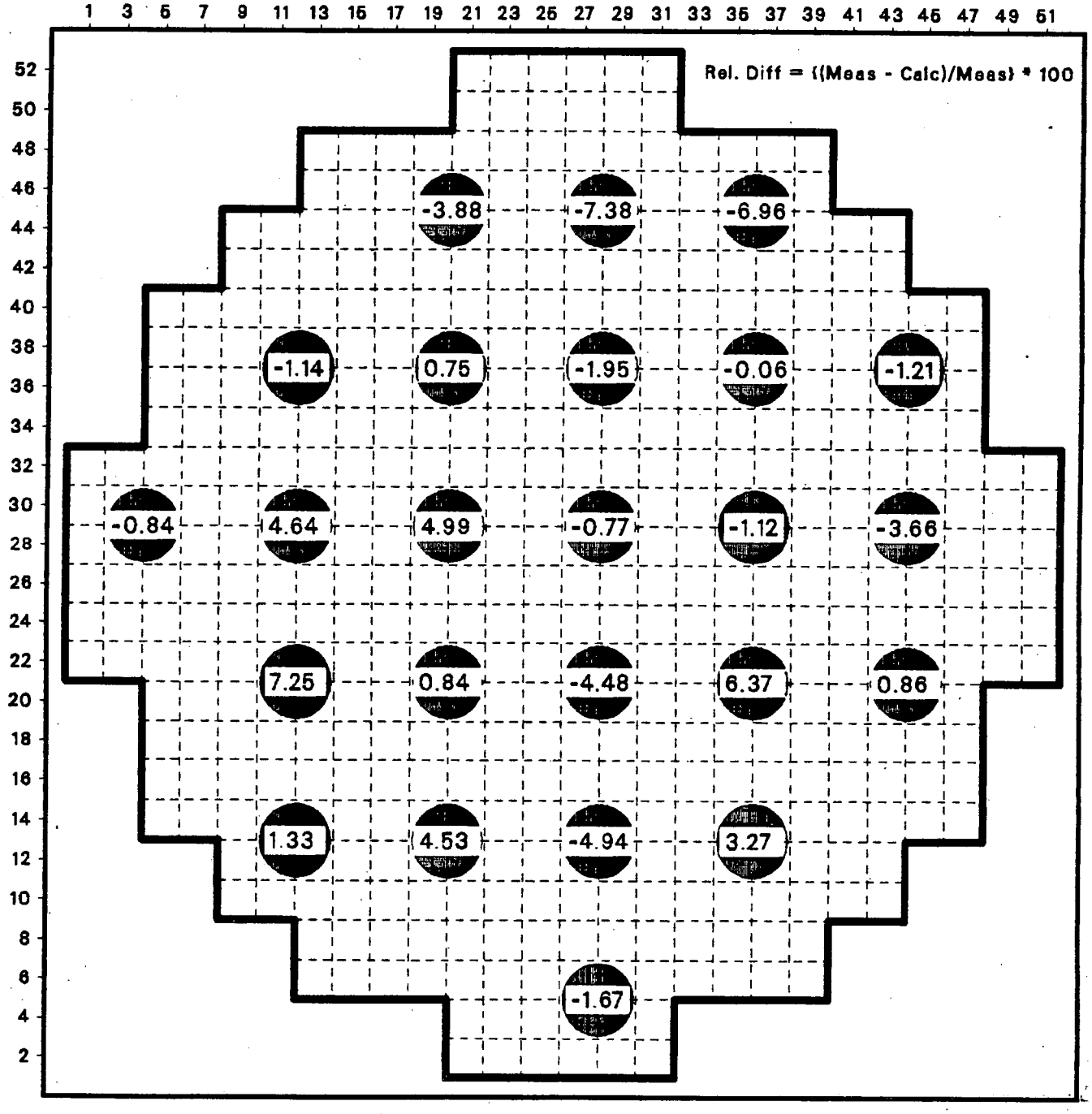

Figure 3.6.17

Measured and Calculated Detector Response

EOC Cycle 8, Trace 20-13

4.651 GWD/MTU, ARO

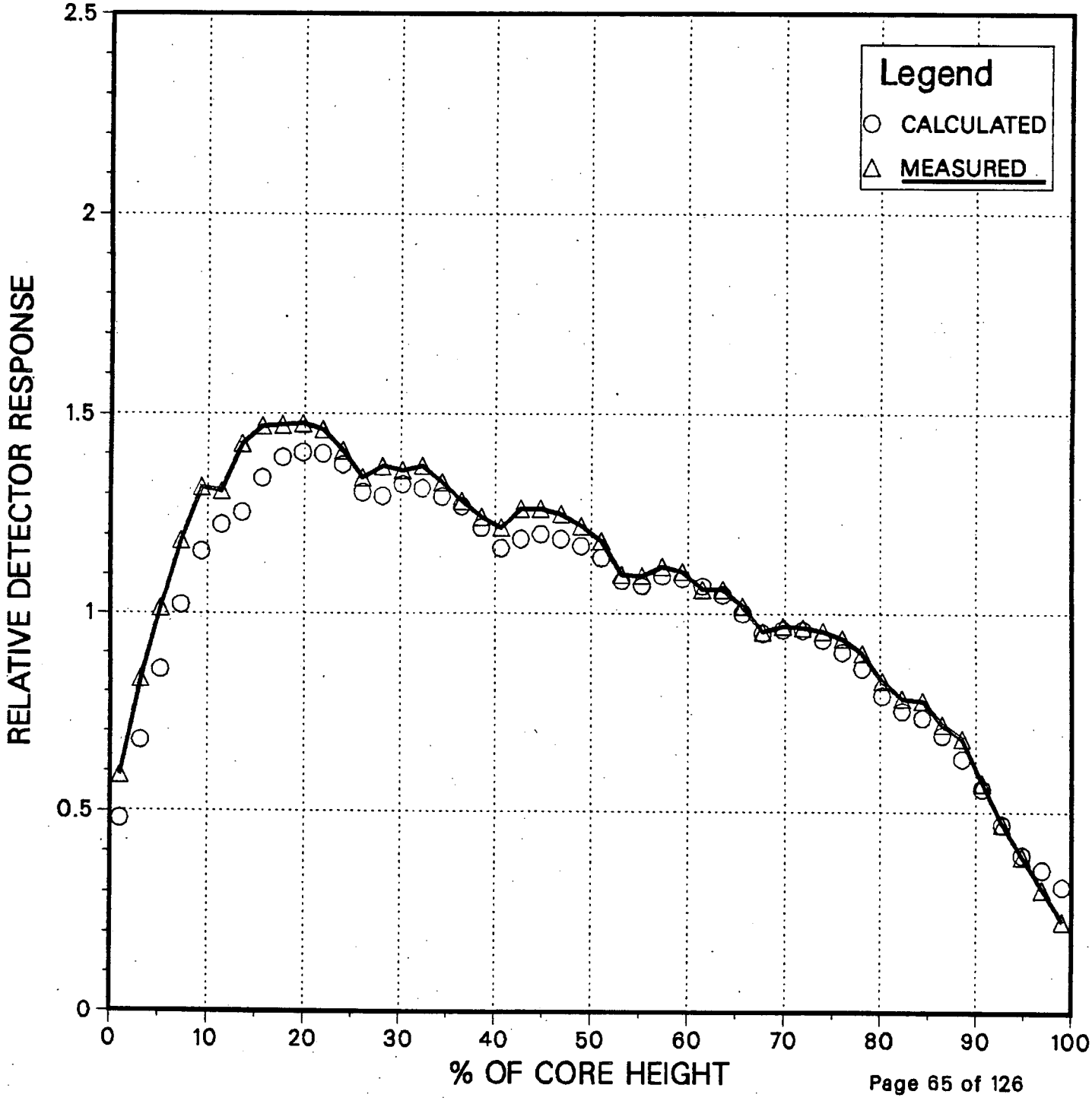

Figure 3.6.18

Measured and Calculated Detector Response

EOC Cycle 8, Trace 44-29

4.651 GWD/MTU, ARO

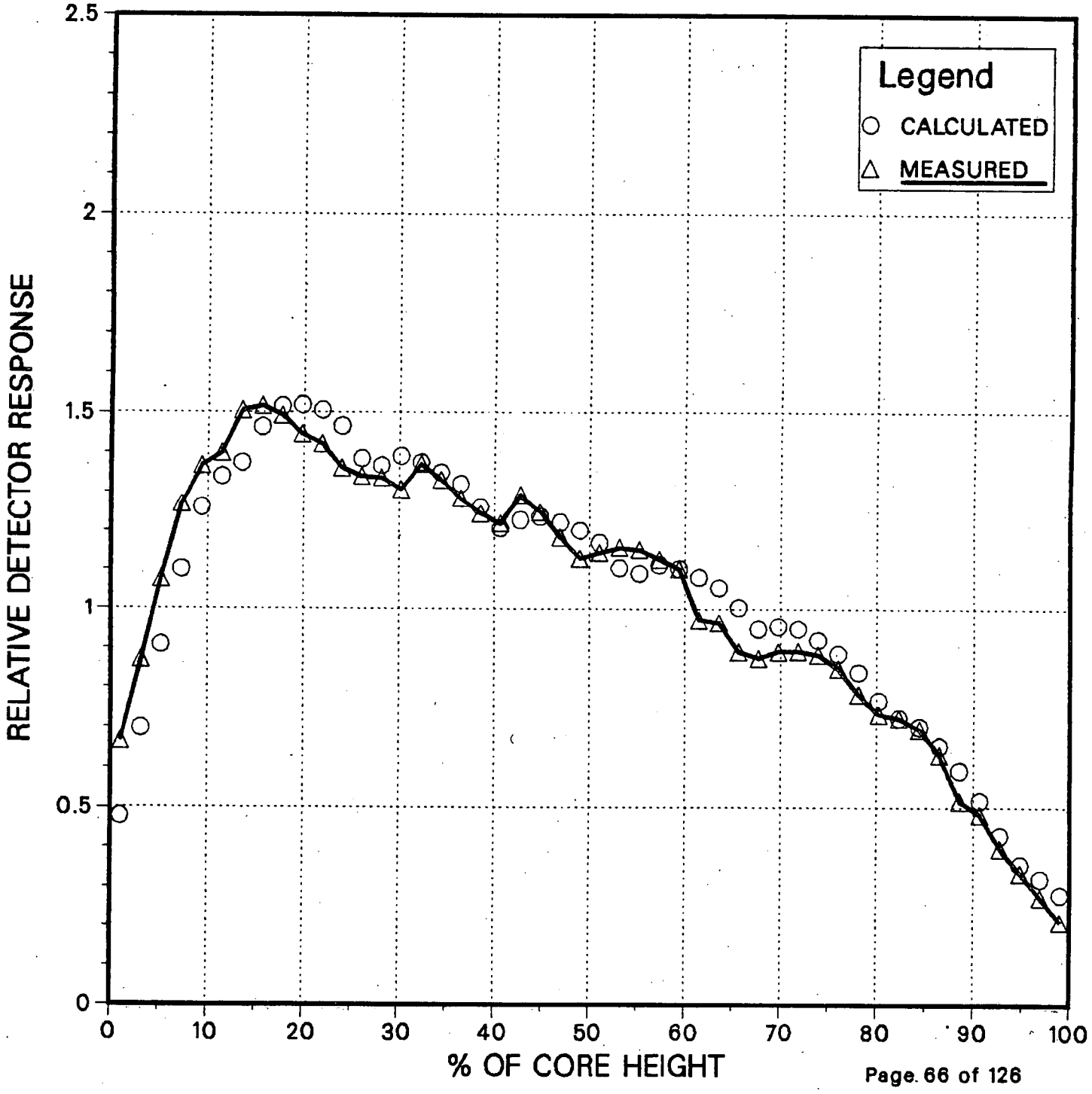

Figure 3.6.19

Measured and Calculated Integrated Detector Responses

BOC 9

1.782 GWD/MTU , B Sequence

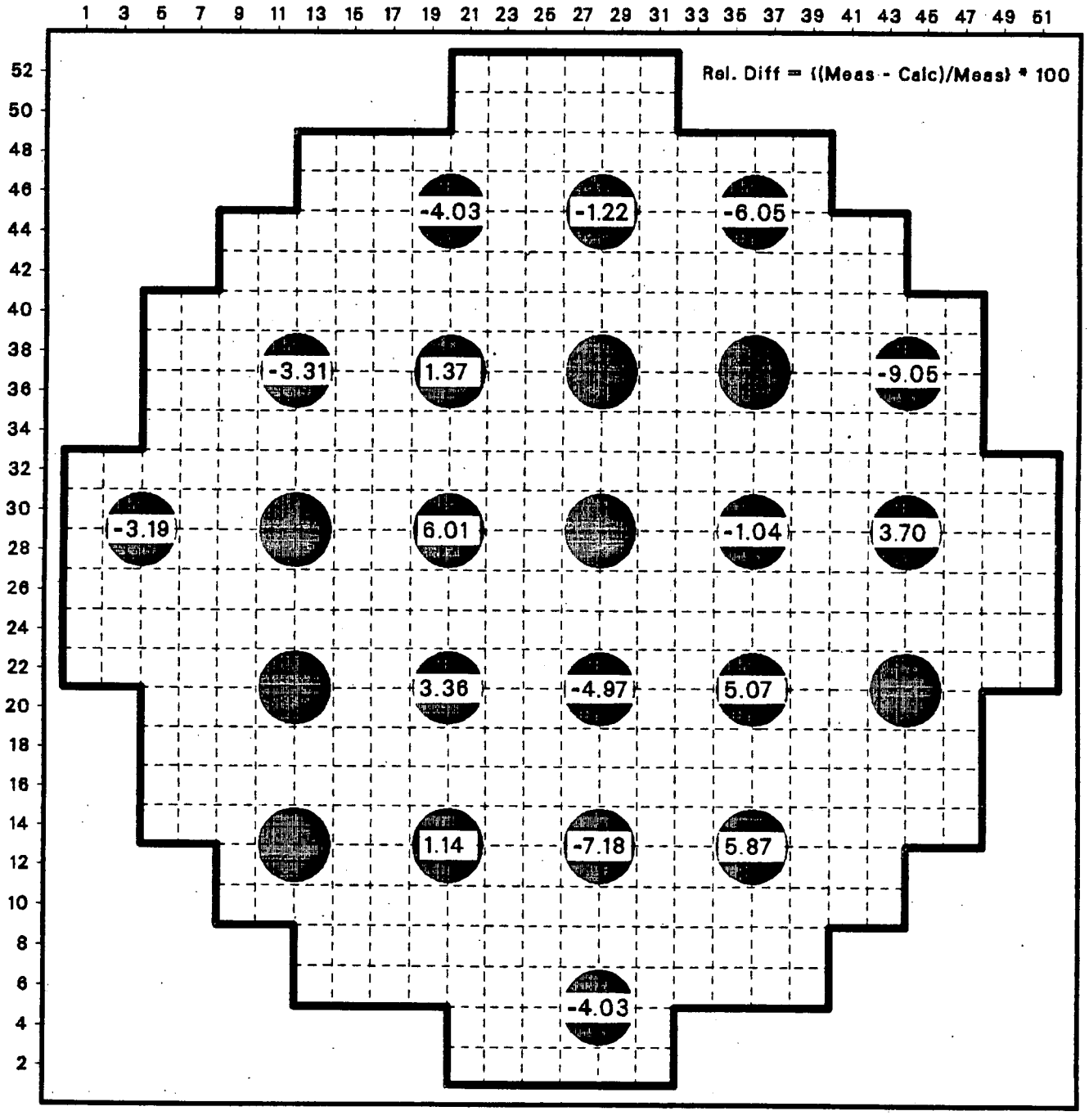

Figure 3.6.20

Measured and Calculated Detector Response

BOC Cycle 9, Trace 12-37

1.782 GWD/MTU, B Sequence

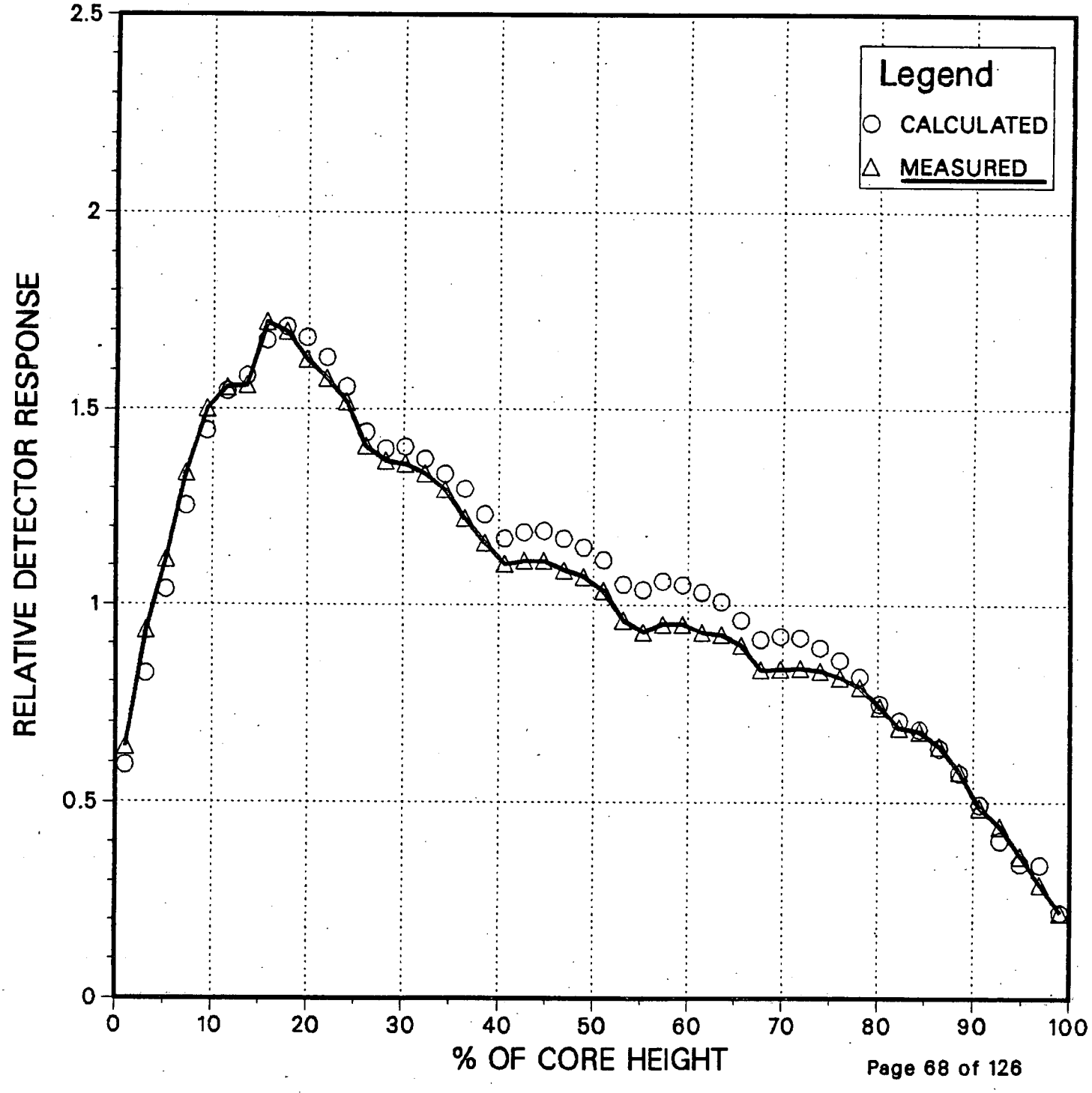

Figure 3.6.21

Measured and Calculated Detector Response

BOC Cycle 9, Trace 44-29

1.782 GWD/MTU, B Sequence

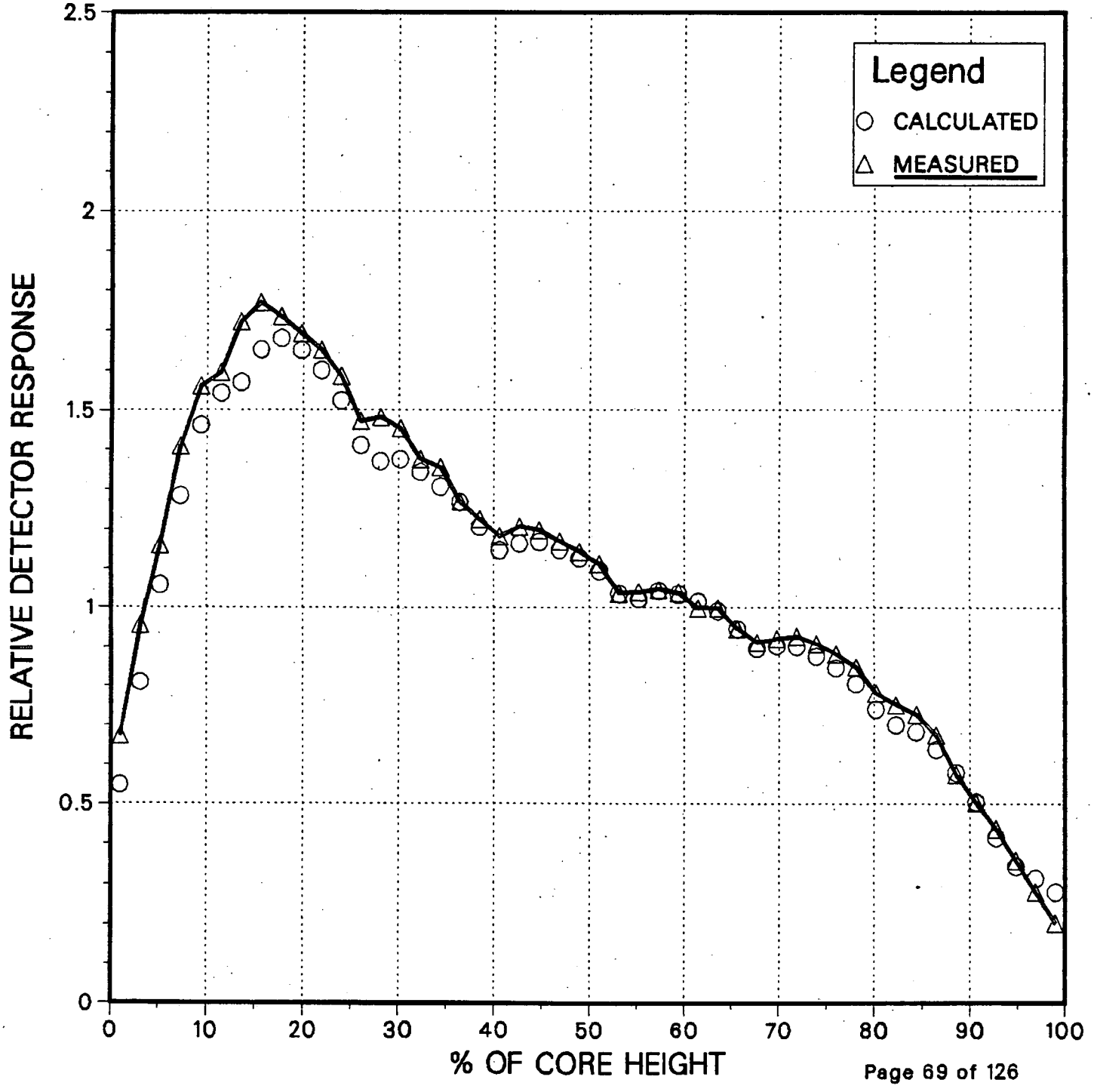

Figure 3.6.22

Measured and Calculated Integrated Detector Responses

MOC 9

2.614 GWD/MTU , A Sequence

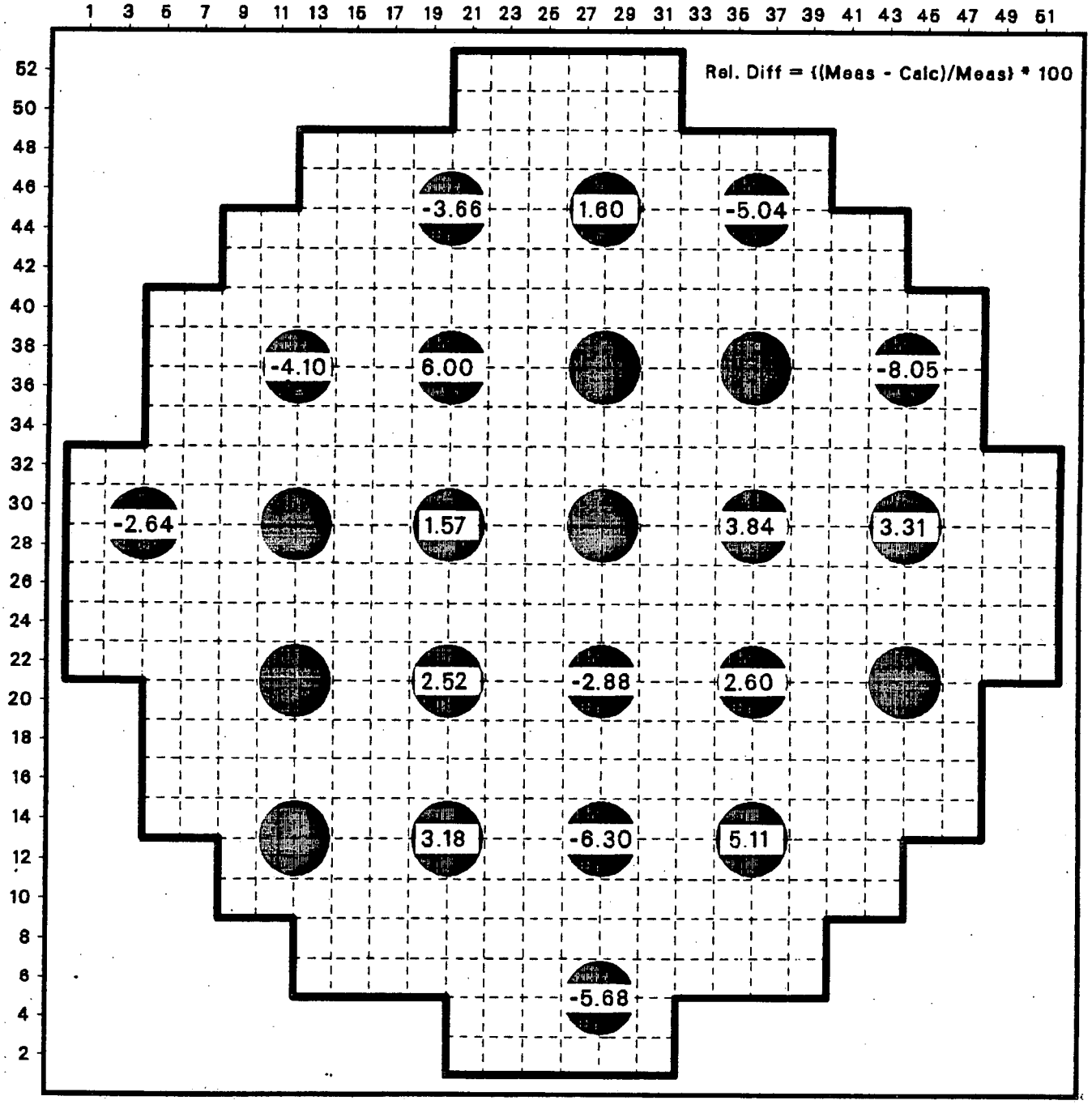

Figure 3.6.23

Measured and Calculated Detector Response

MOC Cycle 9, Trace 36-29

2.614 GWD/MTU, A Sequence

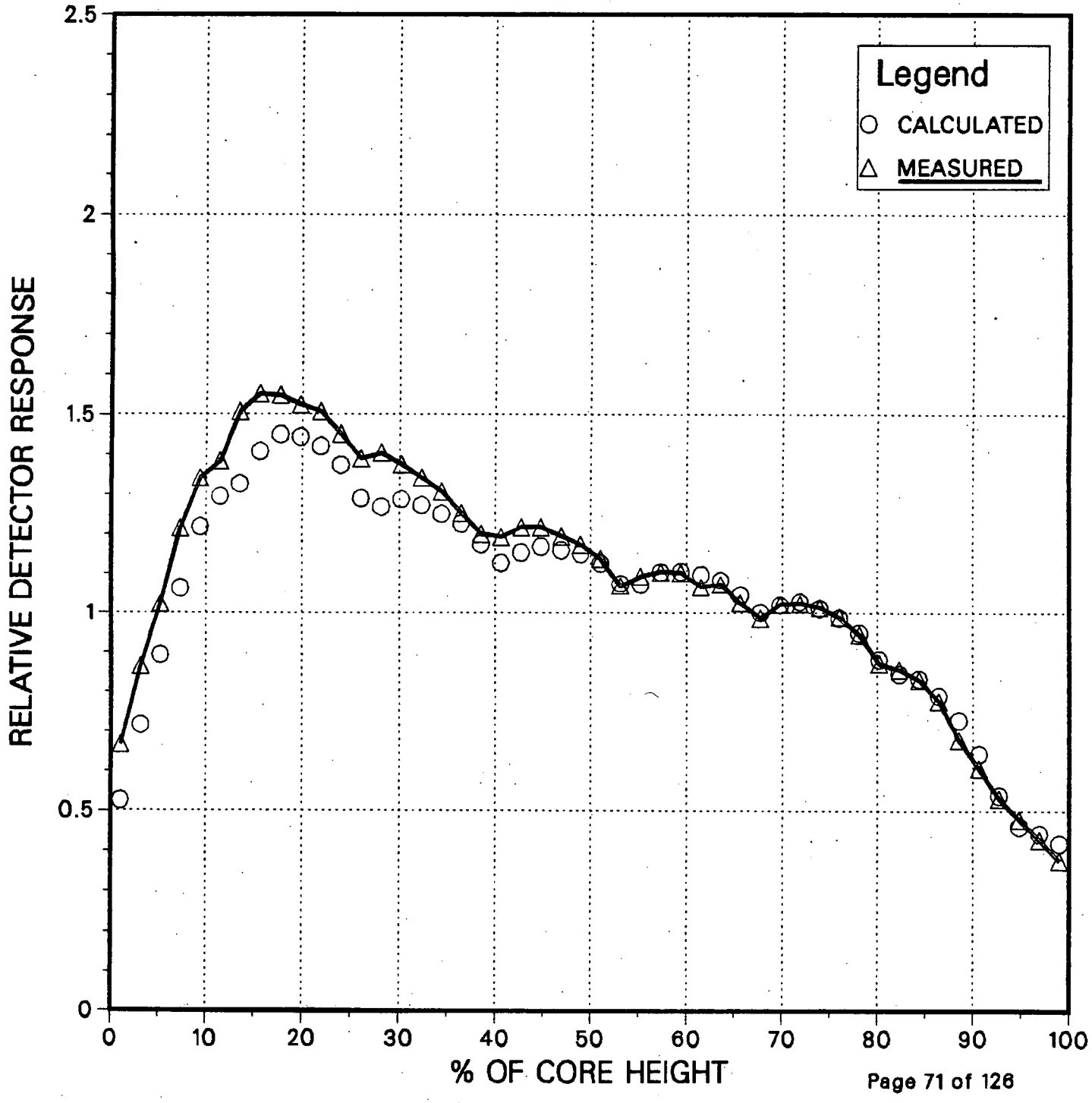

Figure 3.6.24

Measured and Calculated Detector Response

MOC CYCLE 9, Trace 20-45

2.614 GWD/MTU, A Sequence

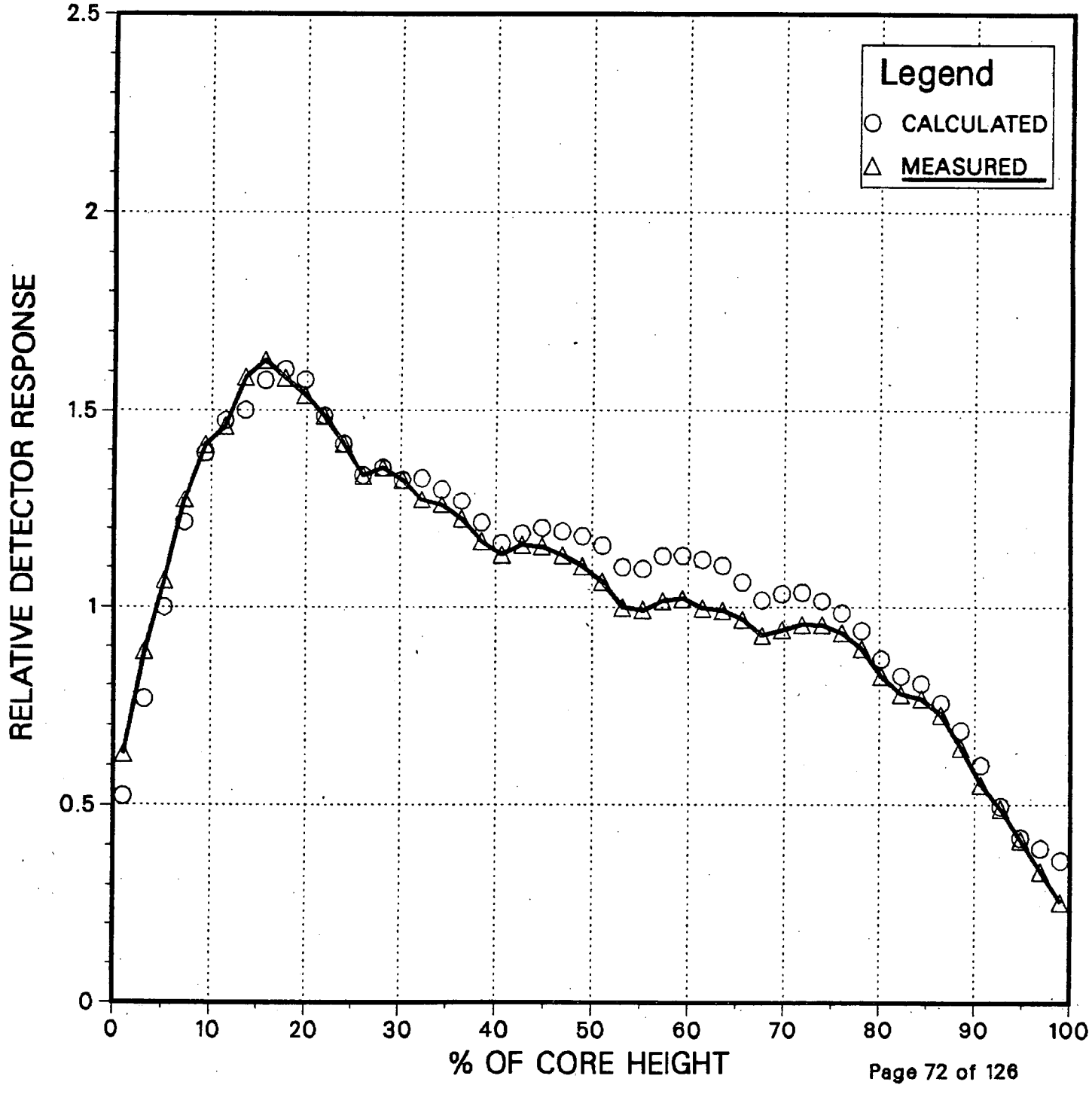

Figure 3.6.25

Measured and Calculated Integrated Detector Responses

EOC 9

4.893 GWD/MTU , ARO

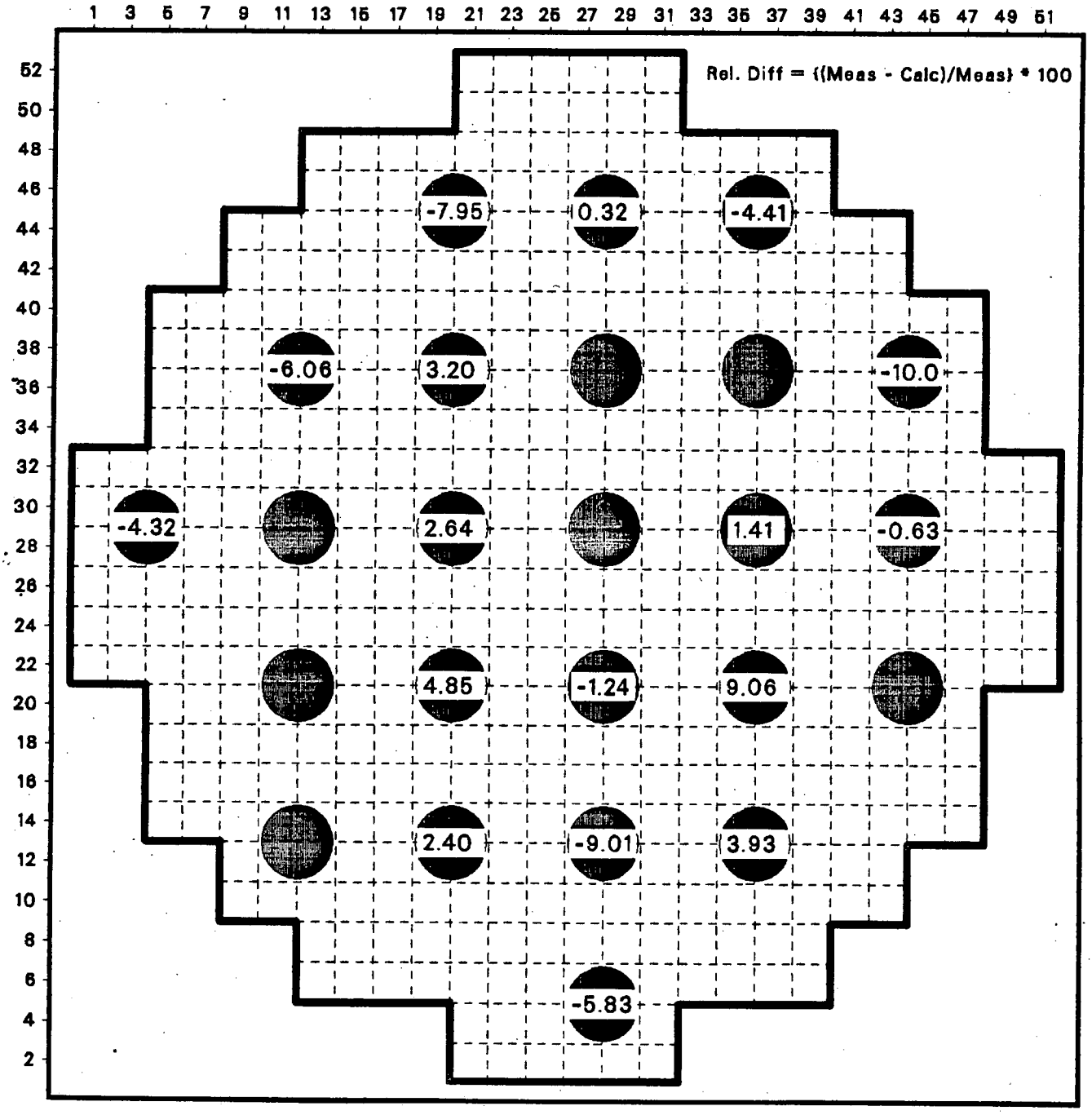

Figure 3.6.26

Measured and Calculated Detector Response

EOC Cycle 9, Trace 20-37

4.893 GWD/MTU, ARO

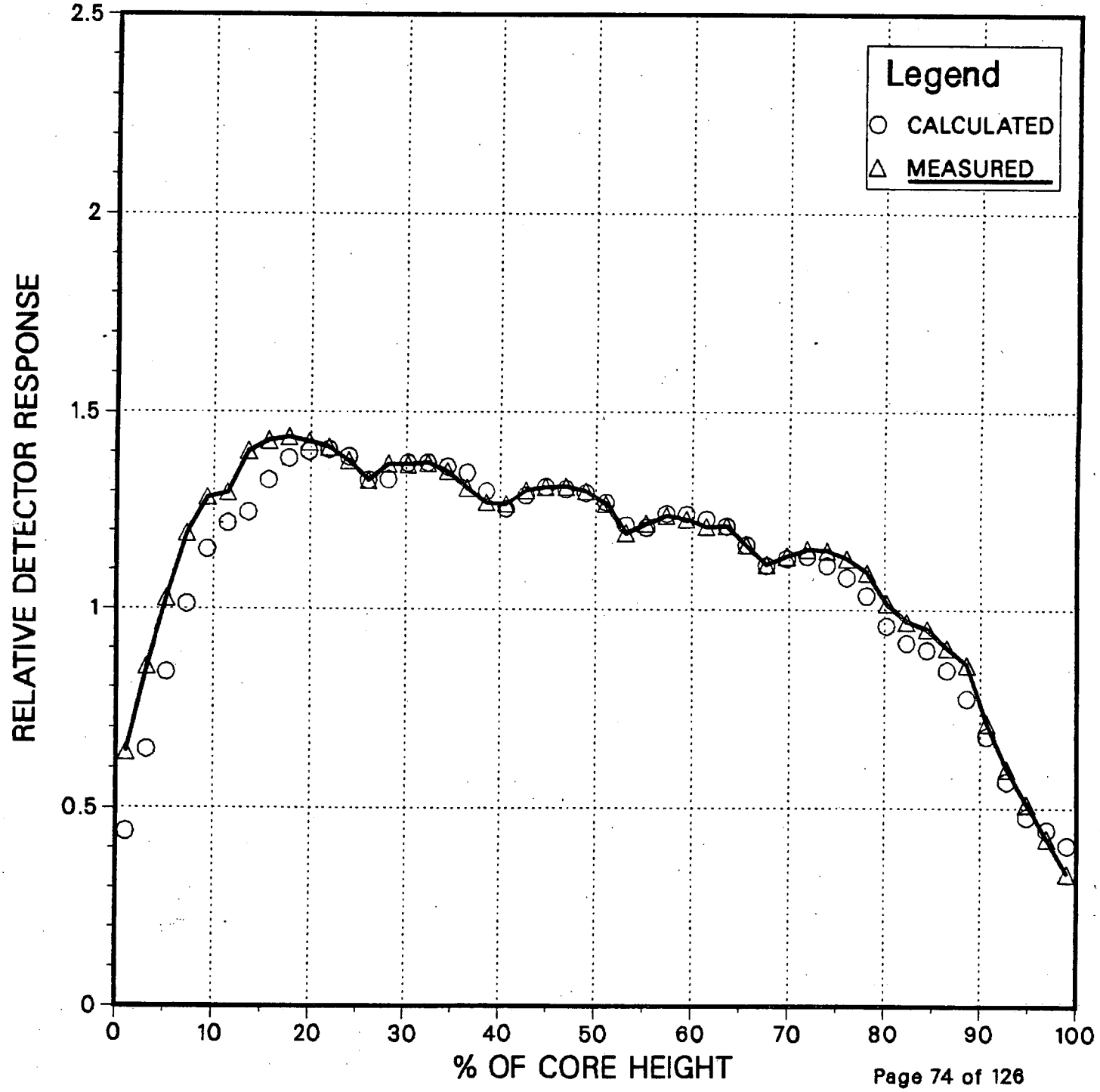

Figure 3.6.27

Measured and Calculated Detector Response

EOC Cycle 9, Trace 36-13

4.893 GWD/MTU, ARO

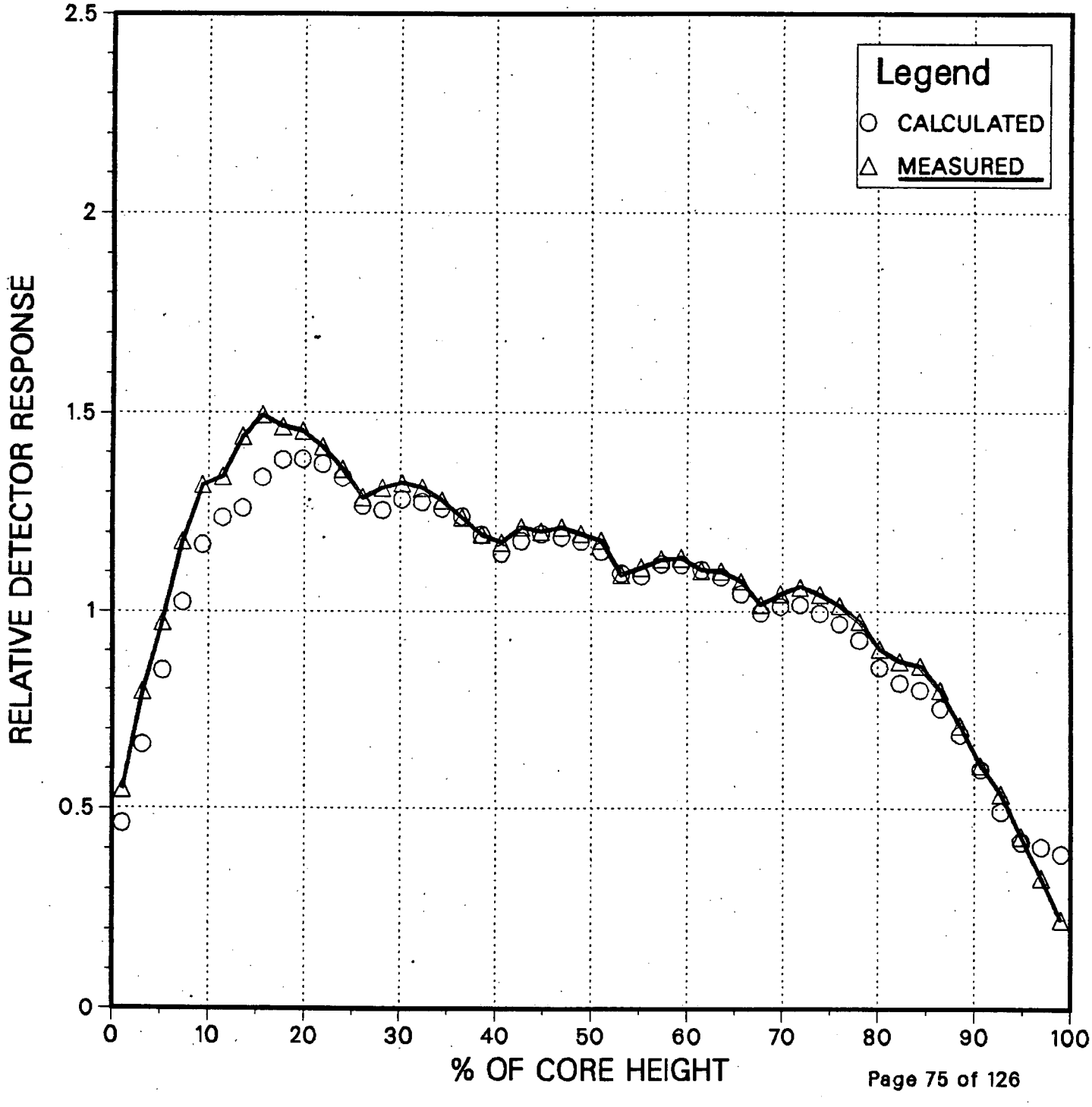

Figure 3.6.28

Measured and Calculated Integrated Detector Responses

BOC 10

1.489 GWD/MTU , B Sequence

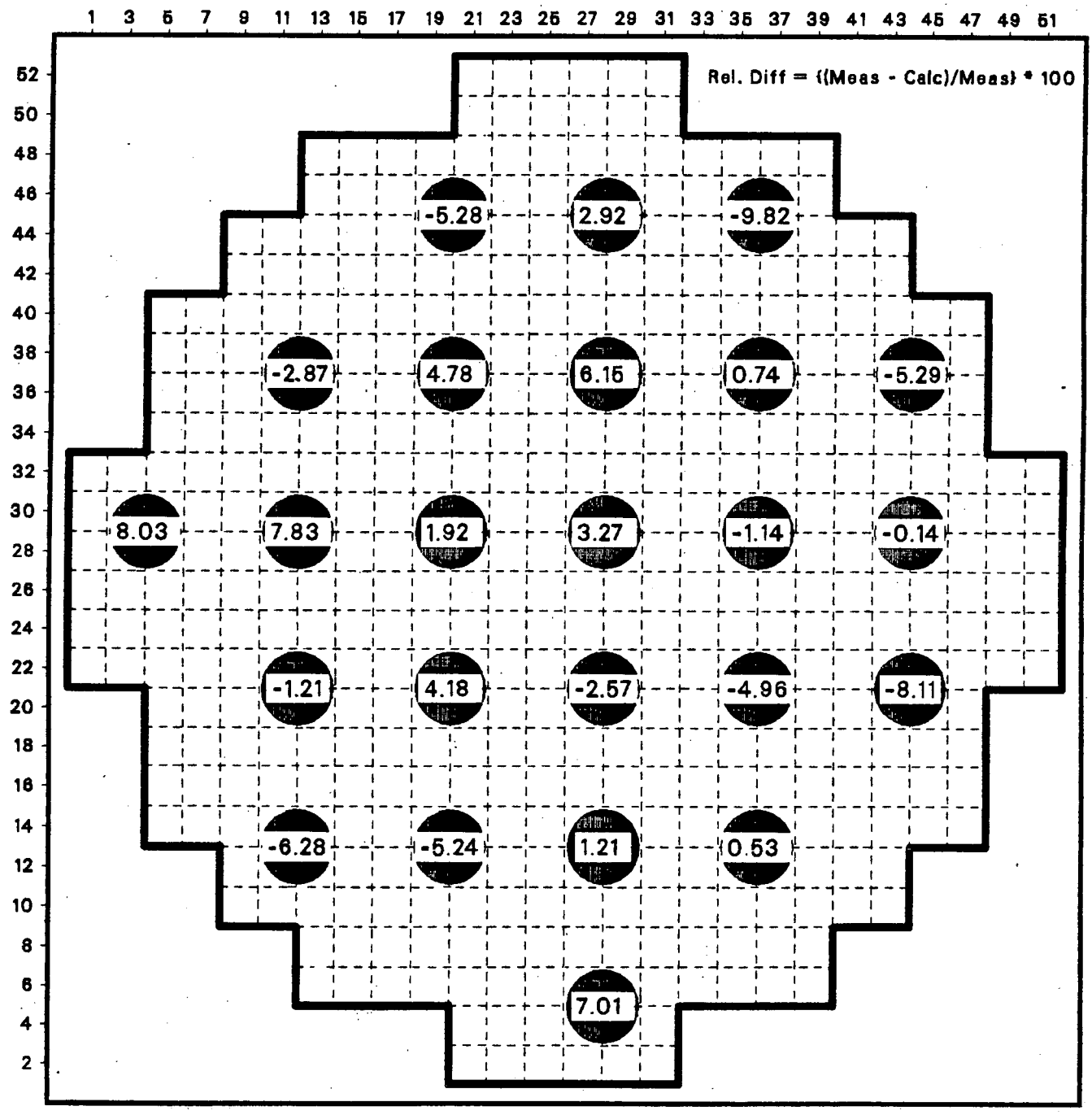

Figure 3.6.29

Measured and Calculated Detector Response

BOC Cycle 10, Trace 20-37

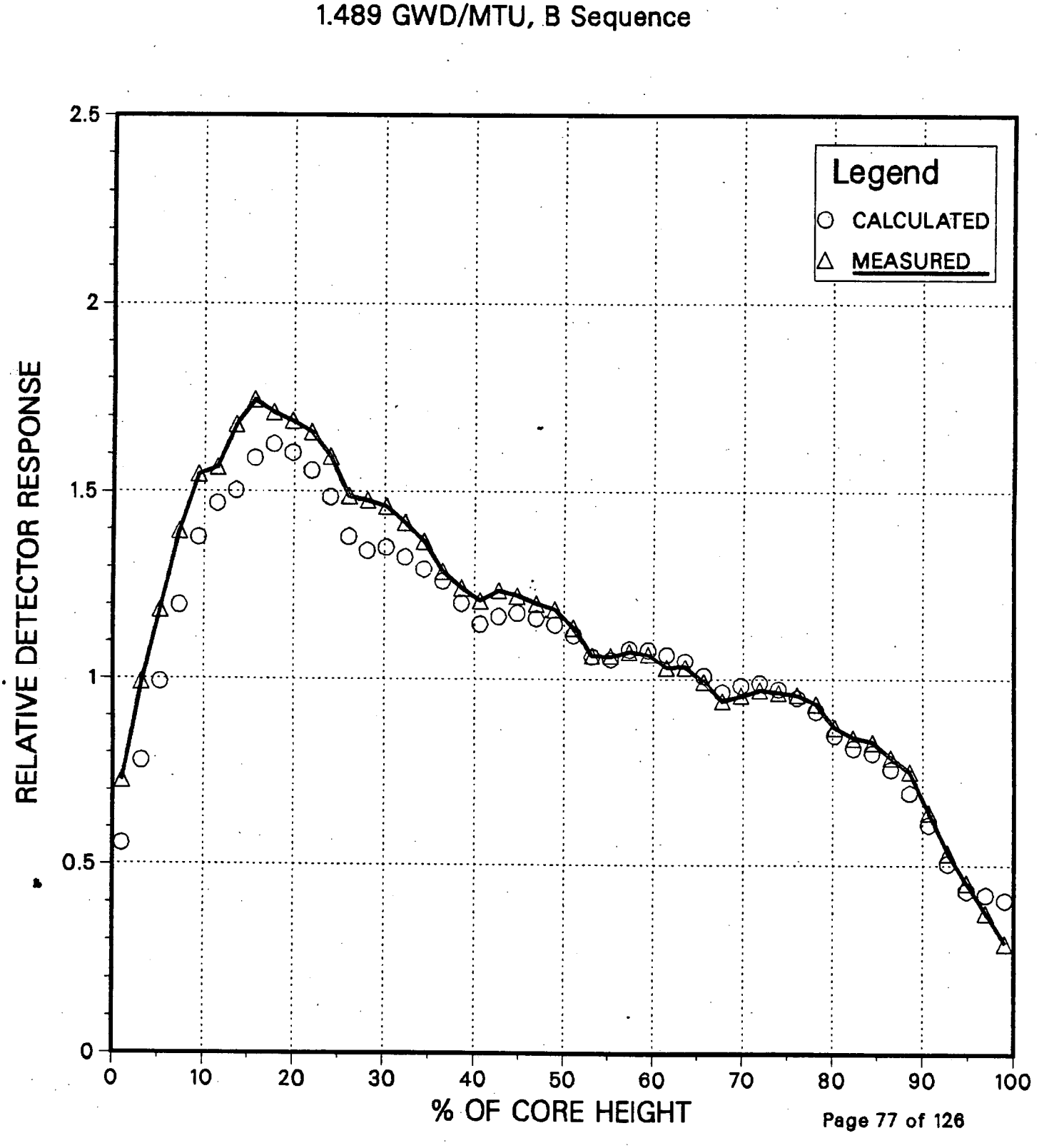

Figure 3.6.30

Measured and Calculated Detector Response

BOC Cycle 10, Trace 36-13

1.489 GWD/MTU, B Sequence

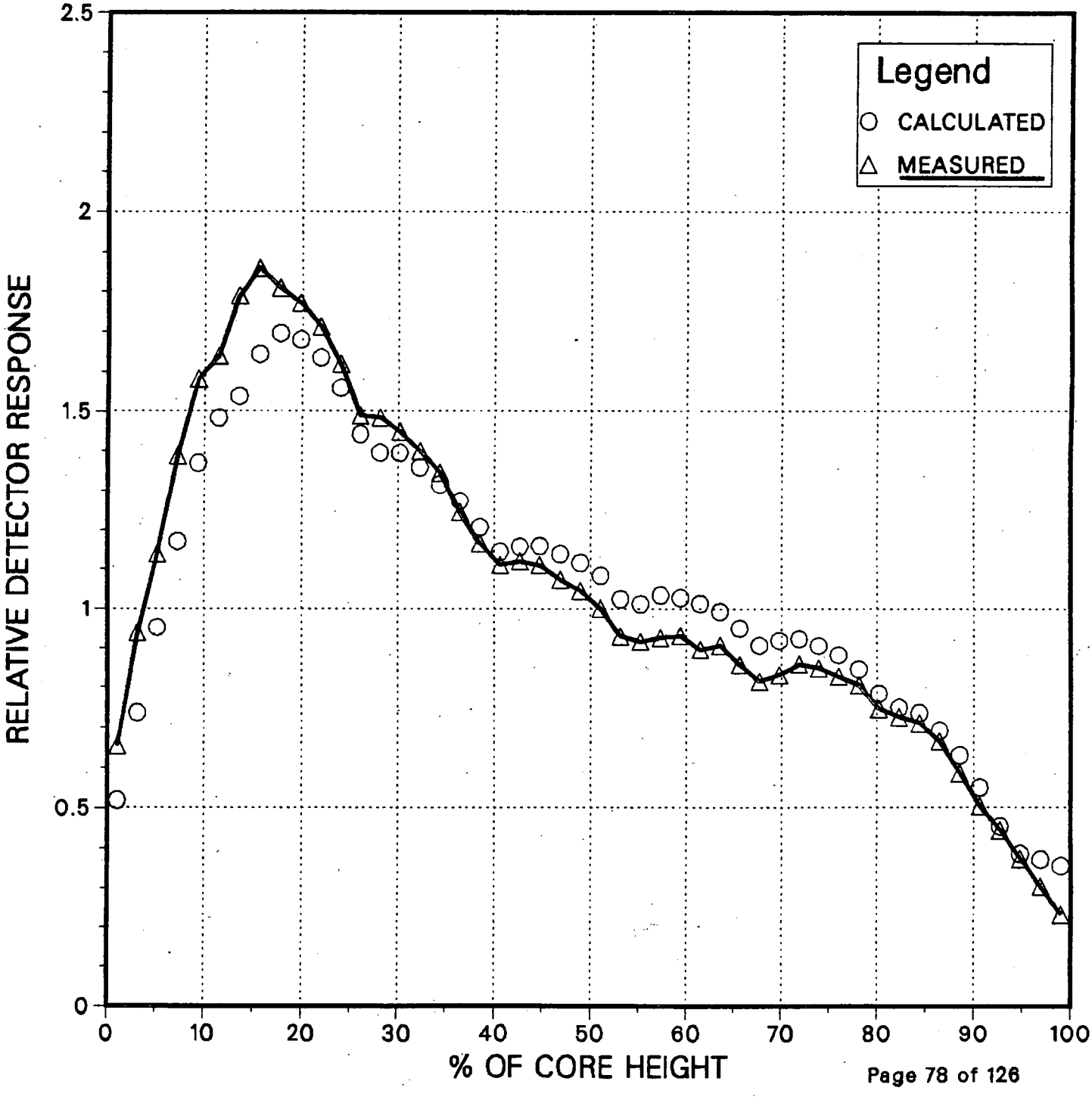

Figure 3.6.31

Measured and Calculated Integrated Detector Responses

MOC 10

3.211 GWD/MTU , A Sequence

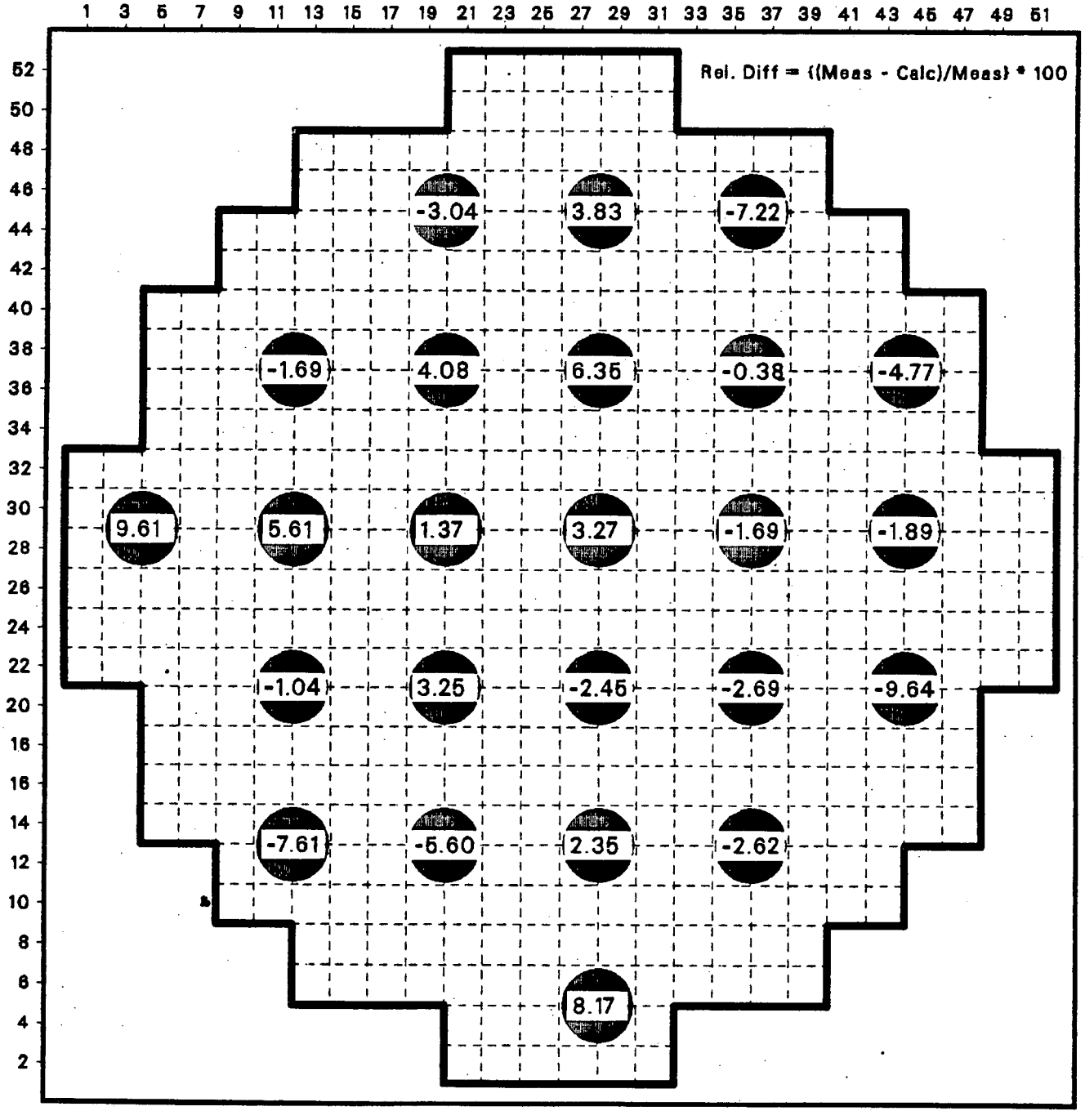

Figure 3.6.32

Measured and Calculated Detector Response

MOC Cycle 10, Trace 28-29

3.211 GWD/MTU, A Sequence

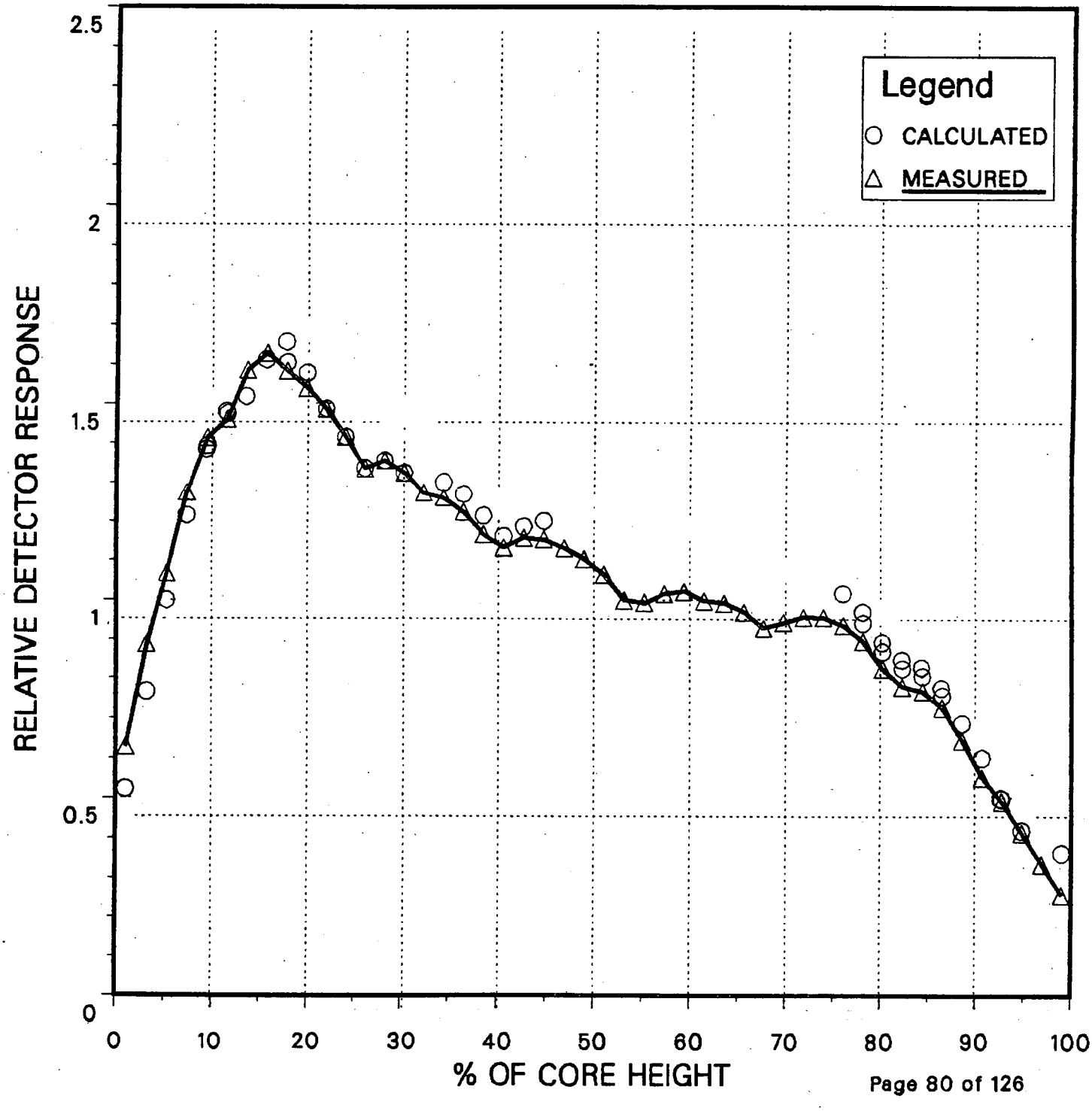

Figure 3.6.33

Measured and Calculated Detector Response

MOC Cycle 10, Trace 28-45

3.211 GWD/MTU, A Sequence

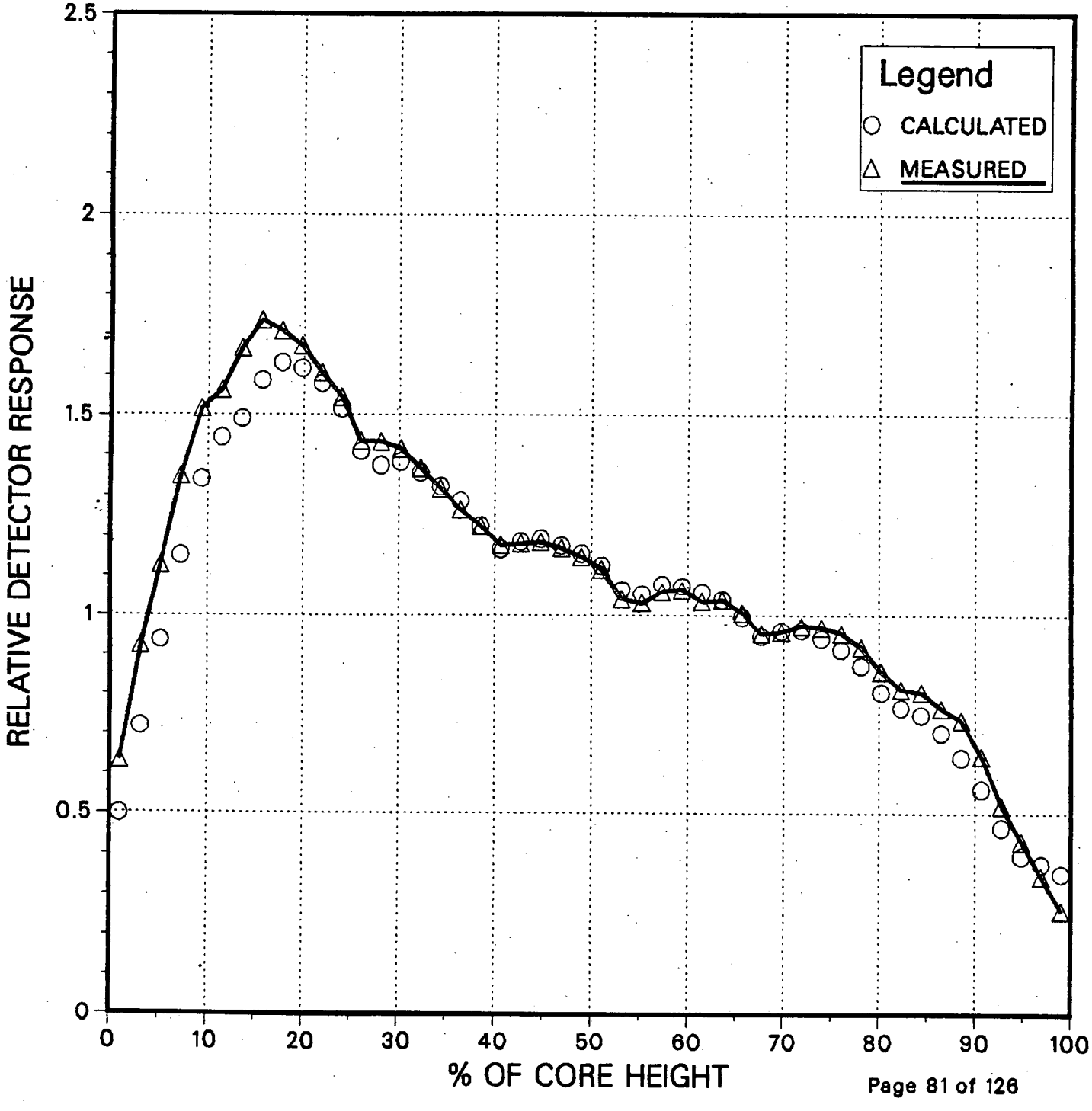

Figure 3.6.34

Measured and Calculated Integrated Detector Responses

EOC 10

4.507 GWD/MTU , ARO

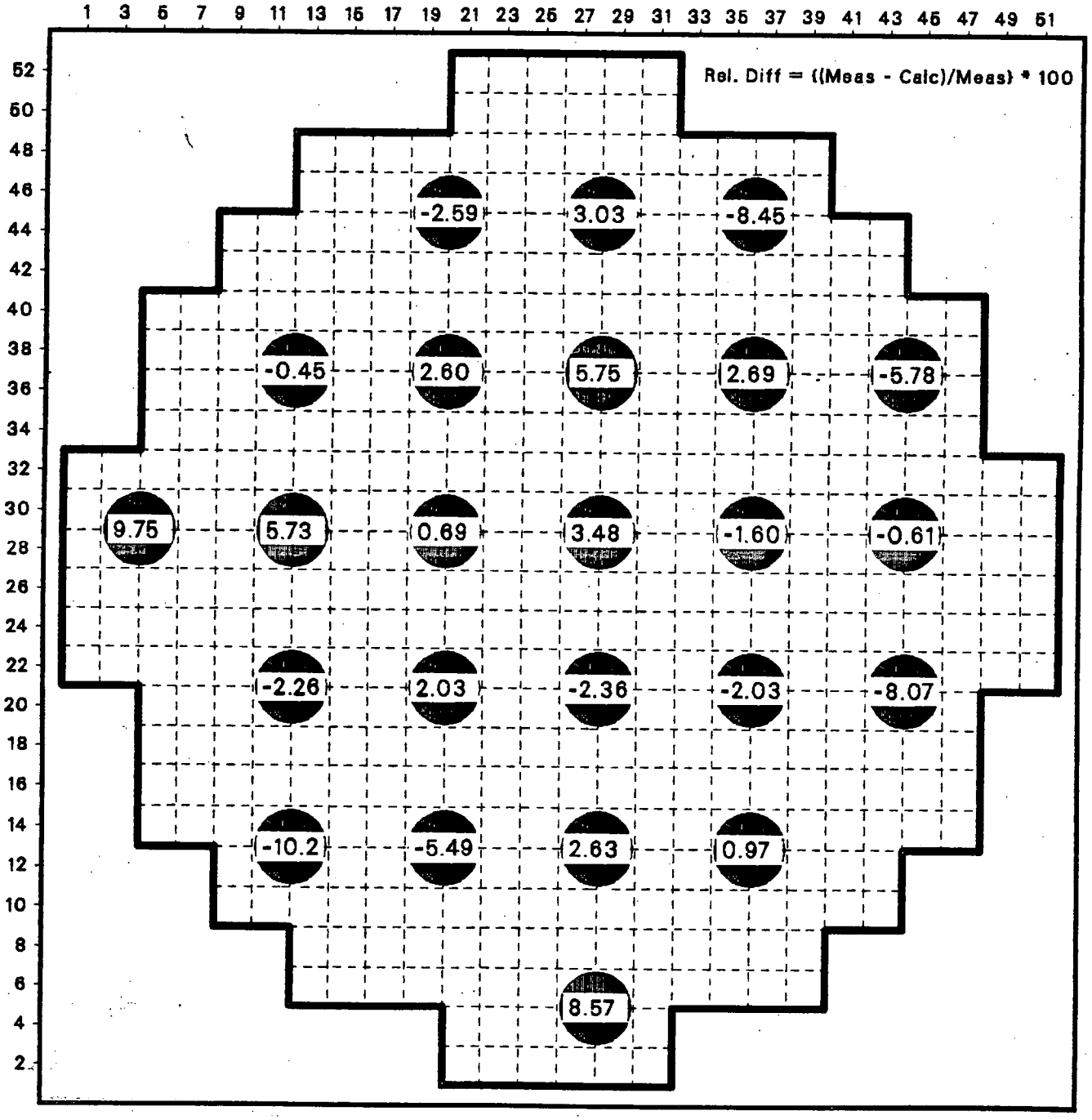

Figure 3.6.35

Measured and Calculated Detector Response

EOC Cycle 10, Trace 28-45

4.507 GWD/MTU, ARO

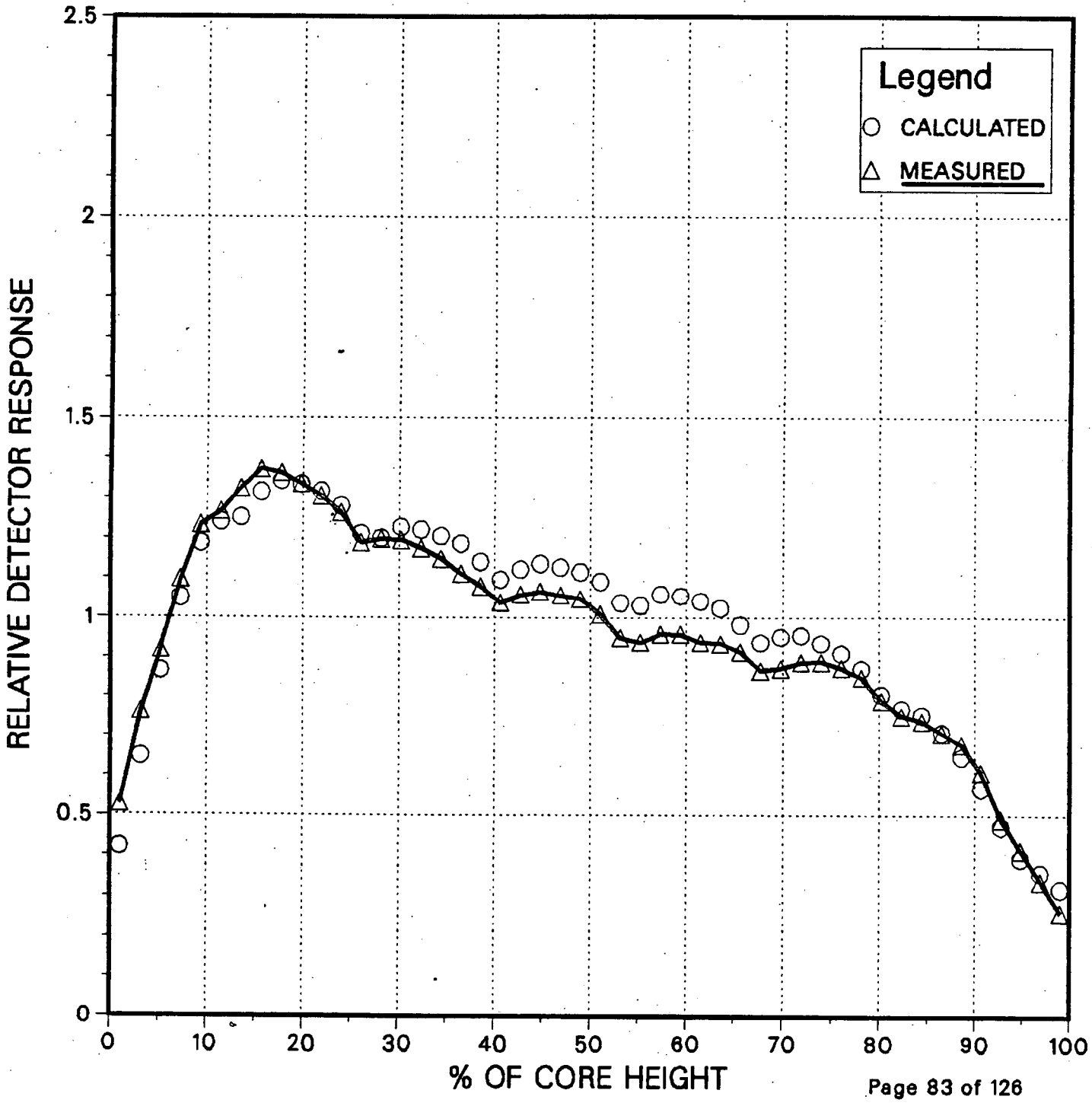

Figure 3.6.36

Measured and Calculated Detector Response

EOC Cycle 10, Trace 28-29

4.507 GWD/MTU, ARO

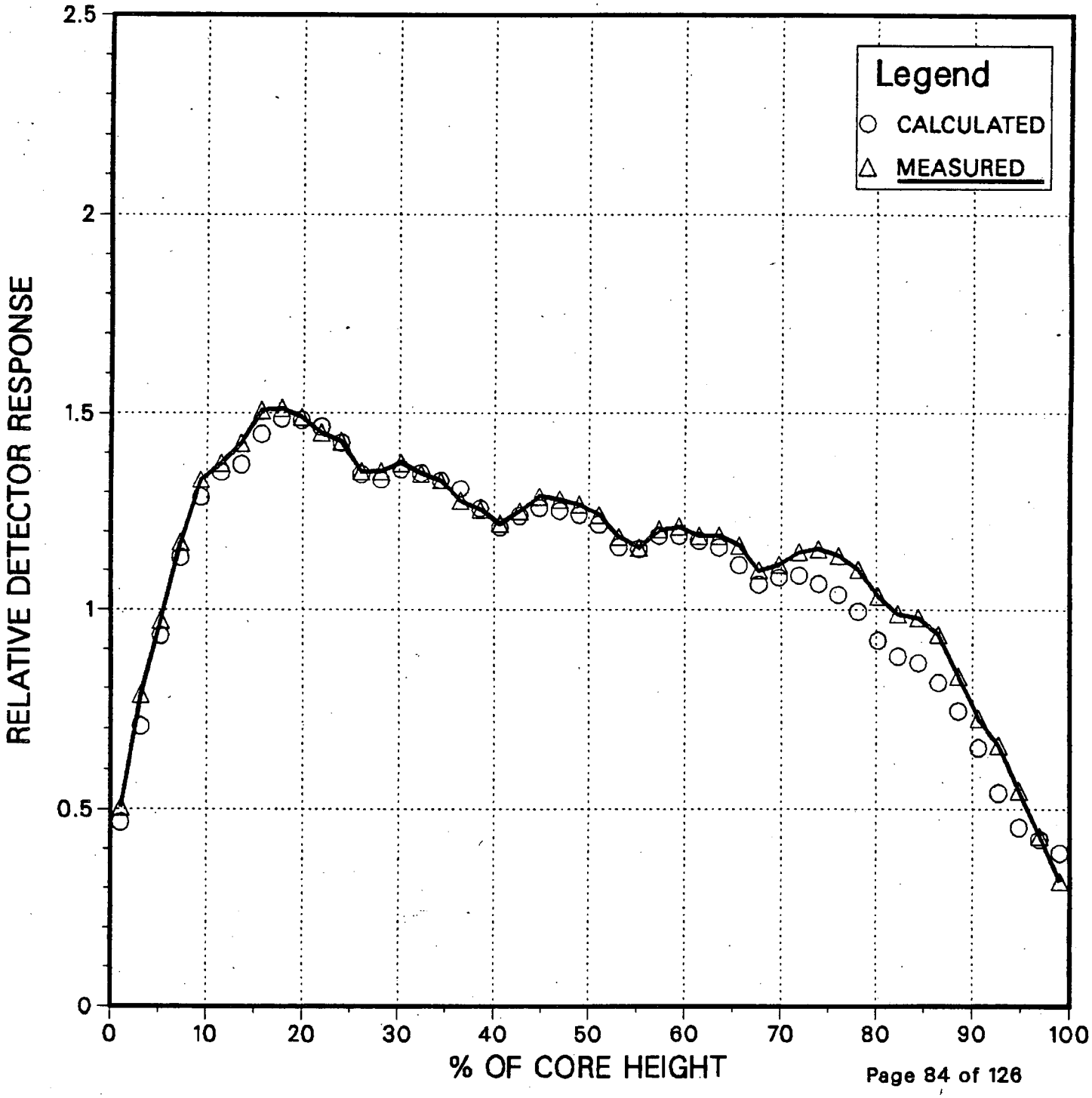

Figure 3.6.37

Observed Differences Density Function Comparison

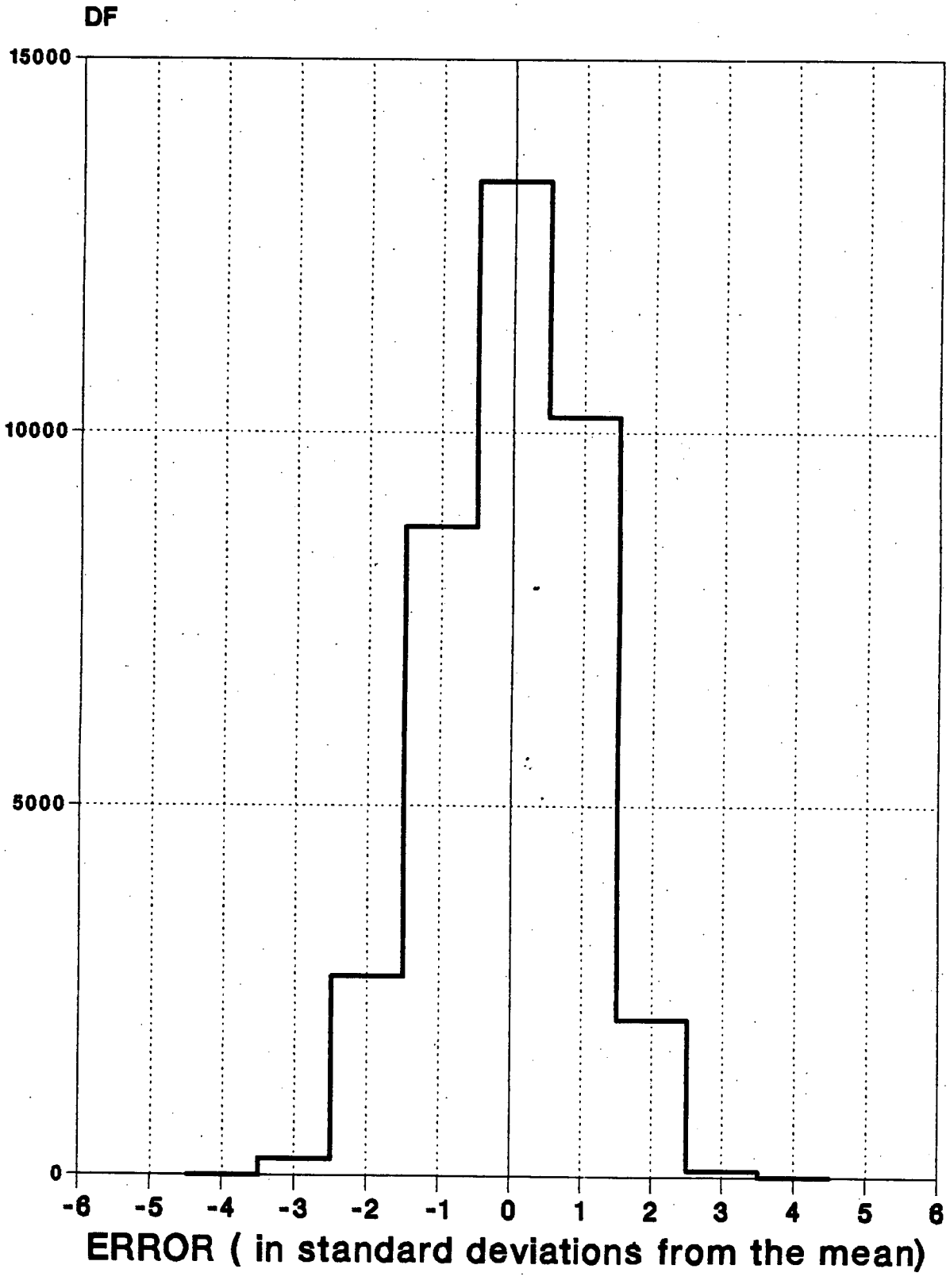

Figure 3.6.38

Cumulative Distribution Function (CDF) Comparison

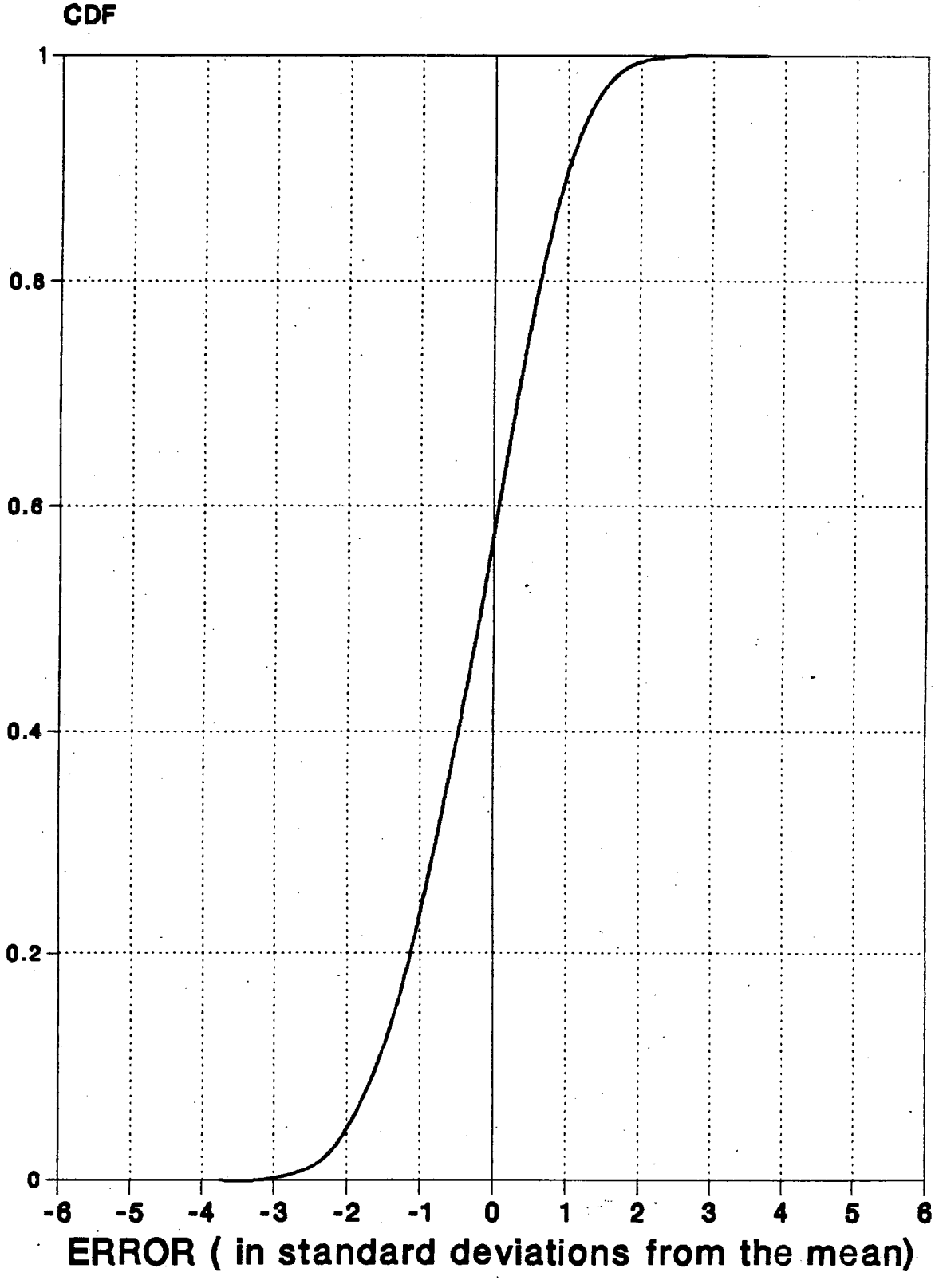

Figure 3.6.39

CDF in the Region of 95th Percentile Model Comparison

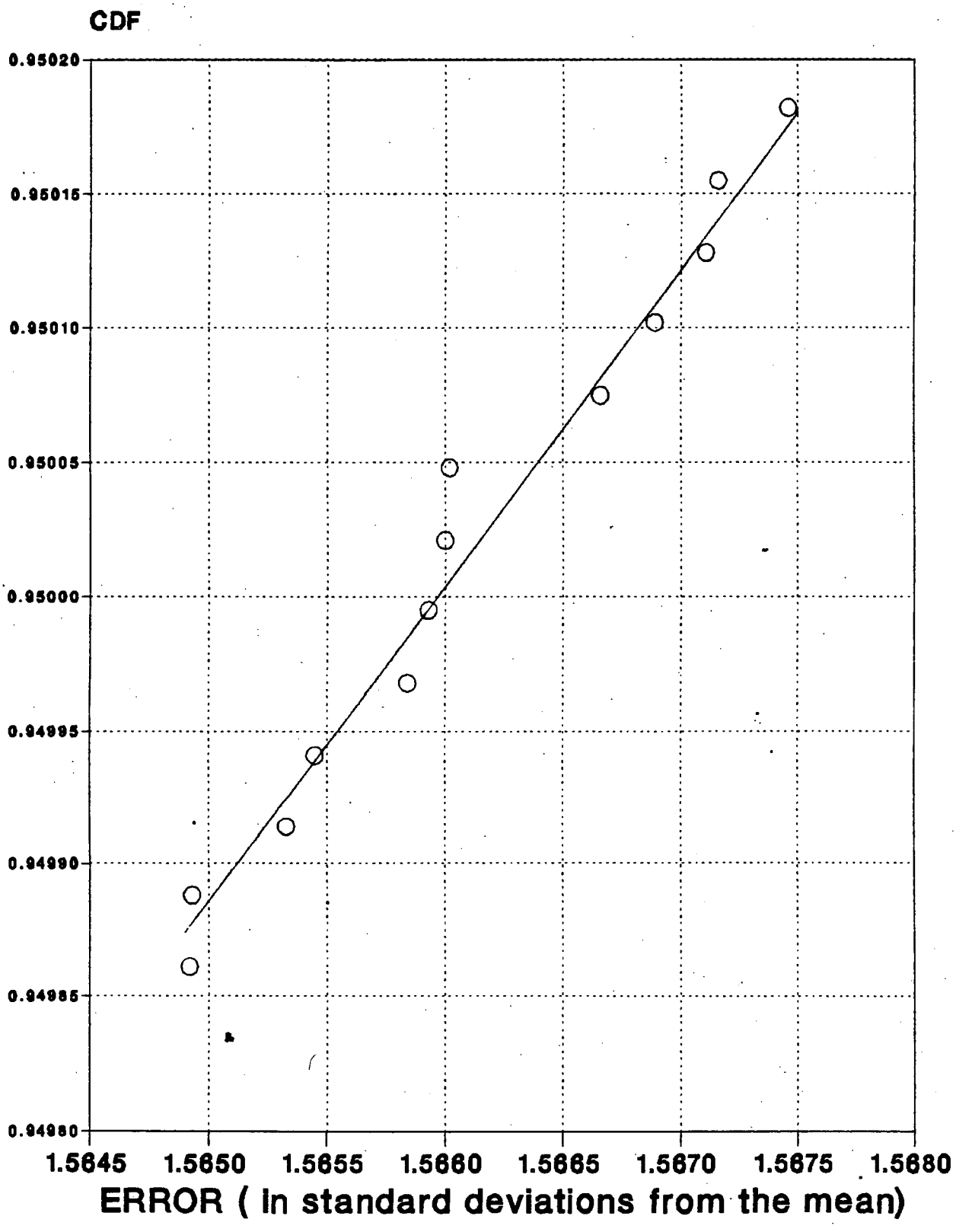

Figure 3.6.40

Observed Differences Density Function
Integrated Reaction Rates Comparison

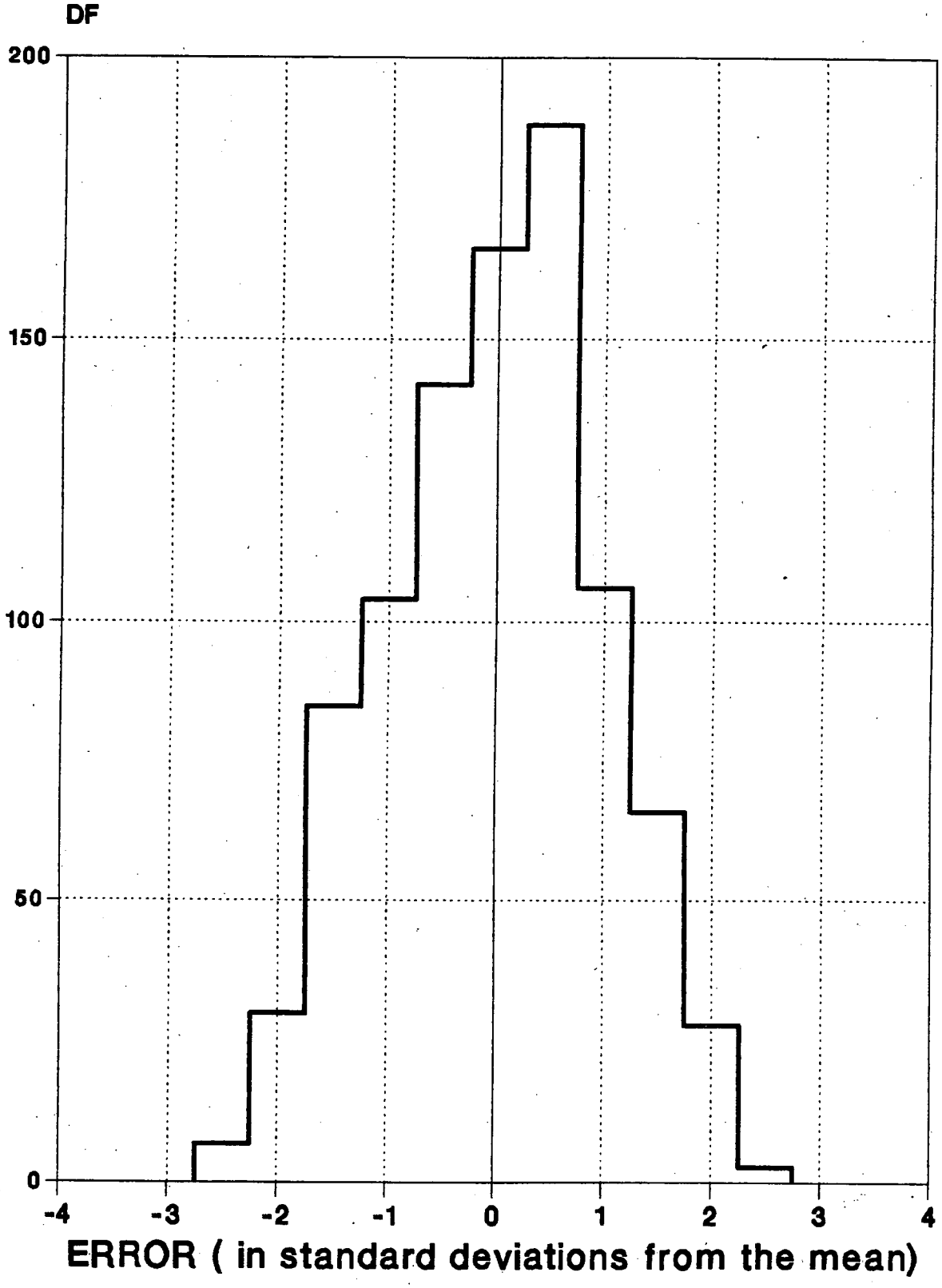

Figure 3.6.41

Cumulative Distribution Function (CDF) For Integrated Reaction Rates Comparison

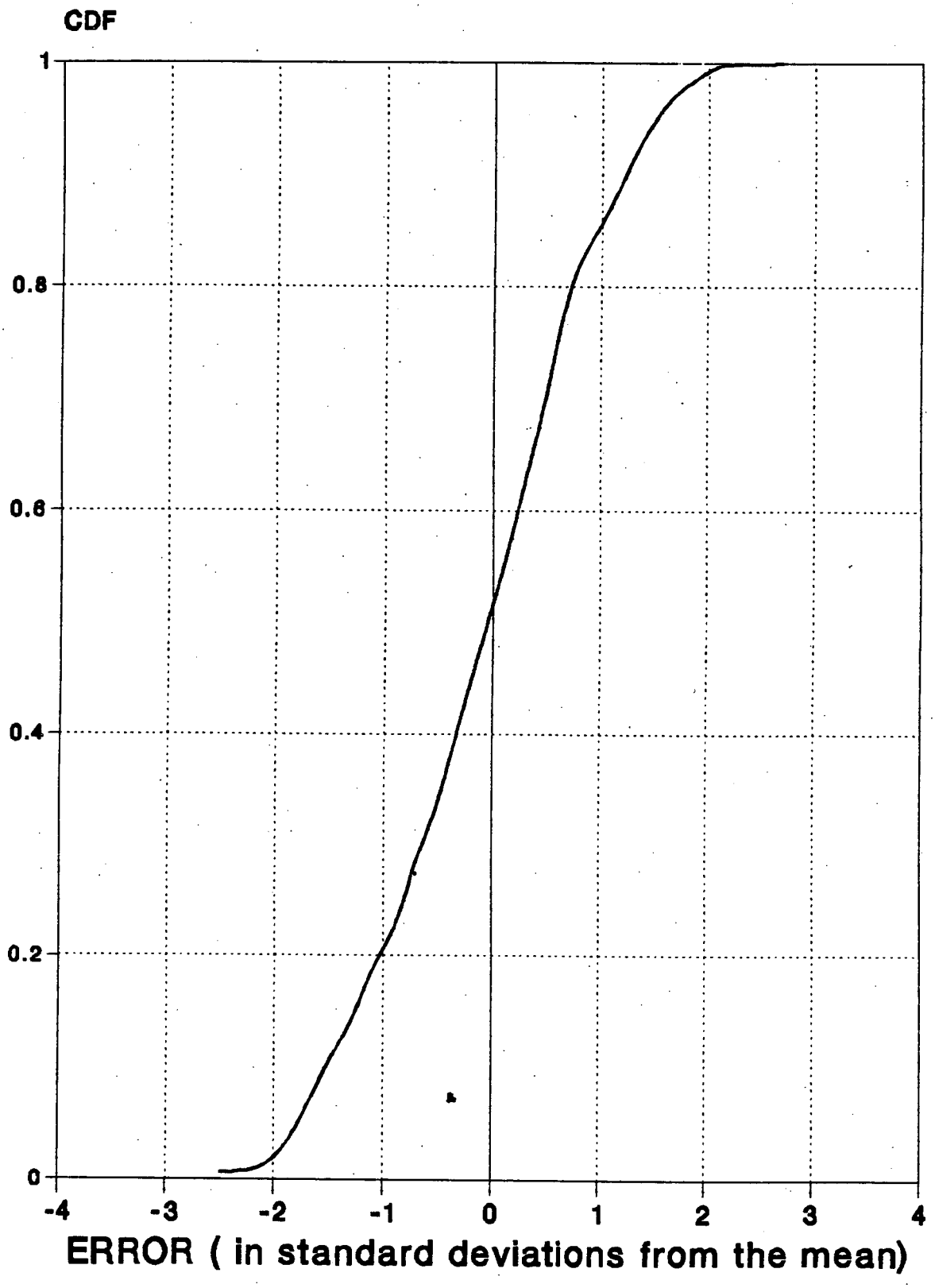

Figure 3.6.42

CDF in Region of 95th Percentile For Integrated Reaction Rates

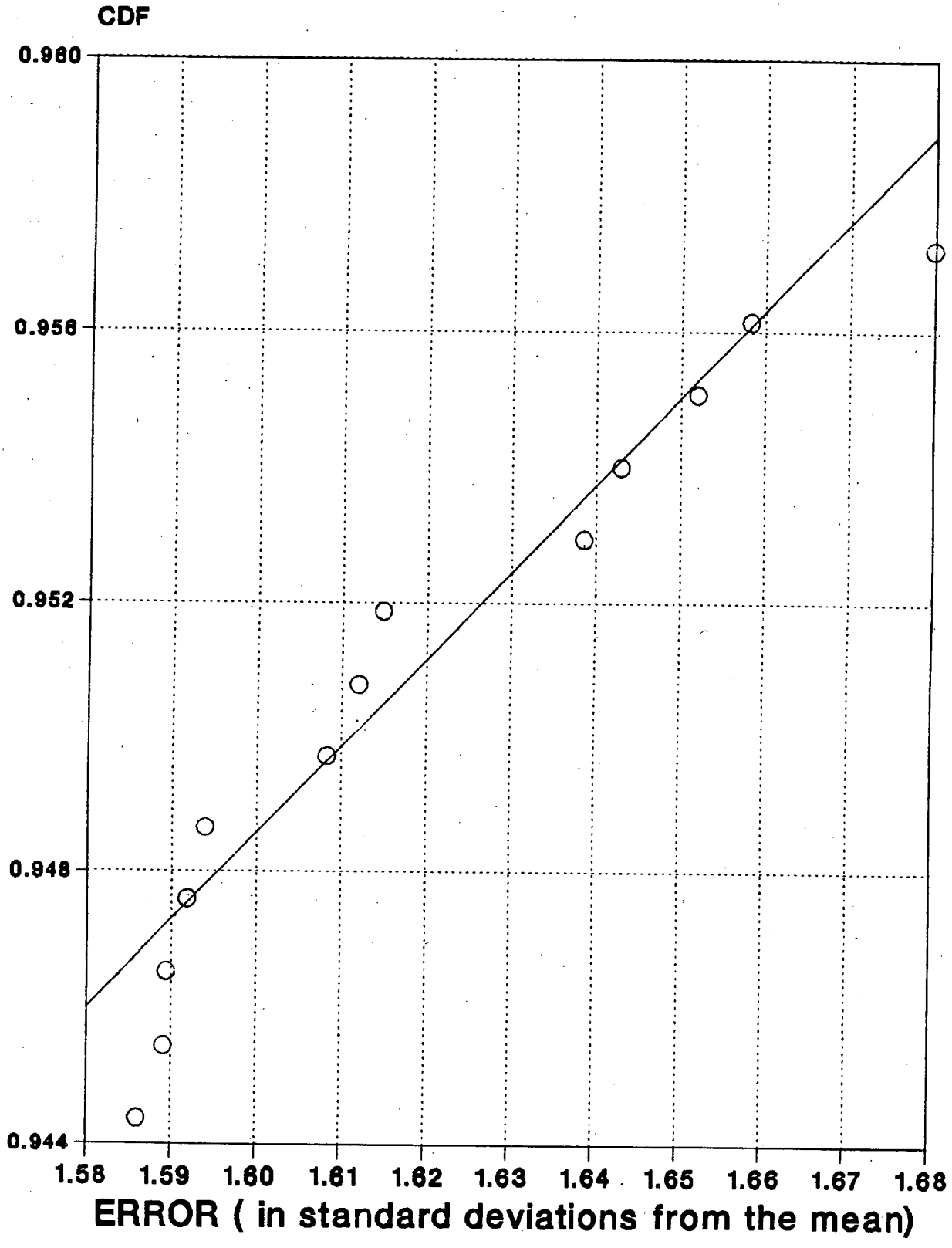

Figure 3.6.43
Standard Deviation vs Measured Instrument Response

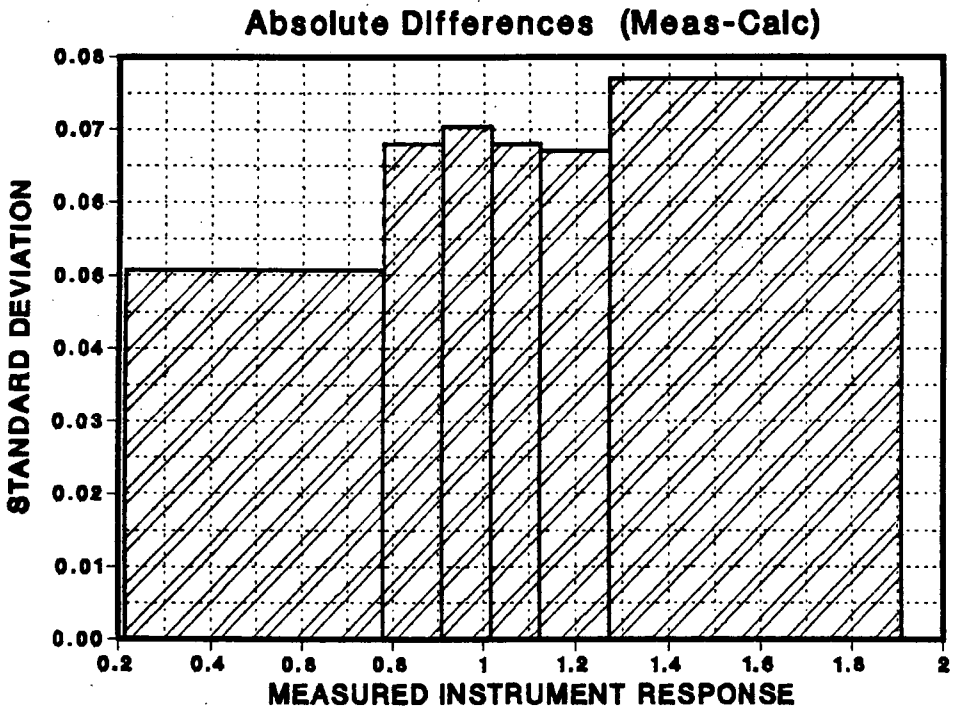

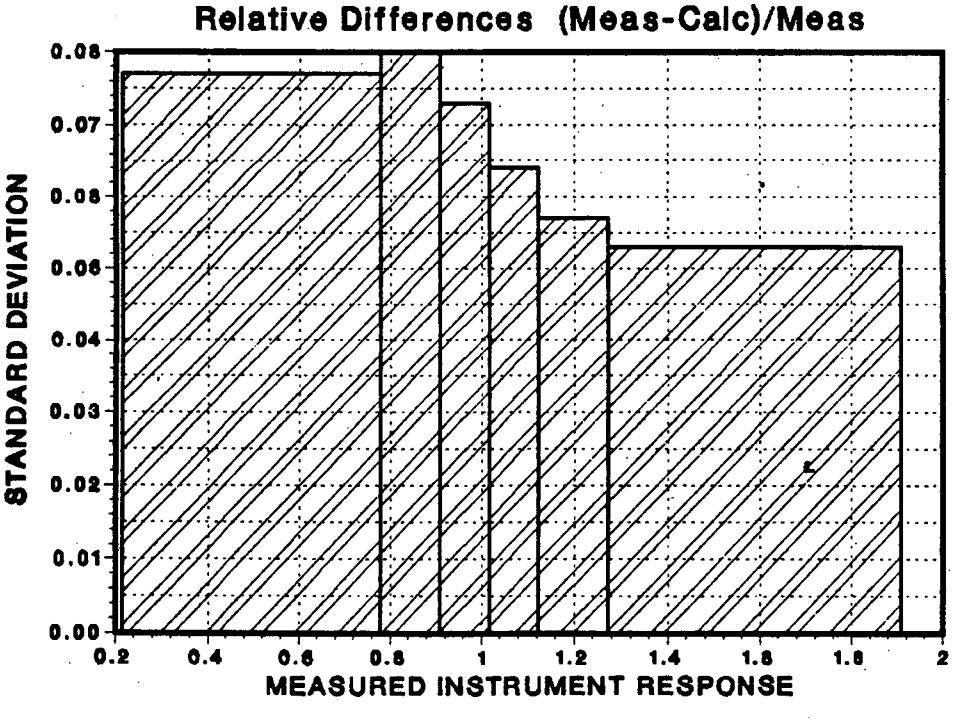

Figure 3.6.44

Gamma Scan Assembly Locations
EOC 8

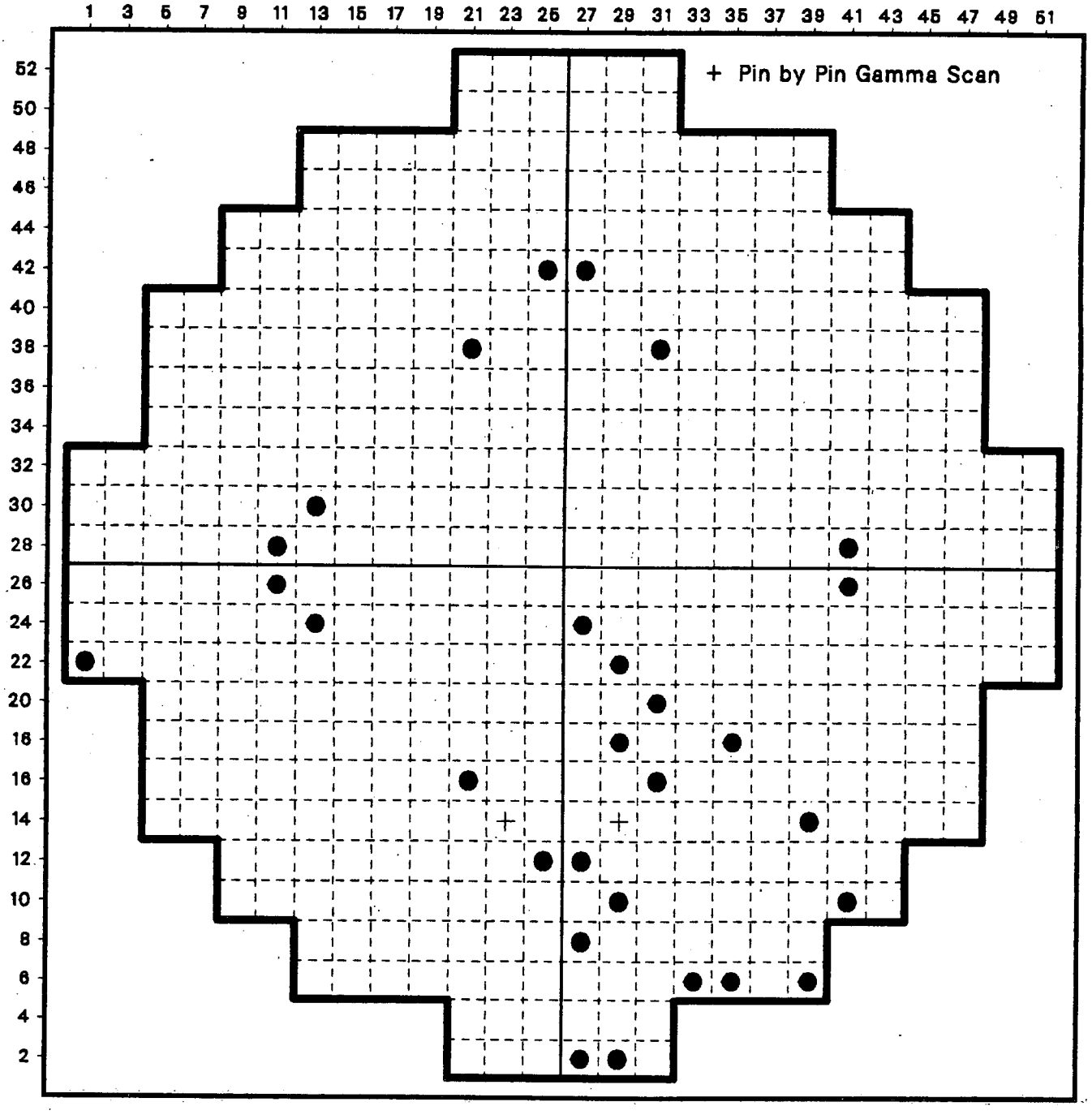

Figure 3.6.45

Gamma Scan Assembly Locations
EOC 9

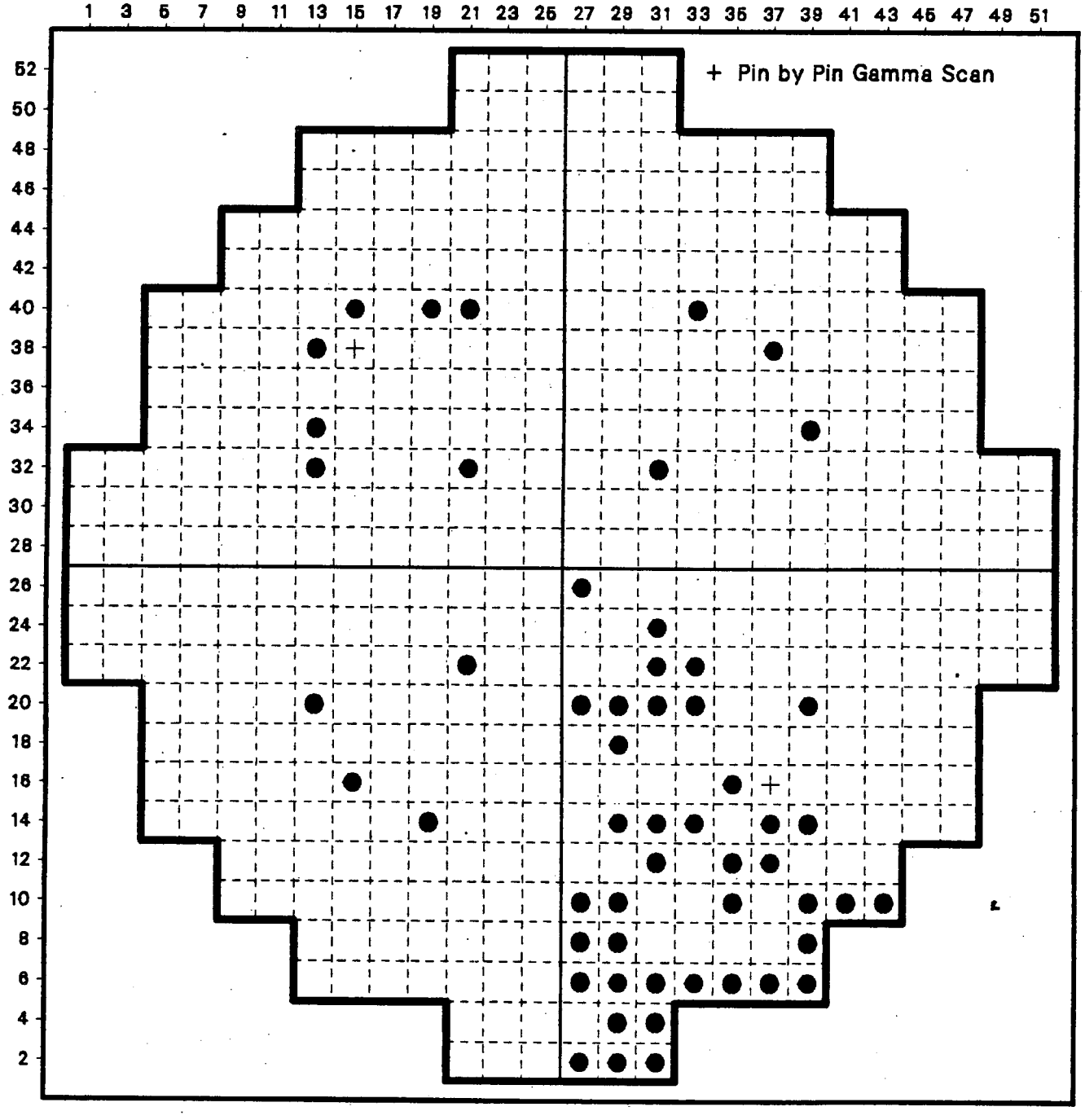

FIGURE 3.6.46

EOC 8 RADIAL GAMMA SCAN COMPARISON

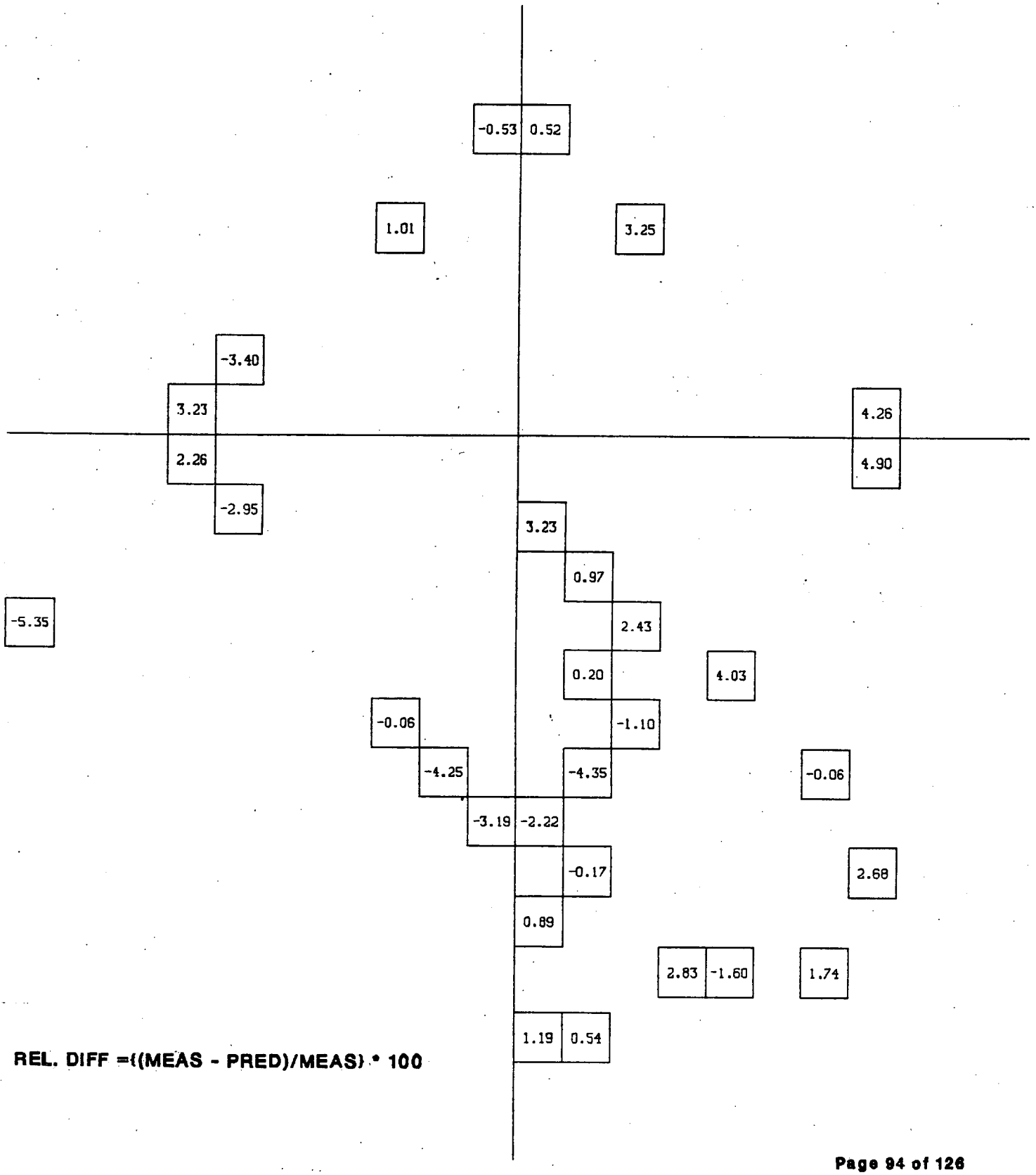

REL. DIFF =((MEAS - PRED)/MEAS) * 100

Figure 3.6.47

EOC 8 Axial Gamma Scan Comparison

Bundle 31-38

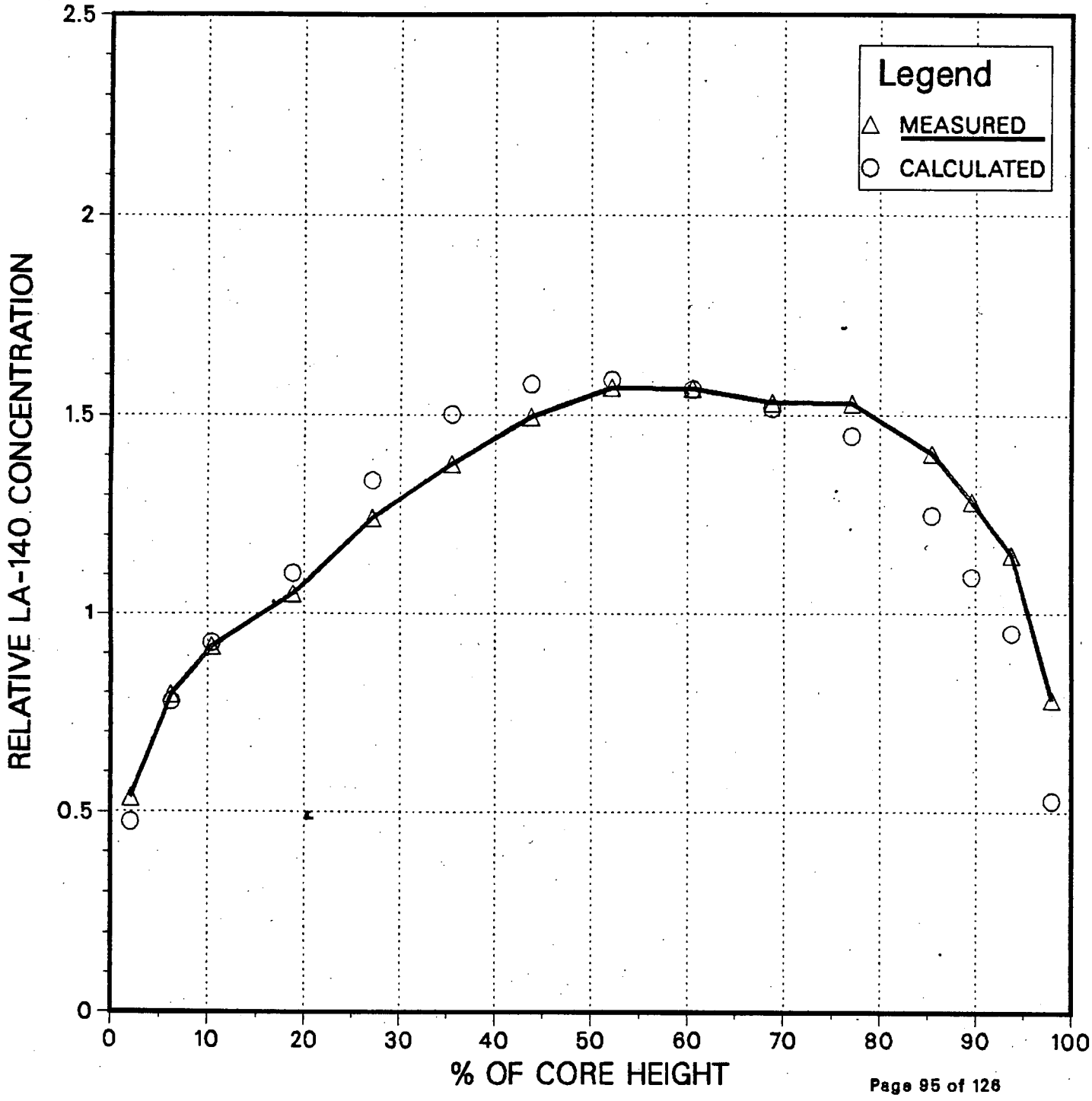

Figure 3.6.48

EOC 8 Axial Gamma Scan Comparison

Bundle 25-12

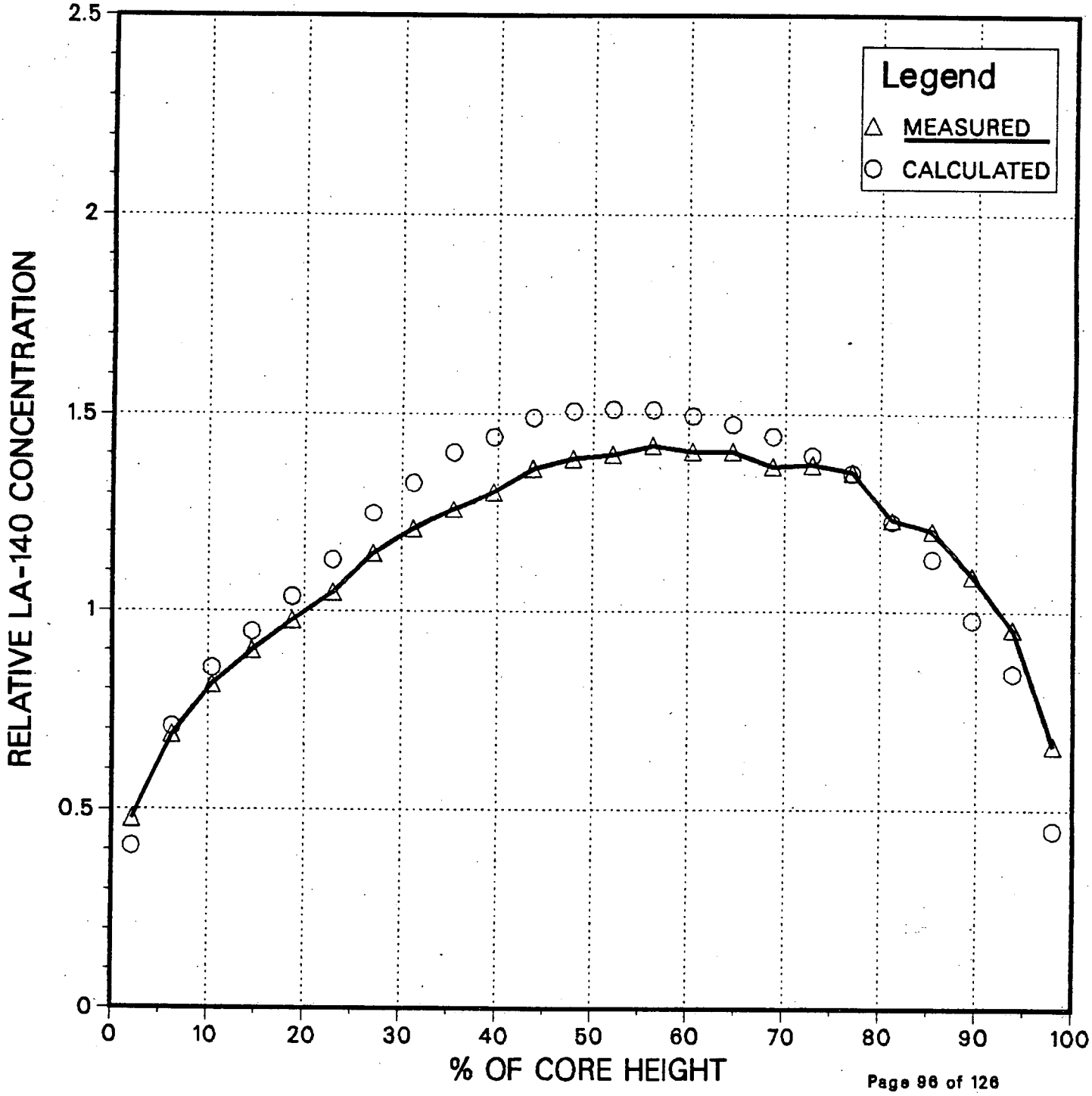

Figure 3.6.49

EOC 9 Radial Gamma Scan Comparison

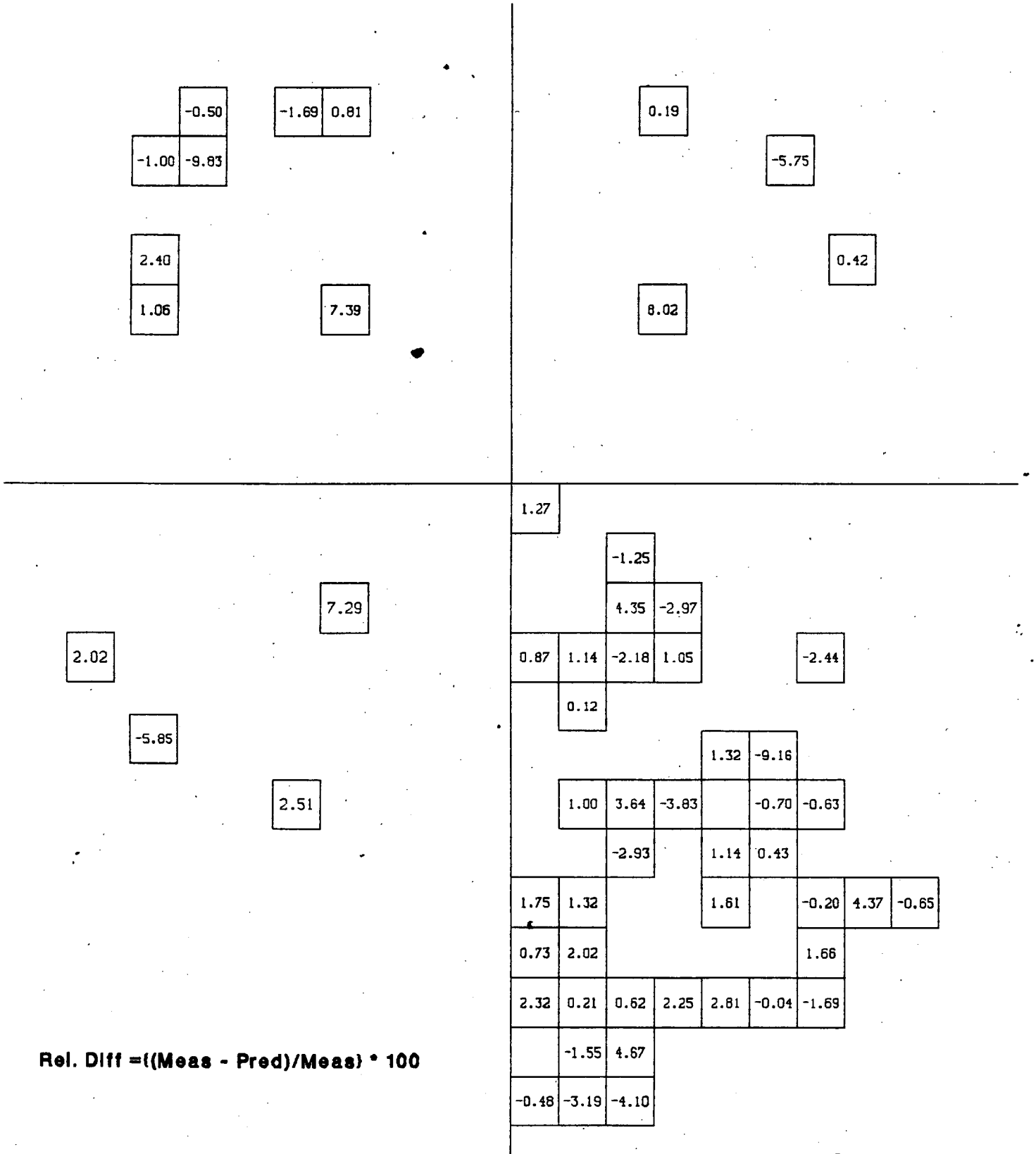

Rel. Diff =((Meas - Pred)/Meas) * 100

Figure 3.6.50

EOC 9 Axial Gamma Scan Comparison

Bundle 33-22

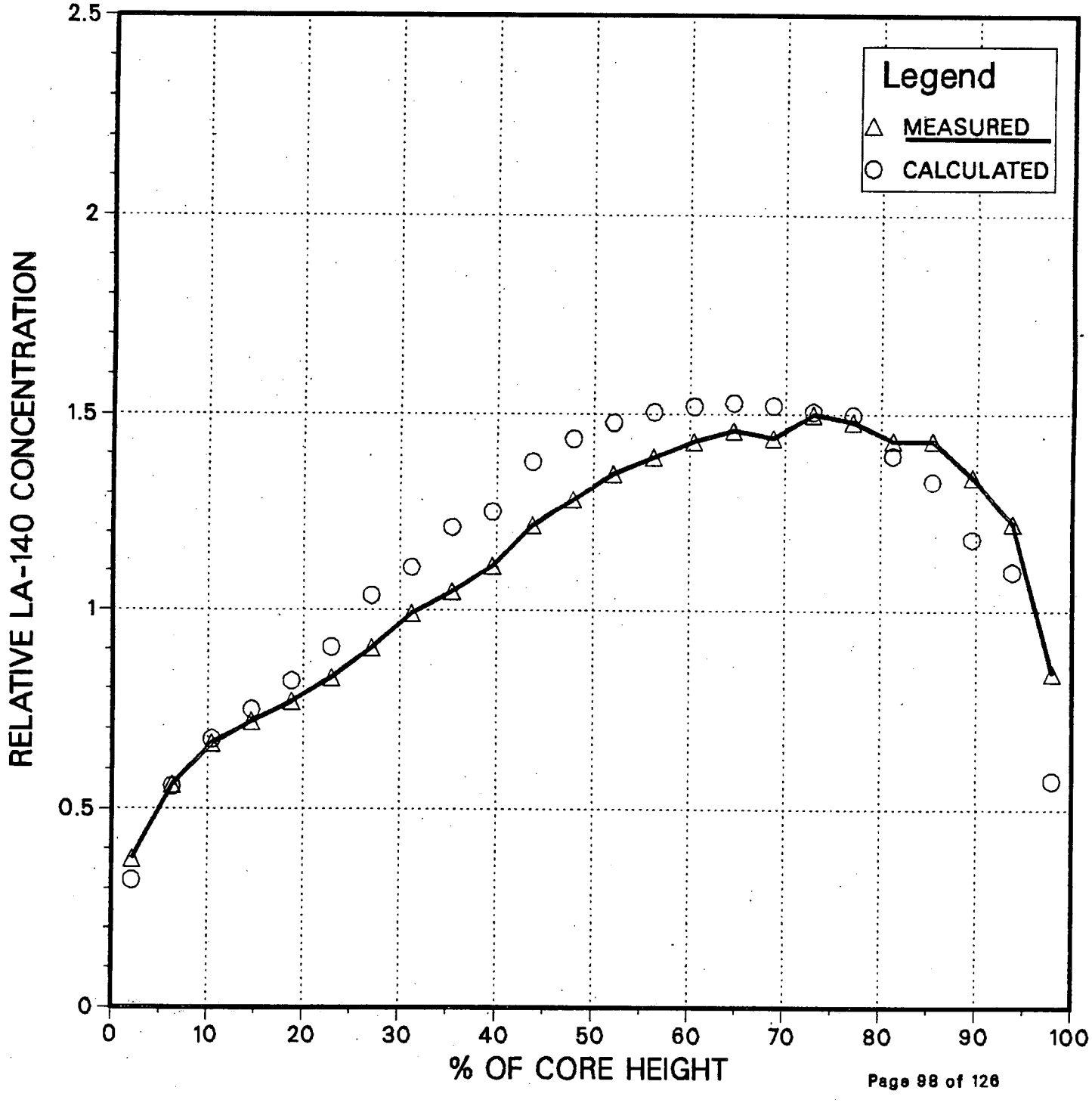

Figure 3.6.51

EOC 9 Axial Gamma Scan Comparison

Bundle 31-14

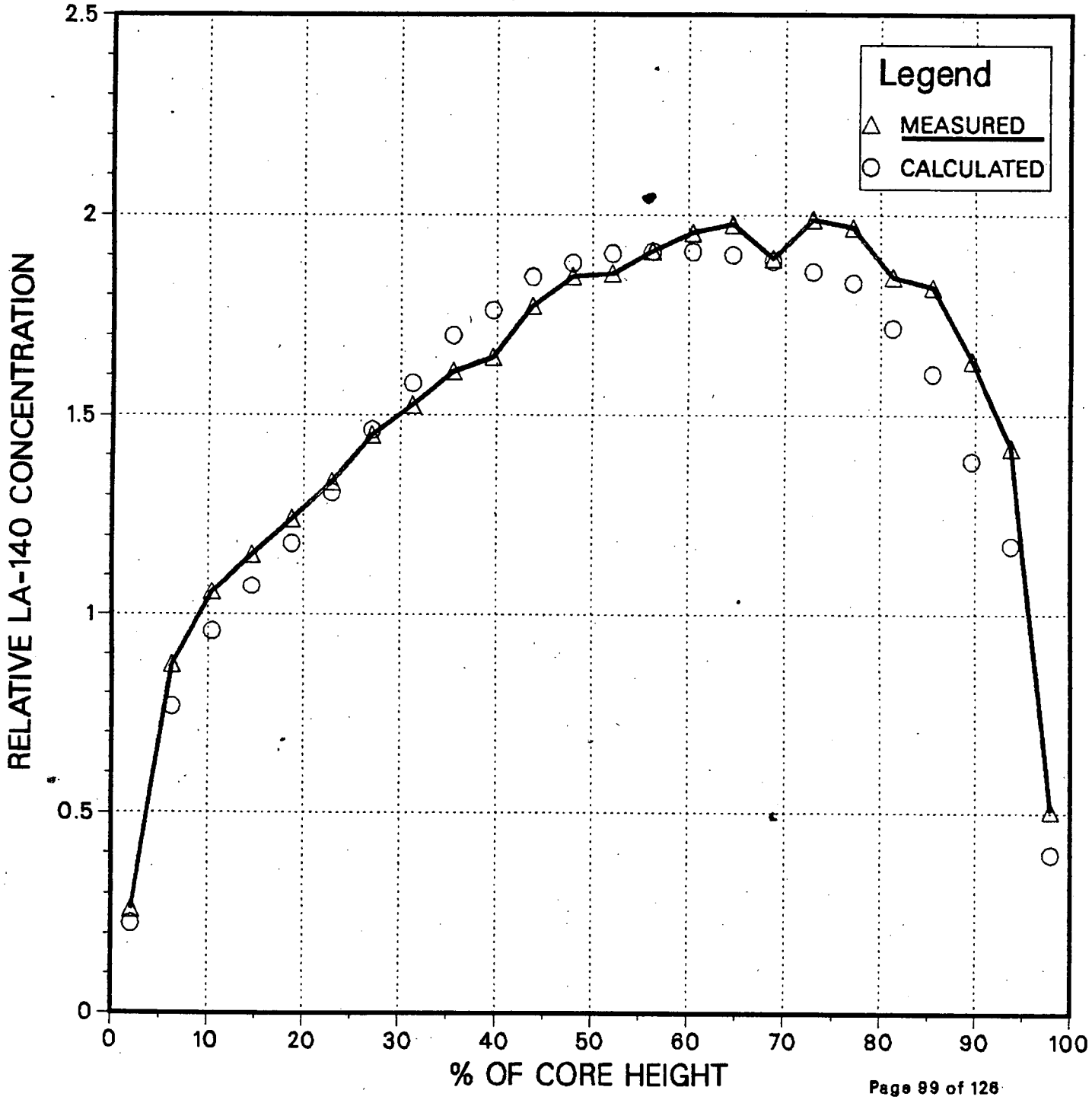

4.0 Model Applications to Reactor Operations

This section describes the methods used in applying the reliability factors and biases to reactor operations. It is not the intent of this section to define the procedures used. However, some aspects of these procedures are presented in order to clarify the approach taken in applying the model reliability factors and biases.

The model will be applied to reactor operations in two primary modes, predictive and monitoring. In the predictive mode, a best estimate of a future core state is desired, and therefore, only power distribution biases are applied to the predictive distribution. Few rod cold critical comparisons, in-sequence cold critical comparisons and hot full power critical comparisons are given below to verify this mode of application.

In the monitoring mode, process computer support and isotopic inventory calculations must be considered.

4.1 Predictive Applications

4.1.1 Few Rod Cold Criticals

NSP has predicted few rod cold criticals around the high worth rod for each cycle of operation in order to verify the predicted model. The resultant cold critical Keff for all few rod criticals calculated for cycles 7 through 10 is:

$$Keff = .9995 \pm .0012$$

Table 4.1.1 gives the detailed information for each critical.

Figure 4.1.1 gives the graphical representation of the criticals for each cycle.

4.1.2 In-Sequence Cold Criticals

NSP has predicted in-sequence withdrawals to cold critical for each cycle of operation to verify the rod withdrawal pattern and to prevent the withdrawal of a high notch worth rod that could scram the reactor.

The resultant cold critical Keff for all in-sequence criticals calculated for cycles 7 through 10 is:

$$Keff = 1.0005 \pm .0021$$

Table 4.1.1 gives the detailed information for each critical.

Figure 4.1.1 gives the graphical representation of the criticals for each cycle.

4.1.3 Hot Full Power Criticals

NSP has predicted the hot full power critical rod patterns for BOC and the resultant rod density for hot full power throughout each cycle.

The resultant hot critical Keff for all criticals calculated for cycles 7 through 10 is:

$$Keff = 0.9917 \pm .0018$$

Table 3.6.1 gives the detailed information for each critical. Figure 4.1.2 gives the graphical representation of the criticals for each cycle. Circled points indicate coastdowns.

4.2 Monitoring Applications

4.2.1 Process Computer

The General Electric Monicore System recently installed at Monticello will be retained. NSP is currently evaluating several options for support of this system for cycles 14 and beyond. GE will supply support for cycle 13 scheduled to startup in October of 1987. The support options are as follows:

1. Continue to have GE supply all support
2. NSP will support with system as installed
3. NSP will support with system modified by replacing Panacea with the NSP CASMO/NDH model.

4.2.2 Isotopic Inventory

The isotopic inventory calculation will be performed by NSP if either option 2 or 3 is decided upon in Section 4.2.1. The calculation of the isotopic inventory for Monticello is based upon a two-dimensional, CASMO calculation. This is the same model as is used to calculate the TIP trace design input. Therefore, the accuracy of the burnup distribution can be verified by the agreement of the measured and calculated reaction rates which is used to evaluate the measurement uncertainties, see Section 3.6 above. The accuracy of the isotopics versus local exposure is described in Section 3.5 above based on measurements at Saxton and Yankee.

TABLE 4.1.1

FEW ROD AND IN-SEQUENCE
COLD CRITICALS

Cycle	Core Ave. Exposure	Temp. °F	F= Few Rod S= Sequence	K_{eff}
7	9.748	101	F	.9995
	9.748	102	S	1.0015
	9.748	118	S	.9991
	9.748	130	S	.9989
	12.033	133	S	.9992
	12.033	172	S	.9975
8	12.119	123	F	.9975
	12.119	123	F	1.0006
	12.119	122	F	.9991
	12.119	122	S	1.0016
	12.119	127	S	1.0046
	12.119	125	S	1.0019
	12.389	141	S	1.0037
9	13.368	99	F	.9990
	13.368	97	F	.9994
	13.368	102	S	1.0003
	13.368	109	S	1.0013
	16.403	134	S	.9971
10	13.520	138	F	.9996
	13.520	139	F	1.0016
	13.520	142	S	.9999
	13.520	145	S	.9999

Statistics

	N	Mean	σ
Few Rod	8	0.9995	0.0012
Sequence	14	1.0005	0.0021
Combined	22	1.0001	0.0019

Figure 4.1.1

Cold Criticals vs Core Average Exposure

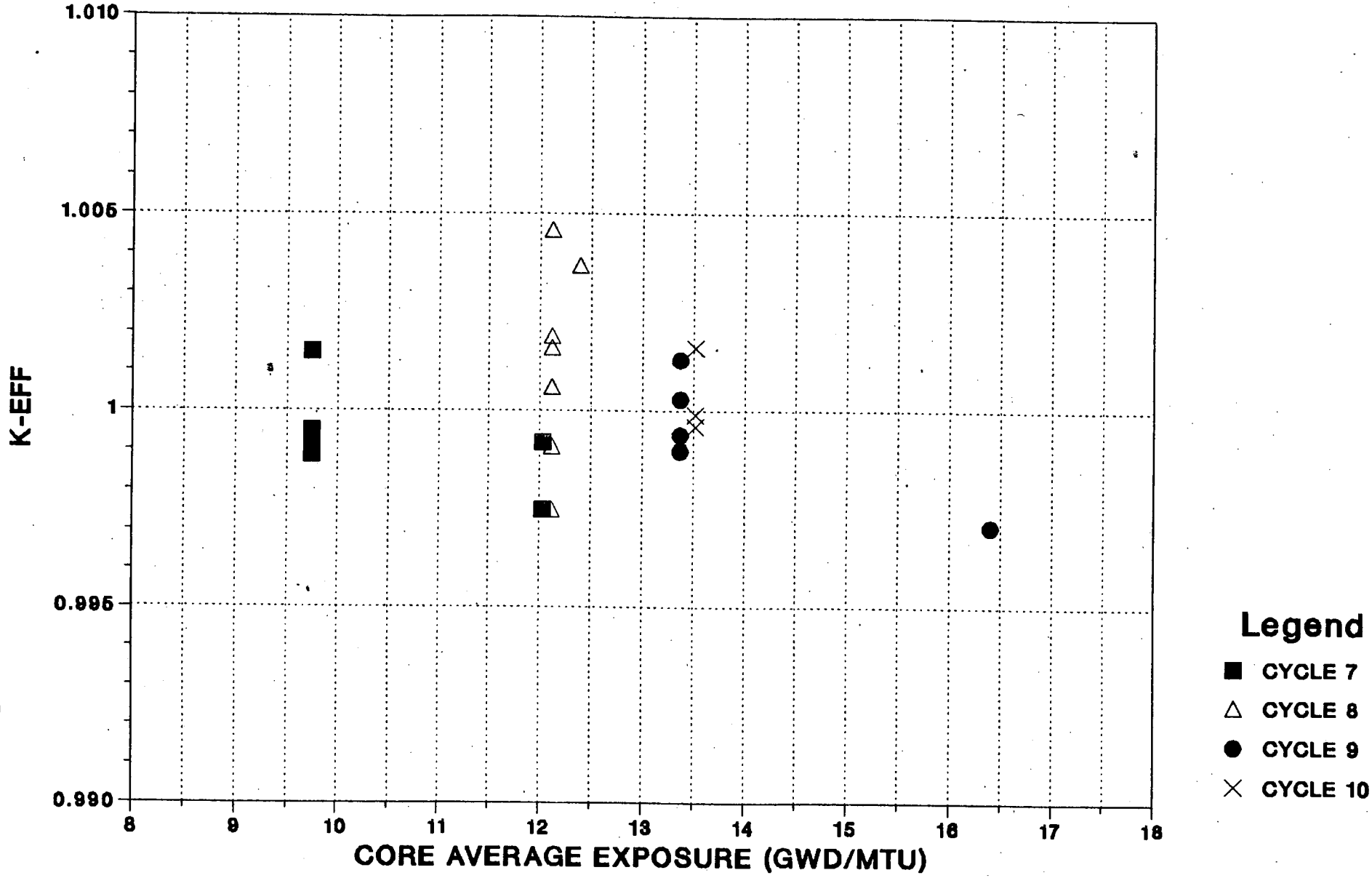

Figure 4.1.2

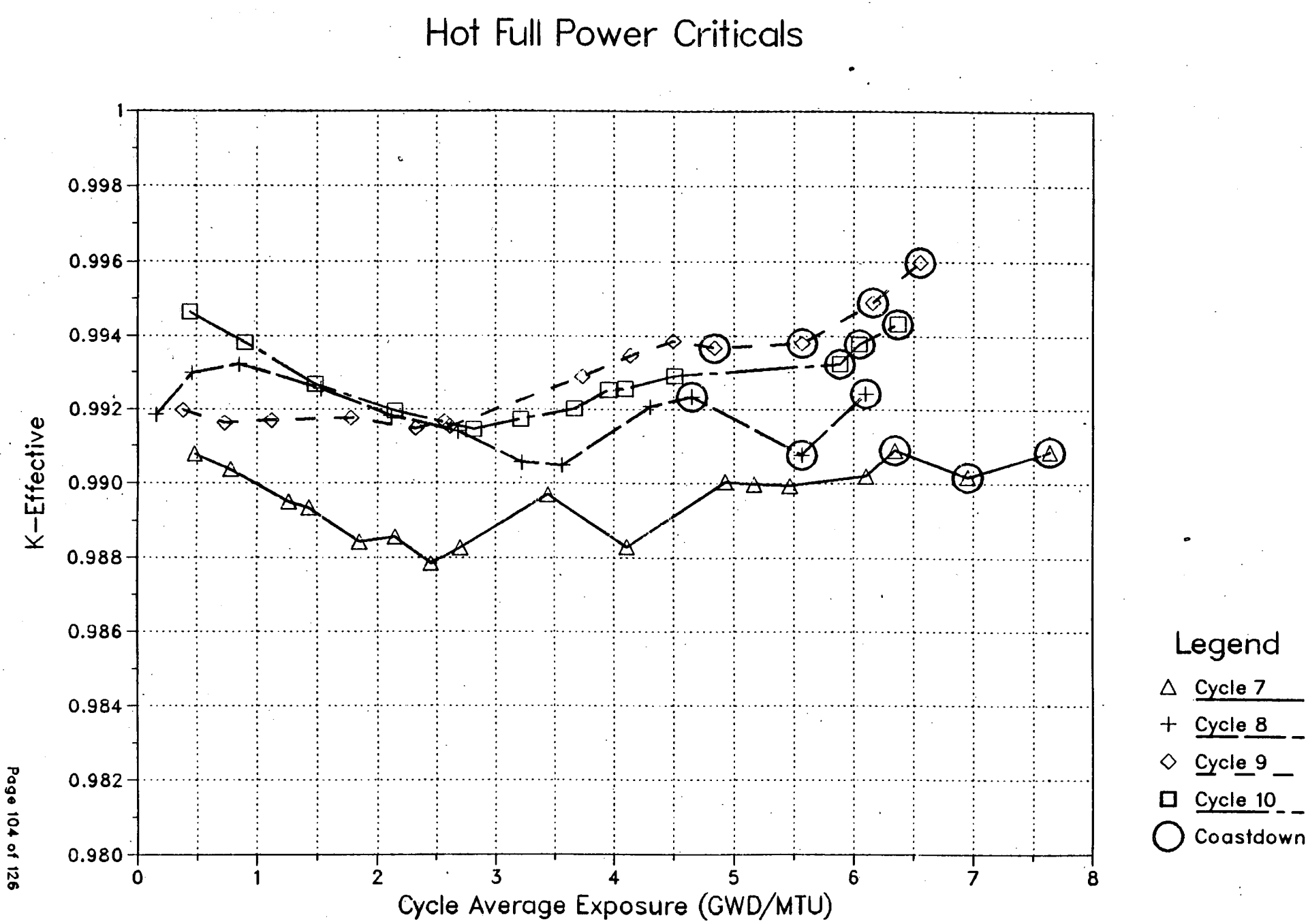
Hot Full Power Criticals
K-Effective
1
0.998
0.996
0.994
0.992
0.990
0.988
0.986
0.984
0.982
0.980
0
1
2
3
4
5
6
7
8
Cycle Average Exposure (GWD/MTU)
Legend
Cycle 7
Cycle 8
Cycle 9
Cycle 10
Coastdown

5.0 Model Applications To Safety Evaluation Calculations

This section describes the methods used in applying the reliability factors and biases to the results of safety related physics calculations. It is not the intent of this section to define the procedures to be used in performing the physics calculations. However, some aspects of these procedures are presented in order to clarify the approach taken in applying the model reliability factors and biases.

In such applications, the question is generally: Will the reload core maintain a safe margin to established safety limits (i.e., peak linear heat generation rate, minimum CPR, shutdown margin, etc.) under normal and non-normal or accident conditions? The question is usually answered by performing cycle specific safety analyses for the limiting transients and accidents.

For each parameter of interest, RF_X and $Bias_X$ are given in Table 3.0.1. The application of the RF_X and $Bias_X$ for each parameter of interest is shown below.

5.1 Linear Heat Generation Rate (LHGR and MAPLHGR)

The linear heat generation rate is defined as follows:

$$LHGR(I,J,K) = P(I,J,K) * LPF(I,J,K) * (1-FLK-FCH)$$

$$LPF(I,J,K) = P_{MAX}(U,E,FT) * L(I,J) * CR(IY)$$

where:

I,J are discrete assembly coordinates
K is a continuous axial coordinate
U is relative water density at location I,J,K
E is exposure in GWD/MTU at location I,J,K
FT is fuel type at location I,J,K
IY designates which of 6 possible control rod conditions exist at location I,J,K. See Reference 5 Part 2 Chapter 15 page 15-54 (EPRI-NODE-B).

$P(I,J,K)$ is the power in an axial slice of assembly I,J

$LPF(I,J,K)$ is the ratio of the power density of the maximum power pin to the average pin power density at location I,J,K

FLK is the fraction of the total nodal power that is produced outside the fuel channel in the leakage flow

FCH is the fraction of the total nodal power in the channel that is not conducted through the cladding

$P_{MAX}(U,E,FT)$ is the maximum pin power divided by the assembly power calculated by CASMO-II as a function of U, E, and FT

L(I,J) is a generic factor used to account for core power shape effect due to neutron leakage calculated from the ¼ core PDQ7 for locations I,J

CR(IY) is a generic factor used to account for the presence of control rods calculated from the ¼ core PDQ7 as a function of IY

The model reliability factor and bias listed in Table 3.0.1 are then applied as follows:

$$LHGR = LHGR(model) * (1+RF_{TPF}) * (1+Bias)$$

where model signifies the best estimate value directly calculated with the 3D simulator.

The Average Planar Linear Heat Generation Rate, APLHGR is defined as follows:

$$APLHGR = LHGR / LPF$$

where LHGR and LPF are as defined above. Therefore, the APLHGR contains the reliability factor and bias presented above. This approach to calculating APLHGR is conservative since the total peaking factor is larger than the axial peaking factor.

5.2 Critical Power Ratio (CPR)

The Critical Power Ratio is defined as the ratio of the bundle power required to produce onset of transition boiling somewhere in the bundle (critical power) to the actual bundle power, i.e.:

$$CPR(I,J) = P_c(I,J) / P(I,J)$$

where:

$P_c(I,J)$ is the critical bundle power in assembly (I,J)
$P(I,J)$ is the actual bundle power in assembly (I,J)

The minimum critical power ratio, MCPR, is defined as the minimum value of CPR in the core, i.e.:

$$MCPR = (P_c(I,J) / (P(I,J))_{min}$$

The model reliability and bias listed in Table 3.0.1 are then applied as follows:

$$MCPR = P_c(I,J) / [P(I,J) * (1+RF_{RPF}) * (1+Bias)]$$

5.3 Control Rod Worths

Rod worths are calculated using the three-dimensional nodal model. Worths are determined by varying the rod position while the independent core parameters such as core power, flow, and void distribution are held constant.

The model reliability factor and bias listed in Table 3.0.1 are then applied as follows:

$$\Delta K_{ROD} = \Delta K_{ROD}(MODEL) * (1 + Bias) * (1 \pm RF_{ROD})$$

The reliability factor is either added or subtracted, whichever is most conservative for each particular application.

The rod worth scram reactivity is input to the one-dimensional kinetics model as a function of the total rod worth, ΔK_{ROD}, as follows:

$$\Delta K_{ROD_K} = \Sigma_I \Delta K_{ROD_I} * CF_{I,K} * RWD_K$$

where:

$CF_{I,K}$ is the source weighted control fraction of group I in axial node K and RWD_K is the relative control rod worth distribution in node K.

5.4 Void Reactivity

For 1D kinetics applications, void reactivity effects are modeled in the transient simulator, DYNODE-B[9], via changes in K_∞ and M^2 relative to an initial transient condition.

The initial transient condition is run with the CASMO/NDH model. Thus the source, power, M^2, and K_∞ distributions are known throughout the core. In a similar manner, DYNODE-B is run for the initial and perturbed conditions. The CASMO/NDH initial case is then perturbed to change the void distribution. The differences in the values of the effective 1-D K_∞ and M^2 distributions between the perturbed and initial cases are computed. From the results, $\Delta K_\infty/\Delta U$ and $\Delta M^2/\Delta U$ are constructed as a function of U, where U is the relative water density obtained from DYNODE-B. These curves are integrated to obtain K_∞ vs U curves.

The model reliability and biases listed in Table 3.0.1 are applied to the $\Delta K_\infty/\Delta U$ function prior to integration; i.e.

$$\Delta K_\infty/\Delta U * (1 + Bias) * (1 \pm RF_{voids})$$

The reliability factor is either added or subtracted, whichever is most conservative, for each application.

For point kinetics applications the reliability factor is applied as follows:

$$\alpha_v = \alpha_v(model) * (1 + Bias) * (1 \pm RF_{voids})$$

5.5 Fuel Temperature (Doppler) Coefficient

For 1D kinetics applications, the Doppler coefficient is a measure of the change in core multiplication associated with a change in fuel temperature. Core reactivity is changed mainly due to Doppler broadening of the U-238 parasitic resonance absorption cross section due to increases in fuel temperature. This effect is calculated by running CASMO/NDH and DYNODE-B cases to develop a $\Delta K_\infty U^{o\frac{1}{2}} / \Delta t_f^{\frac{1}{2}}$ versus $t_f^{\frac{1}{2}}$ curve, where U^o is the initial relative water density and t_f is the fuel temperature obtained from DYNODE-B.

The model reliability factor and bias listed in Table 3.0.1 are then applied at each point as follows:

$$\Delta K_\infty U^{o\frac{1}{2}} / \Delta t_f^{\frac{1}{2}} * (1 + \text{Bias}) * (1 \pm RF_D)$$

This distribution is then integrated to obtain the K_∞ vs $t_f^{\frac{1}{2}}$ curve that is input to the transient code.

Again, the reliability factor is either added or subtracted, whichever is most conservative for each particular application.

For point kinetics applications, the reliability factor is applied as follows:

$$\alpha_D = \alpha_D(\text{model}) * (1 + \text{Bias}) * (1 \pm RF_D)$$

5.6 Delayed Neutrons

For 1D kinetics applications, the delayed neutron constants; β_i and λ_i, are assumed to be uniform throughout the core and constant in time in the transient simulator. The use of constant delayed neutron constants corresponding to the initial conditions is justified by the results in Reference 10 which show that β_{eff} does not change significantly during a transient until the scram is over. Source weighting is used to obtain these constants. The local values of β_i to be used in the weighting are the values taken directly from the infinite lattice calculations (CASMO) without any spectral importance weighting. The reason is that transient simulator source equations relate to the integral of the source over the entire energy spectrum so that the importance of the delayed neutrons does not depend on the energy at which they are born with respect to total source.

The axial-dependent total β's which are entered into the transient simulator are obtained by source weighting of the $\Sigma\beta_i$ over the radial direction at each axial level so that:

$$\beta_K(\text{model}) = \Sigma_R S_\ell \Sigma_i \beta^\ell i / \Sigma_R S_\ell .$$

The reliability factor listed in 3.0.1 is applied as shown:

$$\beta_K = \beta_K (\text{model}) * (1 \pm RF_\beta)$$

For point kinetics, the reliability factor is applied as follows:

$$\beta_{eff} = \beta_{eff}(\text{model}) * (1 \pm RF_{\beta})$$

5.7 Neutron Source Lifetime

In the transient model for 1D kinetics applications, the neutron source lifetime is assumed to be constant in time and is defined as:

$$\ell^*_K = (1/V\nu\Sigma_f)_K$$

where V is the velocity of the source neutrons (cm/s) and source averaging over the radial plane is used for consistency with the transient source solution used in DYNODE-B.

The neutron source lifetime is calculated in the CASMO/NDH model in each node ℓ from a curve fit of $(V\nu\Sigma_f)$ as a function of exposure, moderator density, and control fraction for each fuel type. ℓ_K^* is then source weighted as follows:

$$\ell_K^*(\text{model}) = \Sigma_R \, S_\ell/(V\nu\Sigma_f)_\ell \; / \; \Sigma_R \, S_\ell$$

The reliability factor listed in Table 3.0.1 is then applied as follows:

$$\ell_K^* = \ell^*_K \, (\text{model}) * (1 \pm RF_{\ell^*})$$

For point kinetics applications, the reliability factor is applied as follows:

$$\ell^* = \ell^*(\text{model}) \, (1 \pm RF_{\ell}^*)$$

6.0 REFERENCES

1. NSP Topical "Qualification of Reactor Physics Methods for Application to PI Units" Rev. 1, December 1982.

2. M. Edenius, A. Ahlin, H. Haggblom "CASMO-2 Users Manual," Studsvik Energiteknik AB, Studsvik/NR-81/3.

3. W. R. Cadwell, "PDQ-7 Reference Manual," WAPD-TM-678, Westinghouse Electric Corporation, January 1967.

4. R. Breen, O. Marlowe, C. Pfeifer, "Harmony: System for Nuclear Reactor Depletion Computation,: WAPD-TM-478, Westinghouse Electric Corporation, January 1965.

5. Advanced Recycle Methodology Program (ARMP) System Documentation, EPRI CCM-3 Research Project 118-1, September 1977.

6. M. Edenius, "Studies of the Reactivity Temperature Coefficient in Light Water Reactors," AE-RF-76-3160, AB Stomenergi, 1976.

7. M. Edenius, "Seminar on U-238 Resonance Capture," S. Pearlstein, Editor, page 87, BNL-NCS-50451, 1975.

8. M. Edenius, "Temperature Effects in Thermal Reactor Analysis," Internal Report presented to Oskarshamnuerkets Kraftgrupp AB(OKG), Stockholm, Sweden, employed by AB Stomenergi Studsvik, Sweden.

9. NSP Topical "Monticello Nuclear Generating Plant Safety Evaluation Methods," NSPNAD-8608, Rev. 0, September 1986.

10. J. M. Holzer, et.al. "A Code System to Produce Point Kinetics Parameters for LWR Calculations," ANS Trans, 39, 946-7, 1981.

11. H. D. Kosanke, et al, Gamma Scan Measurements at Monticello Nuclear Generating Plant Following Cycle 8, DOE/ET/34031-10, U.S. Department of Enegry, May 1982; GEAP-22130, General Electric Company, San Jose, California, May 1982.

12. L. M. Shiraishi, et al, Gamma Scan Measurements at Monticello Nuclear Generating Plant Following Cycle 9, DOE/ET/34031-14, U.S. Departement of Energy, Aug 1983; GEAP-30245, General Electric Company, San Jose, California, Aug 1982.

13. M.G. Kendall, A. Stuart, "The Advanced Theory of Statistics," Vol. 1, 3rd. ed., Hafner Publishing Co. N.Y., 1969.

14. D.B. Owen, "Factors for One-Sided Tolerance Limits and for Variables Sampling Plans" Sandia Corporation, March 1963.

APPENDIX A

STATISTICAL METHODS FOR THE DETERMINATION AND APPLICATION OF UNCERTAINTIES

The purpose of using statistical methods is to determine the value X_c (calculated) such that there is a 95% probability at the 95% confidence level that X_c will be conservative with respect to X_t (true value) when applying the calculational methods to safety related reactor analyses.

The first step is to determine whether or not a distribution is normal. If it is, the methods described in Section A.1 are used. If the distribution cannot be treated as normal, but the distributions are known, then the methods described in Section A.2 are used.

If neither of the above methods apply, then the parameter in question is conservatively bounded.

A.1 Application of Normal Distribution Statistics

Separation of Measurement and Calculational Uncertainties

Comparison of measured and calculated reactor parameters includes the effects of both the measurement and calculational uncertainties. Methods used in this report to isolate the calculational uncertainties are described below in terms of the following definitions:

X_T = true reactor parameter

X_M = measured reactor parameter

X_C = calculated reactor parameter

$e_M = (X_M - X_T) / X_T$ = measurement error

$e_C = (X_C - X_T) / X_T$ = calculation error

$e_{MC} = (X_M - X_C) / X_M$ = observed differences

$$\mu_i = \frac{\sum_{i=1}^{n} e_i}{n}$$

$$\sigma_i = \left(\left(\sum_{i=1}^{n} (e_i - \mu_i)^2\right) / (N-1)\right)^{1/2} \quad = \text{standard deviation}$$

If e_M and e_C are independent, then the following relationships exist. (Note that these relationships apply for non-normal distributions as well).

$$\sigma^2_C = \sigma^2_{MC} - \sigma_M^2$$

$$\mu_C = \mu_M - \mu_{MC}$$

Once the σ_C and μ_C have been calculated from historical data, they could be used to apply conservatism to future calculations of reactor parameters, X_C, as follows:

$$X_C = X_C * (1+\mu_C) * (1 \pm K_C\sigma_C)$$

The factor K_c is defined as described in Table A.1.[14] to provide a 95% probability at the 95% confidence level that X_C is conservative with respect to the true value, X_T.

Reliability Factors

It is the objective to define reliability factors which are to be used to increase/decrease calculated results to the point where there is a 95% probability at the 95% confidence level that they are conservative with respect to actual reactor parameters.

For any given application, there is concern only with one side of the component; that is, if the calculated value is too large or too small. Therefore, one-sided tolerance limits based on normal distributions may be used to find a K_c which will give a 95% probability at the 95% confidence level to the reliability factor defined by:

$$RF = K_c * \sigma_c$$

Numerical values of K_c for various sample sizes used to calculate σ_c are provided on Table A.1.[14]

TABLE A.1

SINGLE-SIDED TOLERANCE FACTORS

n	k_c
2	26.26
3	7.66
4	5.15
5	4.20
6	3.71
7	3.40
8	3.19
9	3.03
10	2.91
11	2.82
12	2.74
15	2.57
20	2.40
25	2.29
30	2.22
40	2.13
60	2.02
100	1.93
200	1.84
500	1.76
∞	1.645

n = Number of data points used for σ

A.2 Application of Non-Normal Distribution Statistics

If a distribution is determined to be other than normal, the requirement is that there is a 95% confidence level that X_c will be conservative with respect to the true value X_m. (In the following, the notation used is consistent with that defined in Section A.1). It is thus required that a 95% upper confidence limit be determined for the 95th percentile of the distribution of errors.

In the calculation, a set of error observations (e_i) are determined. The mean (μ_{mc}) and the standard deviation (σ_{mc}) are calculated using the following formulation:

$$\mu_{mc} = \frac{\sum_{i=1}^{n} e_i}{n}$$

$$\sigma_{mc} = \left(\left(\sum_{i=1}^{n}(e_i - \mu_{mc})^2\right) / (n-1)\right)^{\frac{1}{2}}$$

Note that the e_i above are determined from the following:

$$e_i = e_{mc} = (X_m - X_c)/X_m = \text{observed differences}$$

Generally, the e_{mc} are taken from several cycles of operation; thus, they represent the true distribution. The e_i are then transformed to standard measure by the following formula:

$$Z_i = \frac{e_i - \mu_{mc}}{\sigma_{mc}}$$

and the resulting variates (z) are sorted into ascending order and the kth (such that $K \geq .95n$) variate is chosen as an estimate of the 95th percentile of the distribution (See reference 13, page 40-41). This gives a 95th percentile of z to be Q_{95}. This implies that 95% of the errors are likely to be less than Q_{95}.

It remains to calculate a 95% confidence interval on Q_{95}. (The formula for this calculation is taken from reference 13 page 236-243 (See references section 6.0).):

$$\text{Var } Q_{95} = \frac{q(1-q)}{n f_1^2}$$

where: q = the quantile (.95)
n = number of independent observations in the sample
f_1 = ordinate of the density function of the distribution of observed differences at abscissa q

It is necessary to determine if the observations are independent. If they are not independent, it is necessary to reduce the sample size to account for the dependence in the determination of the 95% confidence level.

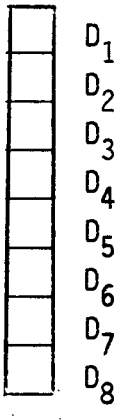

Figure 1. Differences for Nearby Positions

To set notation, let $\delta_{.95}$ be the population 95th percentile for the observed differences, that is $P[D_i \leq \delta_{.95}] = .95$. We wish to determine a 95% upper confidence limit for $\delta_{.95}$ when some of the differences are dependent. For differences observed at adjacent positions, the appropriate measure of association for our analysis can be shown to be

$$C(1) = P[D_1 \leq \delta_{.95} \text{ and } D_2 \leq \delta_{.95}] - (.95)^2$$

We also consider the association of differences observed at locations two apart

$$C(2) = P[D_1 \leq \delta_{.95} \text{ and } D_3 \leq \delta_{.95}] - (.95)^2$$

and, more generally,

$$C(k) = P[D_1 \leq \delta_{.95} \text{ and } D_{1+k} \leq \delta_{.95}] - (.95)^2$$

for k = 1,2,3,4,5,6,7 locations apart. In this example, there are 8 differences D_i, 7 adjacent pairs (D_i, d_{i+1}), 6 pairs with indices two apart (D_i, D_{i+2}) ..., 1 pair $D_1 D_8$.

Let $d_{(s)}$ be the sample 95th percentile with s selected to be the smallest integer not less than .95n. The large sample distribution of $d_{(s)}$ depends on that of

$T(x)$ = number of differences, D_i, that are less than or equal x.

Even with dependence among the D_i,

$$\frac{T(x)-nF(x)}{s.d.[T(x)]} = \frac{\frac{1}{\sqrt{n}}(T(x)-nF(x))}{\frac{1}{\sqrt{n}}\,s.d.[T(x)]}$$

will be approximately standard normal. Here $F(x) = P[D_i \le x]$ and $f(x)$ is the probability density function for the observed differences.

It follows that

$$P[\sqrt{n}(d_{(s)}-\delta_{.95}) \le z] = 1 - P[T(\delta_{.95} + n^{-\frac{1}{2}}z) \le s-1]$$

$$\sim 1 - \Phi\ \frac{-f(\delta_{.95})z}{\frac{1}{\sqrt{n}}\,s.d.[T(\delta_{.95})]}$$

where

$$\left[\frac{1}{\sqrt{n}}\,s.d.[T(\delta_{.95})]\right]^2 = 1/n\ [n(.95)(.05)+2\ \tfrac{7}{8}nC(1) + 2\ \tfrac{6}{8}nC(2)+\ldots+ 2\tfrac{1}{8}nC(7)]$$

$$= (.95)(.05)+\tfrac{14}{8}C(1)+\tfrac{12}{8}C(2)+\tfrac{10}{8}C(3)+\ldots+\tfrac{2}{8}C(7).$$

Under independence $0 = C(1) = C(2) = \ldots = C(7)$ and this expression reduces to its customary value (.95)(.05). If the differences are dependent, the variance of $d_{(s)}$ is

$$1/n\ \frac{(.95)(.05)}{f^2(\delta_{.95})}\ \left[1 + \sum_{k=1}^{7} \frac{2(8-k)C(k)}{8(.95)(.05)}\right]$$

In order to apply this result, we estimate C(1) by

$$C(1) = \frac{\#\text{ adjacent pairs } (D_i, D_{i+1}) \text{ where both} \le d_{(s)}}{\text{Total \# of adjacent pairs}} - (.95)^2.$$

The estimate of C(2) is

$$C(2) = \frac{\#\text{ pairs } (D_i, D_{i+2}) \text{ where both} \le d_{(s)}}{\text{Total \# of pairs } (D_i, D_{i+2})} - (.95)^2$$

and

$$C(k) = \frac{\#\text{ pairs } (D_i, D_{i+k}) \text{ where both} \le d_{(s)}}{\text{Total \# of pairs } (D_i, D_{i+k})} - (.95)^2$$

for k = 3,4,5,6,7. The value of $f^2(\delta_{.95})$ can be estimated as previously suggested. Then, the large sample upper 95% confidence limit for $\delta_{.95}$, adjusted for dependence among differences by location is given by

$$d_{(s)} + \frac{1.645}{\sqrt{n}} \left[\frac{(.95)(.05)}{F^2(\delta_{.95})} \left(1 + \sum_{k=1}^{7} \frac{2(8-k)C(k)}{8(.95)(.05)}\right)\right]^{\frac{1}{2}}$$

One interpretation of this confidence limit, or the variance expression, is that the total sample size n is effectively reduced by the dependence. We estimate the effective sample size to be

$$\frac{n}{1 + \sum_{k=1}^{7} \frac{2\,(8-k)C(k)}{8(.95)(.05)}}$$

If only two terms are used, the effective sample size is estimated to be

$$n \left[\frac{(.95)(.05)}{(.95)(.05) + \frac{14}{8}C(1) + \frac{12}{8}C(2)} \right]$$

It is necessary to obtain an estimate of f_1 (.95) on a short interval of the cumulative distribution function of z in the region of the 95th percentile. The slope of the cumulative distribution function is an estimate of the ordinate of the density function since the density function is simply the derivative of the cumulative distribution function. Thus

$$\sigma Q_{95} = \text{Var } Q_{95}$$

This value then allows an estimate of the 95% confidence limit on Q_{95}. Even though nothing is known about the distribution of Q_{95}, the distribution can be shown to be normal using the following derivation.

$$P[D_1 \leq \delta_{.95} \text{ and } D_2 \leq \delta_{.95}]$$

where $\delta_{.95}$ is the 95th percentile of the distribution of differences. If the differences D_1 and D_2 are independent

$$P[D_1 \leq \delta_{.95} \text{ and } D_2 \leq \delta_{.95}] = P[D_1 \leq \delta_{.95} \text{ and } P[D_2 \leq \delta_{.95}]$$
$$= (.95)(.95) = (.95)^2.$$

The difference

$$P[D_1 \leq \delta_{.95} \text{ and } D_2 \leq \delta_{.95}] - (.95)^2$$

is a measure of association (dependence) from position to adjacent position.

Note that if

$$I(D_1 \leq \delta_{.95}) = \begin{cases} 1 \text{ if } D_1 \leq \delta_{.95} \\ 0 \text{ if } D_1 > \delta_{.95} \end{cases}, \quad I(D_2 \leq \delta_{.95}) = \begin{cases} 1 \text{ if } D_2 \leq \delta_{.95} \\ 0 \text{ if } D_2 > \delta_{.95} \end{cases}$$

then the covariance is

$$C(1) = \text{Cov}(I(D_1 \leq \delta_{.95}), I(D_2 \leq \delta_{.95})) = P[D_1 \leq \delta_{.95} \text{ and } D_2 \leq \delta_{.95}] - (.95)^2.$$

We <u>assume</u> the same covariance for $I(D_2 \leq \delta_{.95})$ and $I(D_3 \leq \delta_{.95})$ ... $I(D_7 \leq \delta_{.95})$ and $I(D_8 \leq \delta_{.95})$. There are about n 7/8 such pairs among the whole set of n observed differences.

Let $d_{(s)}$ be the sample 95th percentile where s is the smallest integer not less than n(.95). When n is large

$$C(1) = \frac{\#\text{ pairs } (D_i, D_{i+1}) \text{ both} \leq d_{(s)}}{\text{Total number of pairs } (D_i, D_{i+1})} - (.95)^2$$

is a good estimate of C(1). Similarly, for the approximately 6n/8 pairs $(D_i,, D_{i+2})$

$$C(2) = \text{Cov}[I(D_1 \leq \delta_{.95}), I(D_3 \leq \delta_{.95})]$$

is estimated by

$$C(2) = \frac{\#\text{ pairs } (D_i, D_{i+2}) \text{ both} \le d_{(s)}}{\text{Total number of pairs } (D_i, D_{i+2})} - (.95)^2$$

and

$$C(k) = \frac{\#\text{ pairs } (D_i, D_{i+k}) \text{ both} \le d_{(s)}}{\text{Total number of pairs } (D_i, D_{i+k})} - (.95)^2$$

Let us now see how to modify the proof that $d_{(s)}$ is asymptotically normal in order to account for the dependence among adjacent differences. It is still true that

(A1) $$P[d_{(s)} \le x] = 1 - P[d_{(s)} > x] = 1 - P[s-1 \text{ or fewer } D_1 \le x]$$
$$= 1 - P[T(x) < s]$$

where $T(x) = \sum_{i=1}^{n} I(D_i \le x) = \#$ differences $D_i \le x$. Moreover, $T(x) - nF(x)$ has mean 0 and, for large samples, is approximately normal under a wide range of dependence structures. Consequently, the sums $\sum_{i=1}^{8} I(D_i \le x)$ are independent of one another and each has the same distribution. Since $T(x)$ is just the sum of these group sums, the central limit theorem gives

$$\frac{T(x) - nF(x)}{\text{s.d.}[T(x)]} \text{ is approximately standard normal.}$$

Consequently, from (A1) and the normal approximation

$$P[\sqrt{n}(d_{(s)} - \delta_{.95}) \le Z] = P[d_{(s)} \le \delta_{.95} + n^{-\frac{1}{2}}z]$$
$$= 1 - P[T(\delta_{.95} + n^{-\frac{1}{2}}z) < s]$$
$$= 1 - \Phi\left[\frac{s - nF(\delta_{.95} + n^{-\frac{1}{2}} z)}{\text{s.d.}[T(\delta_{.95} + n^{-\frac{1}{2}} z]}\right]$$

Now, note that

$$\frac{1}{\sqrt{n}}(s - nF(\delta_{.95} + n^{-\frac{1}{2}} z)) = \frac{1}{\sqrt{n}}(s - nF(\delta_{.95}) - nf(\delta_{.95})n^{-\frac{1}{2}} z + O(1))$$

$$= \frac{1}{\sqrt{n}}(s - n(.95) - n^{\frac{1}{2}} zf(\delta_{.95})) + O(1)$$

$$= -zf(\delta_{.95}) + O(1).$$

Furthermore,

$$\frac{1}{n}\,\mathrm{Var}[T(\delta_{.95} + n^{-\frac{1}{2}}z)] = \mathrm{Var}[I(D_1 \le \delta_{.95} + zn^{-\frac{1}{2}})]$$

$$+ \sum_{k=1}^{7} \frac{2(8-k)}{8}\,\mathrm{Cov}[I(D_1 \le \delta_{.95} + n^{-\frac{1}{2}}z), I(D_{1+k} \le \delta_{.95}\, n^{-\frac{1}{2}}z)$$

which converges to

$$F(\delta_{.95}) - F^2(\delta_{.95}) + \sum_{k=1}^{7} \frac{2(8-k)}{8}\,\{P[D_1 \le \delta_{.95},\ D_{1+k} \le \delta_{95}] - (.95)^2\}$$

$$= (.95)(.05) + \sum_{k=1}^{7} \frac{2(8-k)}{8}\,C(k) = \lim \frac{1}{n}\,\mathrm{Var}[T(\delta_{.95})].$$

Therefore, by (A2),

$$P[\sqrt{n}(d_{(s)} - \delta_{.95}) \le z] \sim 1 - \Phi\left[\frac{-zf(\delta_{.95})}{\frac{1}{\sqrt{n}}\,\mathrm{s.d.}[T(\delta_{.95})]}\right]$$

or $\sqrt{n}(d(s) - \delta_{.95})$ is approximately normal with mean 0 and variance

$$\frac{1}{n}\left[\frac{(.95)(.05) + \sum_{k=1} 2(8-k)C(k)/8}{f2(w_{.95})}\right].$$

As was indicated above, the C(k) may be estimated by C(k) and the large sample normality will still hold. Therefore using Table A.1 to obtain K_c:

$$\sigma\, Q_{95} = K_c\,(\mathrm{Var}\, Q_{95})^{\frac{1}{2}}$$

Thus it is 95% certain that Q_{95} lies in the interval

$$Q_{95} - \lambda\sigma Q_{95} \le Q_{95} \le Q_{95} + \lambda\sigma Q_{95}$$

therefore it is safe to say that we are 95% confident that

$$Q_{95} \le (Q_{95} + \lambda\sigma Q_{95})\sigma_{mc}$$

APPENDIX B

COMPUTER CODE SUMMARY DESCRIPTION

COMPUTER CODE	DESCRIPTION
CAF	Reads CASMO-II output files and generates the input tables and curve fits for each fuel type for the FUN computer program.
CASMO-II	CASMO-II is a multigroup two-dimensional transport theory code for depletion and branch calculations for a single assembly. It calculates the K_∞'s, M^2's and delayed neutron constants used to calculate input to the NDH program and generates cross sections used by PDQ7. Some of the characteristics of CASMO-II are: 1. 69 energy group cross section library. 2. 12 energy groups are used during the two-dimensional transport calculations. 3. Gadolinium effective cross sections are generated by the MICBURN program. 4. A fundamental mode calculation is performed to account for leakage effects. 5. The predictor-corrector approach is used for depletion. 6. Effective resonance cross sections are calculated individually for each pin. 7. A two-dimensional diffusion theory routine is used for automatic generation of effective cross sections for PDQ7. 8. Simple user oriented input.
CAT	Reads CASMO-II output files and generates input cross sections, number densities and chains for the assembly and ¼ core PDQ7. It is also used with the assembly PDQ7 runs to adjust the capture fractions of the assembly PDQ7 until they match CASMO-II. The adjusted cross sections are then input to the ¼ core PDQ7.

COMPUTER CODE	DESCRIPTION
FUN	Reads CAF output files for the fuel types needed and the generic factors generated from the NDH to ¼ core PDQ7 comparisons. It than generates the input models for NDH and SGM.
GAS	Reads NDH output files and calculates the predicted La 140 distribution to be compared to the gamma scan measurements. Outputs the predicted, measured, and difference relative La 140 distribution for input to SPM for statistical analysis.
NDH	NDH is a modified version of the ERPI-NODE-B computer program. The following is a list of improvements made.

1. Base K_∞

NDH - The base K_∞ for the cold model is a function of temperature in °F. There is a multiplier on the base K_∞ as a function of assembly location, core average exposure, for bundles which have been on the periphery, control rods, void history, and relative water density. This multiplier is the result of the generic normalization between NDH and PDQ7.

NODE - The base K_∞ does not have a functional dependence on temperature and the K_∞ multiplier is only a function of assembly location.

2. M^2

NDH - The M^2 has a multiplier which is a function of bundle location, rod presence and core average exposure. This multiplier is the result of the generic normalization between NDH and PDQ7.

NODE - Has no M^2 multiplier.

3. Doppler Reactivity

NDH - The Doppler Reactivity is input as a curve fit which is a function of exposure, relative water density and fuel temperature.

NODE - The Doppler Reactivity is input as a curve fit but does not have the exposure dependence.

COMPUTER CODE	DESCRIPTION
NDH (cont.)	4. Xenon Reactivity

NDH - The Xenon number density is calculated using $\kappa\Sigma_f$ input as a table which is a function of void history and exposure, and σ_a input as a table which is a function of void and exposure. The reactivity is input as $\Delta\rho/N_{xe}$ as a table which is a function of void history and exposure.

NODE - The Xenon number density is calculated using $\kappa\Sigma_f$ and σ_a, both curve fit as a function of relative water density. The reactivity is than calculated internally.

5. Exposure Reactivity Effects

NDH - The exposure reactivity effect is input as a table which is a function of void history and exposure.

NODE - The exposure reactivity effect is input as a curve fit as a function of void history and exposure.

6. Exposure Dependence of Control Rod Worth

NDH - The exposure dependence of control rod worth has an expanded curve fit using both a third and a second order curve fit.

NODE - The exposure dependence of control rods is fit as a linear change with exposure.

7. Control Rod History effect

NDH - The control rod history effect is calculated explicitly using a control rod history array and is a function of gadolinium depletion and exposure.

NODE - The control rod history effect is accounted for by reducing the average relative water density the node has seen.

COMPUTER CODE	DESCRIPTION
NDH (cont.)	8. Exposure Dependence of Void Reactivity
	NDH - The exposure dependence of void reactivity is input as a function of the ratio of instantaneous void and void history, and exposure.
	NODE - Does not have an exposure dependence of void reactivity.
	9. Power to Source Conversion
	NDH - The power to source conversion is done using the ratio of $\kappa\sigma_f/\nu\sigma_f$ vs exposure.
	NODE - The power to source conversion is done using the ratio of $\kappa\sigma_f/\nu\sigma_f$ versus relative water density.
	10. Maximum Number of Axial Nodes
	NDH - Allows up to 24 axial nodes
	NODE - Allows up to 12 axial nodes
	11. Maximum Number of Fuel Types
	NDH - Allows up to 50 fuel types in a three dimensional array.
	NODE - Allows up to 13 fuel types in a two dimensional array.
	12. Other Addtions to NDH Not in NODE
	- Spectrum correction factors used to correct the extrapolated flux assumption in the power correction.
	- A control rod tip correction on power distribution.
	- Power to flow ratio is calculated internally.
	- A correction for Samarium reactivity change during outage has been added.
	- A routine has been added to calculate kinetics parameters for input to transient analysis models.

COMPUTER CODE	DESCRIPTION
NDH (cont.)	- The radial albedos are void dependent. - LHGR, MAPLHGR, and MCPR are calculated. The GEXL correlation is used to calculate CPR. - Automates the collection and processing of data.
NRB	Reads output from ¼ core PDQ7 through PDE and the NDH input model. It then normalizes NDH until it reproduces the PDQ7 results. The normalization factors are the generic factors supplied to FUN for creating NDH and SIGMA models.
MICBURN	MICBURN calculates the burnup of a fuel pin containing gadolinium and generates 69 group effective cross sections as a function of number density for gadolinium to be input to CASMO-II.
PDE	Reads PDQ7 output files and formats them for NRB.
PDQ7	PDQ7/HARMONY is a nuclear reactor analysis program which solves the neutron diffusion equations and performs depletion calculations.
SIGMA	SIGMA calculates the predicted detector reaction rate using the NDH nodal power distribution, CASMO-II detector reaction rate to assembly power factors and generic factors from ¼ core PDQ7. SIGMA outputs the predicted, measured and difference of the detector reaction rates for input into SPM.
SPM	Inputs the predicted, measured and difference of the TIP reaction rates or the gamma scan and calculates bias and reliability factors.
SUN	SUN inputs NDH history files. SUN then shuffles the NDH history file for the next cycle and calculates which bundles have been on the periphery and then moved inside the core.